FERMILAB-PUB-18-594-A

Cosmic Visions Dark Energy: Inflation and Early Dark Energy with a Stage II Hydrogen Intensity Mapping Experiment

(Cosmic Visions 21 cm Collaboration)

Réza Ansari,[1] Evan J. Arena,[2,3] Kevin Bandura,[4,5] Philip Bull,[6,7] Emanuele Castorina,[8] Tzu-Ching Chang,[9,10] Simon Foreman,[11] Josef Frisch,[12] Daniel Green,[13] Dionysios Karagiannis,[14] Adrian Liu,[6,7,15] Kiyoshi W. Masui,[16] P. Daniel Meerburg,[17,18,19,20,21] Laura B. Newburgh,[22] Andrej Obuljen,[23,24,25] Paul O'Connor,[2] J. Richard Shaw,[26] Chris Sheehy,[2] Anže Slosar,[2,*] Kendrick Smith,[27] Paul Stankus,[28] Albert Stebbins,[29] Peter Timbie,[30] Francisco Villaescusa-Navarro,[31] and Martin White[6]

[1] *Université Paris-Sud, LAL, UMR 8607, F-91898 Orsay Cedex, France & CNRS/IN2P3, F-91405 Orsay, France*
[2] *Brookhaven National Laboratory, Upton, NY 11973*
[3] *Stony Brook University, Stony Brook, NY 11794*
[4] *CSEE, West Virginia University, Morgantown, WV 26505, USA*
[5] *Center for Gravitational Waves and Cosmology, West Virginia University, Morgantown, WV 26505, USA*
[6] *Department of Astronomy, University of California Berkeley, Berkeley, CA 94720, USA*
[7] *Radio Astronomy Laboratory, University of California Berkeley, Berkeley, CA 94720, USA*
[8] *Department of Physics, University of California Berkeley, Berkeley, CA 94720, USA*
[9] *Jet Propulsion Laboratory, California Institute of Technology, Pasadena, CA, USA*
[10] *California Institute of Technology, Pasadena, CA 91125*
[11] *Canadian Institute for Theoretical Astrophysics, University of Toronto, Toronto, ON M5S 3H8, Canada*
[12] *SLAC National Accelerator Laboratory, Menlo Park, CA 94205*
[13] *University of California San Diego, La Jolla, CA 92093*
[14] *Dipartimento di Fisica e Astronomia "G. Galilei",Università degli Studi di Padova, via Marzolo 8, I-35131, Padova, Italy*
[15] *McGill University, Montreal, QC H3A 2T8, Canada*
[16] *Massachusetts Institute of Technology, Cambridge, MA 02139*
[17] *Kavli Institute for Cosmology, Madingley Road, Cambridge, UK, CB3 0HA*
[18] *Institute of Astronomy, University of Cambridge, Madingley Road, Cambridge CB3 0HA, UK*
[19] *DAMTP, Centre for Mathematical Sciences, Wilberforce Road, Cambridge, UK, CB3 0WA*
[20] *Kapteyn Astronomical Institute, University of Groningen, P.O. Box 800, 9700 AV Groningen, The Netherlands*
[21] *Van Swinderen Institute for Particle Physics and Gravity, University of Groningen, Nijenborgh 4, 9747 AG Groningen, The Netherlands*
[22] *Department of Physics, Yale University, New Haven, CT 06520*
[23] *SISSA - International School for Advanced Studies, Via Bonomea 265, 34136 Trieste, Italy*
[24] *INFN – National Institute for Nuclear Physics, Via Valerio 2, I-34127 Trieste, Italy*
[25] *Department of Physics and Astronomy, University of Waterloo, 200 University Ave W, Waterloo, ON N2L 3G1, Canada*
[26] *University of British Columbia, Vancouver, BC V6T 1Z1, Canada*
[27] *Perimeter Institute, Waterloo, Ontario N2L 2Y5, Canada*
[28] *Oak Ridge National Laboratory, Oak Ridge, TN 37831*
[29] *Fermi National Accelerator Laboratory, Batavia, IL 60510*
[30] *Department of Physics, University of Wisconsin - Madison, Madison, WI 53706*
[31] *Center for Computational Astrophysics, 162 5th Ave, 10010, New York, NY, USA*

(Dated: October 24, 2018)

* Corresponding author. E-mail: anze@bnl.gov

This document was prepared by Cosmic Visions 21 cm collaboration using the resources of the Fermi National Accelerator Laboratory (Fermilab), a U.S. Department of Energy, Office of Science, HEP User Facility. Fermilab is managed by Fermi Research Alliance, LLC (FRA), acting under Contract No. DE-AC02-07CH11359.

CONTENTS

PREAMBLE

The Department of Energy (DOE) of the United States government has tasked several Cosmic Visions committees to work with relevant communities to make strategic plans for the future experiments in the Cosmic Frontier of the High Energy Physics effort within the DOE Office of Science. The Cosmic Visions Dark Energy committee was the most open-ended, with a broad effort to study periods of accelerated expansion in the Universe, both early and late, using surveys. It has conducted two community workshops and produced two white papers [1–3].

In [1] and [2], intensity mapping of large scale structure was discussed as one possible new observational avenue for the DOE's dark energy program. In the intervening years, an informal working group has been working towards charting a science case and the research and development (R&D) path towards a successful experimental program. The working group has engaged in regular teleconferences and organized one community meeting.[1] This white paper summarizes the work of this group to date.

EXECUTIVE SUMMARY

In the next decade, two flagship DOE dark energy projects will be nearing completion: (i) DESI, a highly multiplexed optical spectrograph capable of measuring spectra of 5000 objects simultaneously on the 4m Mayall telescope; and (ii) LSST, a 3 Gpixel camera on a new 8m-class telescope in Chile, enabling an extreme wide-field imaging survey to 27th magnitude in six filters. DESI will perform a redshift survey of 20-30 million galaxies and quasars to $z \sim 3$ to measure the expansion history of the Universe using baryon acoustic oscillations and the growth rate of structure using redshift-space distortions [4]. Prominent among LSST's science goals are the study of dark energy/dark matter through gravitational lensing, galaxy and galaxy cluster correlations, and supernovae [5].

This white paper proposes a revolutionary post-DESI, post-LSST dark energy program based on intensity mapping of the redshifted 21 cm emission line from neutral hydrogen out to redshift $z \sim 6$ at radio frequencies. Proposed intensity mapping survey has the unique capability to quadruple the volume of the Universe surveyed by the optical programs (see Fig. 6), providing a percent-level measurement of the expansion history to $z \sim 6$ and thereby opening a window for new physics beyond the concordance ΛCDM model, as well as significantly improving precision on standard cosmological parameters. In addition, characterization of dark energy and new physics will be powerfully enhanced by multiple cross-correlations with optical surveys and cosmic microwave background measurements.

The rich dataset produced by such intensity mapping instrument will be simultaneously useful in exploring the time-domain physics of fast radio transients and pulsars, potentially in live "multi-messenger" coincidence with other observatories.

The core Dark Energy/Inflation science advances enabled by this program are the following[2]:

- Measure the expansion history of the universe in the pre-acceleration era at the same precision as at lower redshifts, providing an unexplored window for new physics.
- Observe, or constrain, the presence of inflationary relics in the primordial power spectrum, improving existing constraints by an order of magnitude.
- Observe, or constrain, primordial non-Gaussianity with unprecedented precision, improving constraints on several key numbers by an order of magnitude.

Detailed mapping of the enormous, and still largely unexplored, volume of space observable in the mid-redshift ($z \sim 2-6$) range will thus provide unprecedented information on fundamental questions of vacuum energy and early-universe physics. Radio surveys are unique in their sensitivity and efficiency over this redshift range.

The field of 21 cm intensity mapping is currently in its infancy. Intensity mapping experiments now underway, or proposed, fall into two main classes: those targeting the so-called "Epoch of Reionization" (EoR) at redshift $z \sim 7-20$, and those attempting to observe in the low-redshift range where dark energy begins to dominate the expansion rate around $z \sim 1$. In addition, there are currently operating and proposed large-aperture, high angular resolution radio telescopes targeting a range of redshifts with a limited field of view, appropriate for observations of individual astrophysical objects. The program proposed here will fill the redshift gap for intensity mapping experiments, overlap in survey area with precursor experiments, and take advantage of their progress in addressing the challenges of beam calibration, receiver stability, and foreground component separation. Early science results and operational practicalities from all of these programs will inform the design decisions for next-generation 21 cm surveys.

[1] Tremendous Radio Arrays, https://www.bnl.gov/tra2018/
[2] See Section 2 for quantitative forecasts.

In this document, we lay out a long-term program in three overall stages (see Table II). Stage I will consist of targeted R&D, finalizing and elaborating the science case and collaboration building, which we foresee as the main activities through the early 2020's. This time frame will also see first-generation dedicated intensity mapping experiments release their first datasets. This work will enable Stage II, the construction and operation of a new, US-led, dedicated, radio facility to accomplish the science mission centered on 21 cm intensity mapping in the $z \sim 2 - 6$ range, starting in the mid-2020's and running through the early 2030's. The promises and challenges of this Stage II experiment are the main subject of this paper (see Sections 2 and 3). We designate Stage III to refer to an aspirational but currently speculative program of extending 21 cm intensity mapping to the pre-stellar "Dark Ages" at $z \gtrsim 30$, which could begin in the 2030s; see Section 4.2 for discussion and physics promise.

A new approach to achieving these science goals is now possible thanks to the explosive growth of wireless communications technology enabled by mass-produced digital RF microelectronics and software-defined radio techniques. It is safe to assume that these electronic components will continue to decline in price over the years leading to a construction project. We argue that radio offers the most practical and cost-effective platform for a highly-scaled next-generation survey instrument.

Expertise within the DOE Office of High Energy Physics (OHEP) network can be leveraged to address the needs of the radio frequency intensity mapping program. The principal reasons why this program naturally belongs to the DOE network are not only that the science goals address topics that are traditionally in the cosmic frontier of the DOE OHEP, but also that the difficulty in these measurements calls for an approach involving a single large collaboration tightly integrating experimental design, construction, analysis and simulation. This way of operating has been a traditional strength of the DOE program. There are also concrete synergies at the level of existing expertise within DOE, namely: RF analog and digital techniques for accelerator control and diagnostics; comprehensive detector calibration methodology; high-throughput, high-capacity data acquisition; and large-scale computing for simulations and data analysis. These are coupled with management-side capabilities, including facility operations (with partner agencies) and management of large-scale detector construction projects.

From the standpoint of both physics return and engineering feasibility, we believe that a strong case can be made for including a large scale 21 cm intensity mapping experiment in the DOE's Cosmic Frontier program in the late 2020's timeframe.

1. INTRODUCTION

1.1. Overview and Scientific Promise

The 2014 Particle Physics Project Prioritization Panel (P5) report “Building for Discovery” contained five goals, of which three are amenable to study through cosmological probes. These three are: i) pursue the physics associated with neutrino mass; ii) identify the new physics of dark matter; and iii) understand cosmic acceleration: dark energy and inflation. New knowledge in cosmology that will help us address these topics is acquired by mapping and studying ever increasing volumes of the Universe with improved precision and systematics control. No cosmological theory can predict the locations of individual galaxies or cosmic voids, but such theories can predict the statistical properties of the observed fields, such as correlation functions and their evolution with redshift. Studying fluctuations in the gravitational potential and associated density contrast across space and time thus forms the bedrock of cosmological analysis. Since cosmological constraints are inherently statistical, measurements over increased cosmological volume will lead to tighter bounds. Galaxy surveys at optical wavelengths have been exploring large scale structure (LSS) over increasingly large volumes and are a mature and well tested-technique. However, to keep increasing the maximum redshift and thus measure ever incerasing volumes of the Universe at the same rate, we need a different, higher through-put technique.

In this report we advocate a novel technique: 3D mapping of cosmic structure using the aggregate emission of many galaxies in the (redshifted) 21 cm line of neutral hydrogen as a tracer of the overall matter field. Although currently less mature than optical techniques, we will argue that the coming decade is an ideal time to make large 21 cm surveys a reality. Such surveys will allow us to probe to higher redshifts with higher effective source number densities for a smaller investment. They scale better in cost by relying on Moore’s law in a way that optical surveys cannot. However, these methods need to be developed and validated, and this document aims to set the roadmap for this research.

In the field of low-redshift 21 cm cosmology, one attempts to measure the fluctuations in the number density of galaxies across space [6]. Galaxies typically emit at many wavelengths: their optical emission is mostly integrated starlight, while their emission at low RF frequencies is in synchrotron radiation and also the 21 cm line of neutral hydrogen. This emission comes from the (hyperfine) transition of electrons from the triplet to the singlet spin state; the narrow width of the resulting 21.11 cm line, along with its isolation from other features, allows it to be readily and unambiguously identified in the galaxy’s radio spectrum. Detection of this line in a galaxy spectrum then allows the galaxy’s redshift to be determined with an error that is negligible for any standard cosmological analysis.

Overview: Stage II 21cm intensity mapping survey

- Large-volume cosmological survey optimized for BAO and bispectrum science, covering half the sky at $z = 2 - 6$.
- Main science goals:
  - Expansion history and physics of dark energy in pre-acceleration era
  - Inflationary features in primordial power spectrum
  - Non-Gaussianity of primordial power spectrum
- Reference design:
  - Compact array of 256×256 dishes of 6m diameter, using FFT correlation and redundant calibration.
  - Room-temperature dual-polarization receivers, covering $200 - 500$ MHz.
- 5 years on-sky time, targeted at project start ~ 2025

In the intensity mapping technique, the intention is not to resolve individual galaxies. Instead, one designs radio interferometers with angular resolution limited to scales relevant for studying the large-scale structure traced by those galaxies. In each 3D resolution element (voxel), given by the coarse angular pixel and considerably finer frequency resolution, emission from many galaxies is averaged to boost the signal-to-noise. Even without resolving individual objects, we can still trace the fluctuations in their number density across space and redshift on sufficiently large scales. This allows us to put the experimental signal-to-noise where it really matters for cosmology: on large spatial scales, where our theoretical modeling is most robust.

All neutral hydrogen in the universe below redshift of $z \sim 150$ is in principle amenable to 21 cm observations. This includes the large volumes at $z \gtrsim 30$, the so-called “Dark Ages” before the first luminous objects were created; at $6 \lesssim z \lesssim 30$, when these first objects formed and reionized the universe; and at $2 \lesssim z \lesssim 6$, after reionization but difficult to fully map with large optical surveys. (See Figure 1 for a visual comparison of the volumes accessible to different kinds of observations and in different epochs of cosmic history.) In the Dark Ages and post-reionization era, the 21 cm signal is a theoretically well-understood tracer of cosmic structure, and any science amenable to study through statistics of cosmic fields can be studied using this technique. However, the Dark Ages pose a formidable challenge (to say the least), for several reasons related to the low frequencies at which the associated observations must take place. Thus, we have identified the post-reionization era at $2 \lesssim z \lesssim 6$ as the most natural target for a dedicated next-generation 21 cm instrument, although we will briefly discuss the high-redshift promise in Section 4.

In this white paper, we have not attempted to optimize the many design choices that must go into such an instrument. Rather, we have chosen a configuration that, while somewhat ambitious, is expected to comfortably fit within the cost profile of a typical DOE OHEP project, and performed a first round of forecasts for the scientific capabilities of this configuration. This exercise has allowed us to identify a trio of key science results that could be obtained by an instrument broadly in line with our chosen specifications, and also to explore a range of other applications of such an instrument.

The remainder of this introduction is as follows:

- In Section 1.2, we summarize the three key science results, and a set of ancillary capabilities, associated with our fiducial instrument, which we have dubbed a "Stage II" 21 cm experiment.
- In Section 1.3, we briefly introduce the basic mode of operation of radio telescopes in order to set the context.
- In Section 1.4, we review the landscape of operational or planned post-reionization 21 cm surveys, and place a Stage II experiment in that context.
- In Section 1.5, we introduce and discuss the practical challenges of implementing a Stage II 21 cm experiment.
- Finally, in Section 1.6, we lay out a provisional roadmap for a three-stage 21 cm program, building from "Stage I" (current experiments) through Stage II and beyond.
- In Section 1.7, we describe the synergies between optical surveys and 21 cm experiments and unique advantages of each.

The main text of the paper is devoted to more detailed discussions of the various science cases (Section 2), the challenges and opportunities associated with Stage II (Section 3), and a brief foray into observations 21-cm beyond redshift of $z = 6$ (Section 4), with a discussion of current epoch of reionization experiments (Section 4.1) followed by a discussion of the exciting potential of the Dark Ages a probe of cosmology (Section 4.2). We conclude in Section 5.

1.2. Science capabilities of a large-scale 21 cm experiment

The starting point for a Stage II concept was the realization that the same instrument could help achieve three high-impact science objectives that are deeply connected to some of the biggest problems in fundamental physics. These are:

> **A1. Characterize the expansion history in the pre-acceleration era to the same precision as low-redshift measurements.** The precision of expansion history measurements in the low-redshift era using the BAO technique (see Section 2.3 for a technical description) is close to its theoretical limit due to the finite amount of large-scale information available per redshift. However, the measurement landscape deteriorates very fast for $z \gtrsim 2$, and will not be satisfactory in this range for the foreseeable future. It is imperative to measure the expansion history to better than percent level all the way to $z = 6$, which allows measurement of the energy density in the *dark energy component* with the precision of 10% at those redshifts. In the pre-acceleration era, this is a very difficult measurement, because the total energy density and thus expansion history of the Universe is dominated by the matter density. Consequently, signatures of dark energy are expected to be small in a minimal ΛCDM Universe. There is, however, strong theoretical motivation to explore this particular era, since theoretical explanations for the minimal ΛCDM Universe generally suffer from extreme fine-tuning issues. Alternative explanations to ΛCDM have generic signatures in the $2 \lesssim z \lesssim 6$ range, and percent-level expansion measurements within this range will impose stringent constraints on such theoretical models, which are otherwise unconstrained.

> **A2. Constrain or measure inflationary relics in the shape of features present in the primordial power spectrum.** Sufficiently sharp features in the primordial power spectrum survive mild non-linear evolution and biasing and are predicted in various inflationary models. The amplitude, frequency and phase of the feature are all indicative of the mechanism that sourced the initial seeds of structure and if found would present a breakthrough discovery and unique opportunity in an attempt to understand the physics of the early Universe. It would be highly informative to constrain or detect the presence of oscillatory features with frequencies $\omega_w > 50$Mpc at better than 10^{-3} amplitude relative to inflationary power-law spectrum and improving significantly in a more foreground optimistic scenario.

> **A3. Constrain or measure the equilateral and orthogonal bispectrum of large-scale structure with unprecedented precision.** Primordial non-Gaussianities are generically predicted by non-minimal inflationary models of the early Universe. The size and shape of primordial non-Gaussianities would be indicative of the number of fields present as well as the strength of interactions and self-interactions of the field or multiple fields driving inflation. The huge amount of clean, large-scale statistics from the volume accessible to a high-redshift survey presents a unique opportunity to put unprecedented constraints on non-Gaussianities that are sensitive to the dynamics during inflation. Specifically, the three-

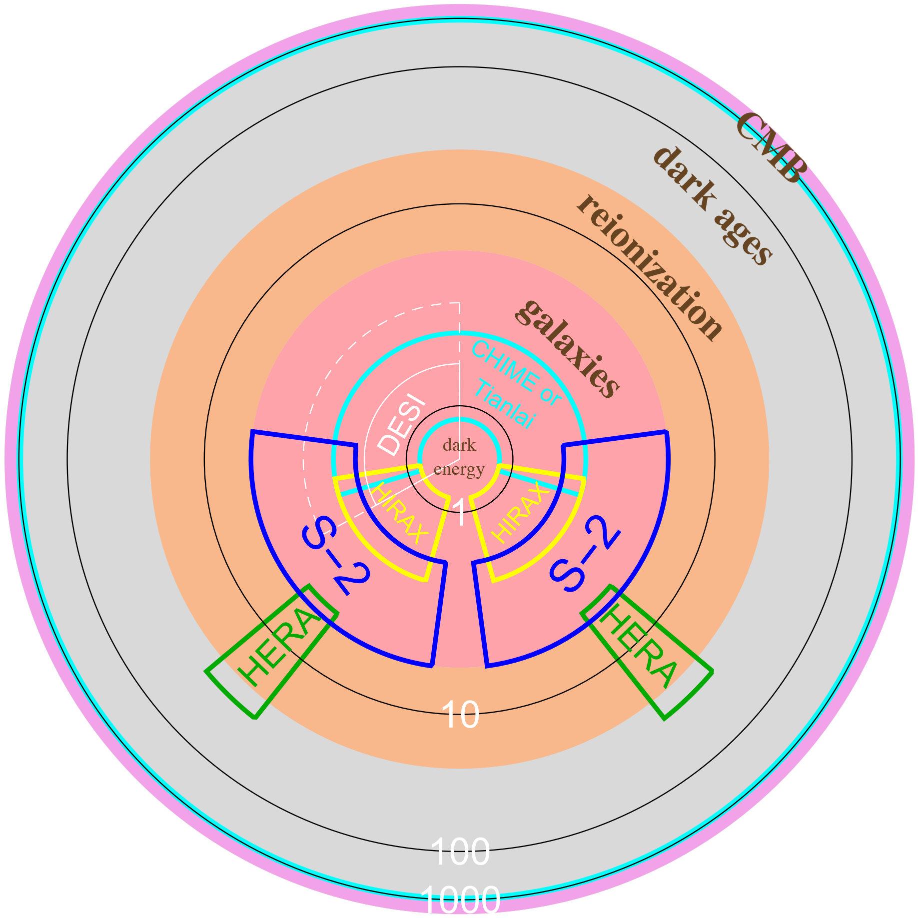

FIG. 1. Plotted is a schematic 2D representation of the observable universe where the *area* is proportional to the *comoving volume* and the distance from center monotonically increases with distance from Earth. Different epochs are color coded: the epoch of galaxies ($z < 6$) pink; the epoch of reionization ($6 < z < 20$) orange; the dark ages ($20 < z < 700$) gray; the epoch of the last scattering ($700 < z < 1300$) cyan; and the early universe ($z > 1300$) purple. The volumes surveyed by various current experiments with dense redshift space sampling are outlined, including the DESI optical spectroscopic survey of galaxies (white) and quasars (white dashed); HI intensity mapping surveys of the intergalactic medium during the epoch of reionization (HERA; green) and lower-redshift galaxies (CHIME/Tianlai; cyan); HIRAX (yellow); and the 21 cm Stage II project proposed here (blue). The wedge sizes give rough representations of the covered volume.

> point correlation function of Fourier modes of the density field (the so-called bispectrum) is amenable to measurement using high-redshift LSS surveys, and its amplitude in different configurations (corresponding to the three points forming squeezed, equilateral, or folded triangles) is directly connected to different inflationary models. Moreover, these types of non-Gaussianities (equilateral and orthogonal) cannot be constrained using bias constraints in the power spectrum and are therefore not amenable through cosmic variance cancellation techniques that are forecasted to put stringent constraints on squeezed non-Gaussianities. In other words, a high-redshift survey of the universe will most likely present the only viable opportunity to improve over CMB constraints.

All three objectives described above could be achieved with a next-generation 21 cm experiment, which we designate a Stage II experiment. Our fiducial configuration consists of a close-packed 256×256 array of 6 m dishes, operating from 200 to 500 MHz. This configuration is an ambitious but realizable expansion over the current generation 21 cm experiments. Section 2.1 contains a technical arguments motivating this particular choice of fiducial experimental parameters. The precise configuration of the array and other experimental details are expected to evolve and be further developed depending on key science targets and experience obtained with predecessors of a Stage II 21 cm experiment. However, having an explicit experiment allows us to make concrete forecasts that set the context for further optimization.

The objectives outlined above directly follow from the ability of 21 cm emission to obtain a pristine picture of large-scale structure with essentially no tracer shot-noise. In the following, we list some of the other new capabilities that will be enabled by a Stage II experiment:

B1. **Quadruple the observed volume at an increased fidelity.** The volume between $z = 2$ and $z = 6$ is approximately three times the volume between $z = 0$ and $z = 2$, and contains structures whose clustering statistics are easier to predict than at lower redshifts (see Figure 6). 21 cm intensity mapping can probe this volume with a very high effective number of sources, allowing for straightforward extraction of cosmological information from these measurements. While we have identified several well-motivated uses of the large number of linear modes present in this volume as our main scientific goals, other, yet to be discovered, statistical quantities describing and constraining fundamental physics are also likely to improve equally due to generic $\sqrt{N}$ scaling of error on any derived statistical quantity.

B2. **Constrain models of modified gravity.** When combined with additional observations, the 21 cm data will also provide measurements of the growth of fluctuations in the universe at high redshifts. Such measurements can, in principle, distinguish between dynamical dark energy and modified gravity.

B3. **Measure information from scales and redshifts not directly present in the survey.** Couplings between different Fourier modes of the cosmic density field will allow us to reconstruct modes that are not directly present in the survey through their effects on the observed small-scale modes. In particular, the tidal effect of large-scale modes on the small-scale power will give access to the large-scale modes (which may otherwise be obscured by foregrounds in certain scenarios). Furthermore, gravitational lensing effects on small scales will provide information about lower-redshift structure. Three-dimensional 21 cm observations will provide several source "screens" for lensing analyses; the signal to noise of a joint analysis of all such screens will exceed that for the next generation CMB lensing reconstruction in cross-correlation.

B4. **Improve measurements of parameters that encode deviations from the minimal cosmological model, including neutrino mass, radiation content of the early universe, and curvature.** 21 cm observations can, in conjunction with other synergistic measurements, aid in constraining these parameters. In particular, we should achieve an independent detection of neutrino mass and constrain the radiation content to within a factor of few of the guaranteed correction due to electron-positron annihilation.

B5. **Potentially directly detect the expansion of the Universe.** The Universe expands at the Hubble rate and in principle this expansion can be detected by observing sources drift in redshift over the time of experiment. The advantage of radio observations is that the clocks stable enough to drive the digitization circuits at the required time stability are nearly off-the-shelf equipment.

B6. **Explore the physics of fast radio bursts (FRBs).** This instrument will also likely detect millions of FRBs as we discuss in Section 2.12. The physics of FRBs is currently poorly understood, but in some models they could act as standard candles or alternatively their dispersion measure in conjunction with kinetic Sunyaev-Zeldovich effect measurements from CMB could open another possible window into the expansion and growth history of the universe.

B7. **Explore modified gravity using pulsars.** The same instrument that can be used for cosmology will also be able to observe numerous pulsars and study general relativity through precision changes in pulsar timings.

Using our fiducial Stage II 21 cm configuration, we will perform a detailed exploration of all possible science targets identified above in Section 2.

1.3. Observing the universe with a radio telescope

Radio telescopes observe the electromagnetic radiation at radio frequencies and for 21 cm this means at frequencies below 1.42GHz. A traditional single-dish radio telescope contains a focusing element, typically a parabola that focuses the incoming radiation onto a radio receiving element. Such parabola coherently adds all radio waves coming from a given direction. Such a telescope can observe a single pixel in the sky at once and the bigger the parabola, the higher is its resolution, with the sky response function scaling as roughly λ/D, where $\lambda = \lambda_0(1+z)$ is the observing wavelength (redshifted from rest-frame λ_0) and D is the parabola size. Because radio wavelengths are very long (compared to typical optical wavelengths, for example), the size of the reflector needs to be very large to achieve a fine resolution.

In Figure 2 we schematically show the signal observed by one such single-receiver pointed at a typical direction on the sky (and assuming it could observe signal from 200MHz to 1420Mhz). The signal would be dominated by the emission from our own galaxy – shown as the red line. This emission is very strong, but at the same time very smooth, which gives us a handle at subtracting it. The blue lines illustrates what the 21-cm signal would look like: at low redshift it would correspond to individual over-densities traced by small objects, while at high redshift the structure in the radial directions blurs into a continuous field.

It has long been recognized, that instead of combining the signals by optically adding them, one can add them electronically. This concept, known as aperture synthesis (for which the Nobel prize was awarded in 1974 to Martin Ryle) led to a class of instruments called radio interferometers. In such telescopes, the collecting area of a single dish is replaced with several individual smaller elements, that do not need to be, but are are often smaller dishes themselves. Signals form individual receivers are combined and allow one to synthesize an effective dish whose total collecting area is the sum of individual collecting areas and whose resolution matches that of a dish with the same size as the largest separation between individual elements. But the most

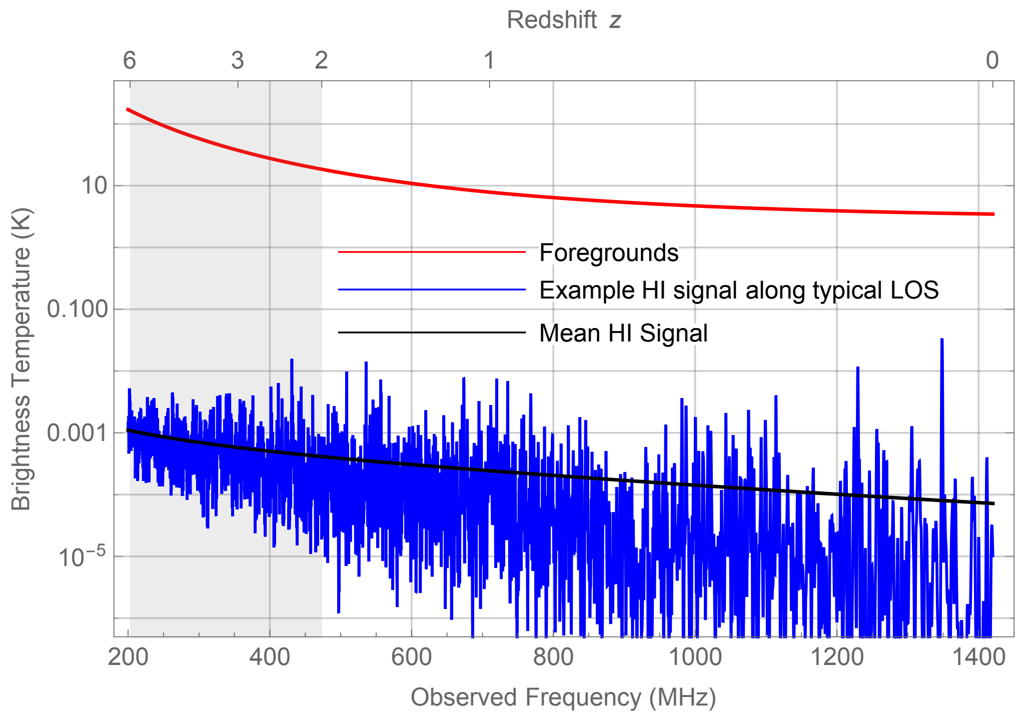

FIG. 2. Illustration of 21cm emission spectra, showing observed brightness temperature as a function of observed frequency and source redshift. *Red:* Average emission from galactic foreground sources (see Equation D1) varying between a brightness of a few K to a few hundred K. *Black:* Mean signal from cosmological HI, following Eq. B1, smaller by about five orders of magnitude; *Blue:* Example realization of the HI signal that would be seen with one beam along a typical line of sight. At low redshifts the matter signal is dominated by a few peaks, indicating the growth of structure; while at earlier times the fluctuations around the mean are smoother. The grey band highlights the redshift range z=2–6.

important advantage is that multiple beams can be synthesized concurrently which can cover all of the primary field of view of individual elements. This can lead to an exponential increase in sensitivity compared to traditional single-element dishes.

In order to perform aperture synthesis, the signal from every pair of elements needs to be correlated and hence the difficulty increases as the square of the number of individual elements forming an interferometer. Therefore, traditional interferometers employed at most a few tens of elements. In the 21^{st} century, however, digital technology allows the possibility of doing the signal combination digitally, leading to telescopes made of thousands of receiving elements. This progression in technology moved the complexity first from the problems of mechanical engineering in making large receiver dishes to that of building and replicating analogue electronics and finally to processing massive amounts of digital data. As we will see later, part of this white-paper continues this trend by arguing for digitization as soon as possible after the signal enters the system.

1.4. Post-reionization 21 cm surveys: the state of the art

21 cm cosmology has only been made possible recently through developments in infrastructure (e.g. high-throughput computing and commodification of low noise radio-frequency technology) that allow for correlations at full bandwidth at the necessary scale. Tools and techniques have been developing rapidly, and the first steps towards extracting cosmological information from 21 cm observations have already been demonstrated.

The first detection of the redshifted 21 cm emission in the intensity mapping regime was achieved by Chang et al. in 2010 [7]. The measured 3D field, obtained from the Green Bank Telescope (GBT) 800 MHz receiver, spans the redshift range of $z = 0.53$ to 1.12 and overlaps with 10,000 galaxies in the DEEP2 survey [8] in spatial and redshift distributions. This enabled a cross-correlation measurement on $9h^{-1}$ Mpc scales at a 4σ significance level. This detection was the first verification that the 21 cm intensity field at $z \sim 1$ traces the distribution of optical galaxies, which are themselves known tracers of the underlying matter distribution. It presents an important proof of concept for the intensity mapping technique as a viable tool for studies of large-scale structure.

A continuing observing campaign to expand the GBT 21 cm IM survey in both sensitivity and spatial coverage has yielded two subsequent publications: an updated cross-power spectrum at $z \sim 0.8$ [9] between 21 cm and optical galaxies in the

Name	Optimized	Steerable	Type	Elements	Redshift	First light
Existing w data:						
GBT	N	Y	Single Dish	1 dual-pol on 100 m dish	$\sim$0.8	2009
Dedicated experiments:						
CHIME	Y	N	Cylinder Interferometer	1024 dual-pol over 4 cyl	0.75 – 2.5	2017
HIRAX	Y	limited	Dish Interferometer	1024 dual-pol $\times$ 6 m dishes	0.75 – 2	2020
TianLai Dish	Y	Y	Dish Interferometer	16 dual-pol $\times$ 6 m dishes	0 – 1.5	2016
TianLai Cylinder	Y	N	Cylinder Interferometer	96 dual-pol over 3 cyl	0 – 1.5	2016
OWFA	N	Y	Cylinder Interferometer	264 single-pol	$\sim$ 3.4$\pm$0.3	2019
BINGO	Y	N	Single Dish	$\sim$60 dual-pol sharing $\sim$50 m dish	0.12 – 0.45	2020
Dedicated R&D:						
BMX	Y	N	S. Dish + Interferometer	4 dual-pol $\times$4 m off-axis dishes	0 – 0.3	2017
NCLE	Y	N	Satellite	3$\times$5 m monopole ant. at Earth-Moon L_2	$>$ 17	2018
PAON-4	Y	limited	Dish Interferometer	4 dual-pol $\times$5 m dishes	0 – 0.14	2015
Non-dedicated:						
MeerKAT	N	Y	Single-Dish	64 dual-pol $\times$ 13.5 m dishes	0 – 1.4	2016
SKA-MID	N	Y	Single-Dish	$\sim$ 200 dual-pol $\times$ 15 m dishes	0 – 3	2023
Proposed Here:						
Stage II	Y	limited	Dish Interferometer	65,536 dual-pol $\times$ 6 m dishes	2 – 6	$<$2030

TABLE I. List of current and planned experiments. The "First light" column refers to first light for 21 cm observations for non-dedicated experiments. In the "Optimized" column, we note whether the telescope has been designed with intensity mapping as its primary scientific goal. The HIRAX and PAON-4 dishes can only be steered by manual human intervention. For MeerKAT and SKA-MID, dishes will likely be used in a single-dish mode, with interferometric capability used only for gain calibration.

WiggleZ survey [10], and an upper limit on the 21 cm auto-power spectrum [11]. Combining the cross- and auto-power spectrum measurements yields a $\sim$3-σ measurement on the combination of the cosmic HI abundance $\Omega_{\rm HI}$ and bias $b_{\rm HI}$ parameters, $\Omega_{\rm HI} b_{\rm HI} = 0.62^{+0.23}_{-0.15} \times 10^{-3}$ [11]. Further analysis of 800 hours of GBT observations taken during 2010-2015 is currently ongoing.

No experiment has detected the 21 cm power spectrum in auto-correlation. While this should be possible with non-dedicated experiments in terms of statistical significance, the instrumental challenges are currently too large. However, this situation should change with the advent of dedicated instruments.

There are currently five main experiments that are presently being built or are in the commissioning phase to measure LSS with the 21 cm intensity mapping technique with dedicated instrumentation: CHIME in Canada, HIRAX in South Africa, Tianlai in China, OWFA in India, and BINGO, a UK/Brazil experiment. In addition, there are several smaller efforts dedicated to R&D, such as BMX at Brookhaven National Laboratory and PAON at Nançay in France. We list the main properties of these instruments in Table I. These small-scale experiments will teach us about the viability of the intensity mapping technique, for example by providing testbeds for calibration, foreground removal, and RFI mitigation techniques.

Of the listed experiments, CHIME is currently the most advanced, and has recently upgraded from a prototype to the full instrument. It consists of 4 cylindrical radio antennas with no moving parts, observing the entire accessible sky which passes above it as the Earth rotates. It operates from 400-800 MHz, equivalent to mapping LSS between redshift $z = 0.75$ to 2.5. We expect the first cosmology results from CHIME in the next 3 years, which should include foreground removal or mitigation techniques for intensity mapping measurements of LSS in 21 cm emission. Note that CHIME has already shown promise related to one of its other science goals, having recently announced the first detection of a low-frequency fast radio burst [12].

Another experiment often mentioned in this context is the SKA[3] (Square Kilometre Array). The SKA1-MID mid-frequency dish array is a formidable instrument, but is optimized for a variety of radio astronomy goals other than intensity mapping. In many aspects the comparison is similar to new generation of extremely sensitive optical telescopes that have mirror-sizes exceeding 30m, but are nevertheless not competitive for survey-science optical cosmology due their small field of view and focus on diffraction-limited imaging of individual objects. For intensity mapping, SKA1-MID suffers from a similar mismatch in scales to which it is sensitive compared to the proposed Stage II experiment. While it will typically act as an interferometer with several hundred large dish elements, the baseline distribution best matches the scales relevant to imaging of individual objects rather than intensity mapping of large-scale structure. As a workaround, the SKA1-MID array will instead be used

[3] https://www.skatelescope.org/

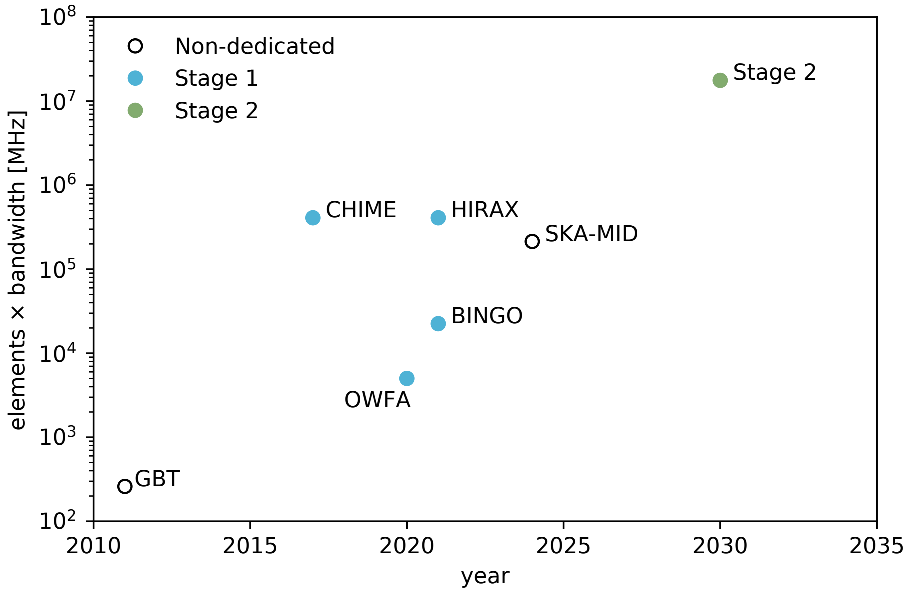

FIG. 3. Representation of improvements from current-generation to future proposed experiments in a figure of merit analogous to optical etendue measure: number of receiving elements × bandwidth. See text for discussion.

as a collection of single dishes for intensity mapping, perhaps using interferometry only as a calibration tool. This will have relatively poor angular resolution at $z \gtrsim 1$ however, leaving it sensitive mostly to only the radial BAO feature [13]. Additionally, individual elements of SKA1-MID are highly capable fully-steerable dishes that can operate up to 14 GHz. Dedicated designs for 21 cm intensity mapping survey science typically use transiting arrays instead, since one wants to maximize the sky coverage rather than point at objects of interest, and reduce mechanical costs; 21 cm intensity mapping also requires considerably lower maximum frequencies and corresponding dish-surface accuracy requirements (i.e. 500 MHz for our Stage II experiment and never higher than the frequency of $z = 0$ neutral hydrogen at 1420 MHz). It is clear that the SKA1-MID instrument has been optimized for different science goals and has therefore embarked on a different set of trade-offs to an optimal 21 cm experiment. As such, it will not be directly competitive with dedicated instruments for many of the science cases discussed in this document, and thus does not present an obstacle to DOE for entry into this field. The same is true for the SKA1-LOW instrument, which partially overlaps in frequency coverage with our proposed Stage II experiment (i.e. at the high redshift end of our band), but has a greater focus on Cosmic Dawn and Epoch of Reionization science, and will not be competitive with Stage II for BAO measurements for example (see [14] for cosmological forecasts for SKA1-MID and SKA1-LOW surveys). Nevertheless, as the largest and most complex radio astronomical facility to be constructed in advance of Stage II, we expect SKA to offer a number of valuable lessons in terms of calibration and data analysis techniques, computing infrastructure, and data management.

In Figure 3, we plot the same information as Table I, but compressed into in a figure of merit analogous to optical etendue measure:

$$\mathrm{FoM} = \text{number of receiving elements} \times \text{bandwidth} \,. \tag{1}$$

This equation is motivated by the expression for the system temperature contribution to noise (see Eq. D2 in Appendix D) and it is necessarily a very crude simplification. Most importantly, it does not take into account the surface area of reflector material and would naturally drive you towards a field of dipole antennas at fixed cost. While this might be the right answer in the absence of systematic effects, the current consensus is that some directionality of individual elements is desirable. Moreover, a compact interferometric array with the same figure of merit will in general perform better than a traditional radio array with the same figure of merit for the science discussed in this paper. Finally, observing at different central frequency affects the result in a non-trivial way: the sky noise is lower at higher frequencies, but the volume per unit bandwidth is larger at lower frequencies and the Universe is more linear at higher redshifts.

Nevertheless, with these caveats in mind, the figure of merit in Eq. (1) is a rough proxy of instrument capability and Figure 3 shows the improvement with time of the current and proposed experiments. To visually demonstrate the capability of a Stage II experiment, we refer reader to Figures 4 and 5. These figures display how the proposed instrument would faithfully measure the structures in the Universe up to very high redshifts at the large scales relevant to cosmological analysis.

We again iterate that this section was focused on the post-reionization experiments. There is a vibrant community of epoch of reionization 21 cm experiments and ideas for even higher redshift. These share many of the technical issues with the Stage II experiment even though the science is considerably different and are discussed in Section 4.

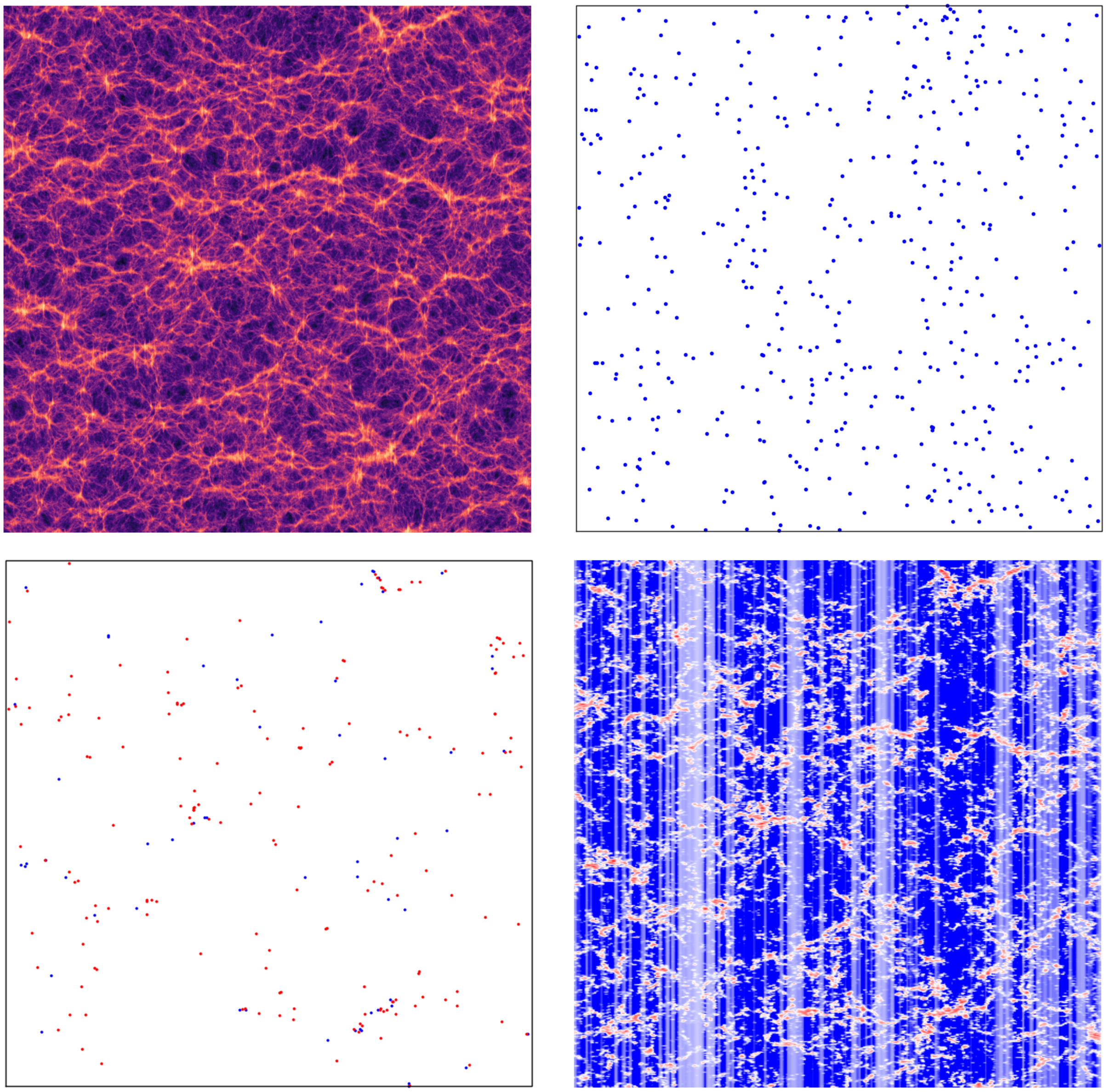

FIG. 4. This figure shows the same slice of the simulation at redshift $z = 3$ as "seen" by different probes. We show a $300 \times 300 \times 4\,h^{-1}$Mpc slab of an approximate simulation with horizontal direction corresponding to transverse direction and vertical direction to radial direction in redshift space. The upper left plot shows the underlying dark matter density. The upper right plot shows the LSST sources, where structure is erased due to photometric redshift errors. The lower left shows a putative drop-out spectroscopic survey selecting $m_{\rm UV} < 24.5$ (blue and red dots) and those going to just $m_{\rm UV} < 24$ (blue dots). The lower right plot shows a raw image from a Stage II-like instrument. The vertical striping is due to foreground removal and there is a visible smoothing in the transverse direction. The plot uses logarithmic scaling with a non-linear color scale to make features more visible. See Appendix E for discussion of assumptions that went into making of this figure and Figure 5.

1.5. Practical challenges

There are several known issues for achieving 21 cm cosmology goals compared to traditional galaxy surveys. These call for a coherent development plan that will allow this technique to reach its full potential. We stress that the challenges are in the instrument and not fundamental to the signal: with sufficient care, we can build a calibrated system that will be dominated by statistical rather than systematic errors. These complications and our suggested mitigation for a successful survey are:

- **Loss of small-$k_\parallel$ modes**. The foreground radiation is orders of magnitude brighter than the signal, but spectrally smooth (see Figure 2 for a schematic illustration). Thus, the signal can be isolated but only for modes whose frequency along

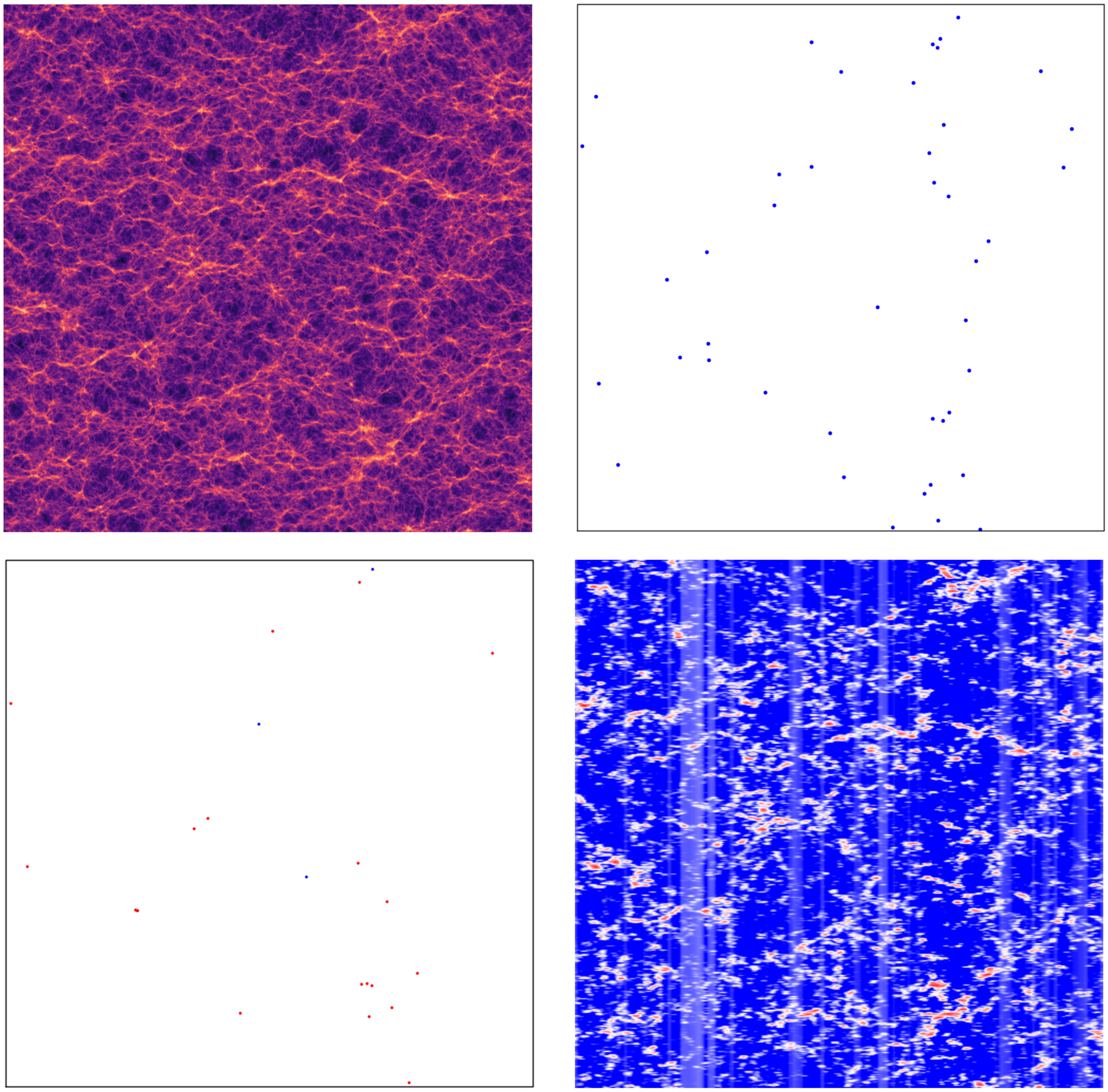

FIG. 5. Same as Figure 4 but at $z = 5$. Compared to lower redshift, the number of sources tracing the structure decreases further to become completely shot-noise dominated. The transverse smoothing for the Stage II experiment becomes more pronounced, but it nevertheless captures the richness of the underlying dark matter structures.

the line of sight ($k_\parallel$) is sufficiently large. As a consequence, the low-$k_\parallel$ modes are lost and this precludes direct cross-correlation with tomographic tracers such as weak lensing. However, as we discuss, these modes can be reconstructed from their coupling to the measurable small-scale modes, with non-trivial precision for a sufficiently aggressive system.

- **The foreground wedge**. Interferometers are naturally chromatic instruments, since their fringe patterns—and therefore the cosmological lengthscales that they probe—are dependent on frequency. This can cause extra spectral features to be imprinted on the (in principle) spectrally smooth foregrounds. For a power spectrum measurement, this results in a set of Fourier modes on the $k_\perp$-$k_\parallel$ plane ("the foreground wedge") that are heavily contaminated by foregrounds. This problem becomes more important at higher redshift and is acute for epoch of reionization experiments. We note that there is nothing fundamental about this problem: the mathematics behind the wedge are well-understood [15, 16], and thus an appropriate analysis pipeline applied to a well-calibrated system with sufficient baseline coverage can in principle perfectly separate the foregrounds from the signal even inside the wedge [17, 18]. The problem is therefore primarily a technical challenge rather than a fundamental limitation. We discuss our modeling of, and assumptions about, the foreground wedge in Appendix C.

Roadmap	**Stage 1** Post-Reionization Pathfinder ($0 < z < 2$)	**Stage 2** Post-Reionization Experiment ($2 < z < 6$)	**Stage 3** Dark Ages Experiment ($30 < z < 150$)	**Context**
2018 – 2020	**Decadal Survey submission.** Community building.			LSST/DESI ongoing. S1 results (CHIME).
2020 – 2025	Diverse R&D based on test-beds and simulated data. Participate in Stage 1 Pathfinder experiments.	Collaboration forming. CD0/1.		LSST/DESI ongoing. S1 results (HIRAX, Tianlai). **P5 submission + results.** **Decadal Survey results.**
2025 – 2030	Firm science case. Optimize S2 experiment design.	Start phased construction. Early data acquisition.		LSST/DESI ending. SKA1 results expected.
2030 – 2035		Finish phased construction. Main data acquisition.	Feasibility study. Preliminary design.	SKA2 comes online. NASA LSSM launches.
2035 – 2040		**Final analysis and results.**	Construction.	?
2040 –			Data acquisition. **Analysis and results.**	?

TABLE II. Notional roadmap of the proposed 21 cm cosmology program.

- **The mean signal is not measured.** Because the mean signal is not measured, the redshift-space distortions are related to the growth parameter $f\sigma_8$ via an unknown constant. Therefore, in absence of additional information, 21 cm observations cannot use the redshift-space distortions as a direct probe of growth. However, there are several ways around this problem as we discuss later in the text. Most promising is to use cross-correlations or directly quantify the mean signal from a statistical sample of hydrogen systems (damped Lyman-α [DLA] and high column-density [HCD] systems) in the Lyman-α forest.

These issues need to be studied in detail, both in theoretical terms and through a vigorous experimental program. We argue that major US agencies should support this research program in order to allow truly competitive experiments to become reality in the coming decades.

1.6. Roadmap

This white paper argues for a long-term development of the 21 cm cosmology program in the USA, led by the Department of Energy but working in conjuction with other agencies where shared science warrants cooperation. In particular, a similar model to that of LSST is envisioned, in which DOE takes up particular aspects of the development which are well matched to its expertise and a collaborating agency takes over some of the other aspects that might not be an optimal fit for the DOE. To this end, we argue for a staged approach that includes three nominal steps leading to a Dark Ages experiment, as outlined in Table II.

- Our first step in the roadmap is an era of vigorous research and development, probably in conjuction with a small-scale test-bed experiment. During this stage, the following should be accomplished:
  - **Refine the scientific reach of a Stage II experiment.** In Chapter 2 we start this process by describing some of the exciting science that is achievable using a straw man design. The design of the instrument should be driven by science and not the other way round, but in practice one needs to start with a given design to see the ballpark science achivable and then iterate until a convincing science-driven experiment design emerges. Our Chapter 2 is the first step in this direction.
  - **Advocate for support from major scientific commissions.** In particular, the 2020s *Astronomy and Astrophysics Decadal Survey* and the next P5 report will need to strongly endorse this technique to keep it a viable option.

  - **Resolve technical challenges.** There are numerous technical challenges, particularly in terms of calibration and data analysis. We suggest a two-pronged approach: first to benefit from the experience of current-generation experiments in mitigating these challenges, and second to support instrumentation development and theoretical progress using a combination of computer simulations, lab experiments, and small, dedicated pathfinder instruments. We describe this program in greater detail in Section 3.
  - **Optimize a Stage II instrument configuration.** Parameters like redshift range, number of elements and their optical designs, calibration schemes, etc. can crucially affect scientific outcome. We will refine and optimize the array parameters to both minimize the systematic effects and maximize possible science.
  - **Maintain flexibility in approach.** New exciting scientific developments obtained with optical surveys will be considered when designing the 21 cm array proposed here. For example, a sign of early dark energy might motivate a shift towards higher redshift, while evidence for a non–cosmological-constant equation of state parameter, $w \neq -1$, might favor lower redshift. Moreover, if fast radio bursts turn out to have useful cosmological applications, they might also affect various design choices. The most important point is that sufficient resources must be available at this stage to develop the technique and maximize its promise.

- The next step is a post DESI/LSST experiment, which we call a Stage II experiment in this document, becoming reality in the later part of the next decade. To reach interesting cosmological constraints, the experiment will have to be an order of magnitude larger than current experiments. In this document we consider a particular fiducial Stage II experiment operating at redshifts $z = 2 - 6$, whose parameters we discuss in Section 2.1. This is motivated by the intuition that this volume of the universe is least explored and might offer new low-hanging fruit. However, this particular aspect of the design, as any other, remains on the table to be changed and optimized as we learn more about the most compelling scientific targets.

- If successful, we expect this could be followed by a Dark Ages experiment. This is the most vaguely defined and forecasted instrument, and will require significant improvements and R&D, pushing its timeframe to two or three decades from now. To motivate an experiment probing the high redshift 21 cm signal, we discuss some of the unique science opportunities in Section 4.2. The most important aspect is that there exists a long-term scientific opportunity which could be built on top of the Stage II experiment.

1.7. Synergies with optical surveys

Optical galaxy surveys are now a mature observational tool, having gone from pioneering surveys of a few thousand galaxies, through definitive detections of cosmological clustering signals like baryon acoustic oscillations, to now routinely producing precision cosmological constraints. This successive, multi-generational development path continues, as next-generation experiments like DESI are poised to improve over current experiments by an order of magnitude in depth, and by pushing to significantly higher redshifts.

The 21 cm intensity mapping technique is much earlier along its development track, and must yet pass through a series of milestones before it can be considered truly competitive with optical surveys. We can already discern some of the main synergies with the optical surveys:

3D information. Optical galaxy surveys fall into two categories: either they survey a huge sample of galaxies at low redshift resolution (photometric) or survey a subset of selected galaxies at high redshift resolution (spectroscopic). However, in both cases we have additional information about galaxies: from photometric surveys the actual image of the galaxy can be used to infer not just galactic morphology, but also gravitational lensing and the detailed optical spectra can be used to infer physical properties of the galaxy, such as star formation. 21 cm surveys on the other hand provide an avenue that identifies galaxies and at the same time recovers their redshifts (in an aggregate sense) allowing an efficient mapping of the full 3D structure in our Universe. This inevitably loses some information that can be present in the full optical survey, but offers a complementary path towards a cost-effective survey at high redshift.

Shot noise vs sample selection. Any point tracer of large-scale structure suffers from the fact that we are sampling a continuous field using a finite number of objects. This Poisson component, also known as shot noise, acts as a source of noise in any statistics derived from the large-scale structure observable. To reduce shot noise, one needs to take spectra of more objects, but most often there simply are not enough objects up to a given flux, limiting the ability to mitigate shot noise. In 21 cm observations, we are measuring integrated intensity from all objects, even the very small and faint ones, and so the shot noise is lower by several orders of magnitude. In fact, all Stage I experiments will be limited by continuous sources of noise (sky noise and thermal amplifier noise) and only Stage II will start to be sensitive to the underlying shot noise. On the other hand, optical surveys allow one to slice the galaxy sample into individual sub-samples that can be selected to have certain properties. Together, both techniques offer complementary views of the same underlying structure.

Scaling with redshift. Optical measurements excel at lower redshifts, but they become increasingly difficult as the redshift range of surveys is pushed towards the more distant universe. First, observations must be performed in the infrared, where they suffer from brighter sky that has many more sky-lines which are also more variable than in the optical. Second, the infra-red detectors are more expensive and less efficient than optical charge-coupled devices (CCDs). Third, the objects themselves are fewer in number and fainter, since we are observing a younger universe. In radio, the primary limitation is from foreground emission; however, the same foreground removal techniques vetted by previous generations of 21 cm experiments can be applied because the foregrounds do not fundamentally change across the redshift range of interest. In addition, at higher redshifts, the same bandwidth covers more cosmic volume and requirements on things like reflector surface accuracy become less demanding. In short, for the $z < 1.5$ universe, optical surveys offer many advantages and offer an excellent tool for studying the universe down to the smallest scales, but radio techniques scale better towards higher redshift.

2. SCIENCE CASE FOR A POST-REIONIZATION 21 CM EXPERIMENT

This section focuses on preliminary science forecasts for a Stage II 21 cm experiment to demonstrate the potential science reach of such an instrument. A *Stage* II *experiment* refers to an experiment that will build upon the current, non-US, Stage I, pathfinder telescopes such as CHIME and HIRAX. We focus on redshifts after reionization ($z < 6$) that will be mostly unexplored by optical surveys. We design an array to probe these redshifts, based on what would be possible with current technology at a price-point that is consistent with a medium-size high-energy-physics experiment. In this Chapter we envision a realistic experiment that is "shovel-ready", assuming the technical challenges discussed in the next chapter are feasible and Stage I experiments do not uncover any unexpected significant issues.

We will describe the science potential that our proposed design could achieve, briefly in Section 2.1 and then in more detail in the following subsections. We conclude with a discussion of other relevant science. We emphasize that this design is intended as a first exploration of the capabilities of a large project of this type, so we have not attempted any detailed optimization. In later stages of the planning process the science goals and instrument parameters will be refined further with a proper flowdown study, likely motivating various modifications or improvements to the design choices we present here.

2.1. Science drivers and the straw man experiment

As outlined in the introduction, there are three main science drivers for the proposed experiments: measurement of the properties of dark energy in the preacceleration era (goal A1), constraints or detection of inflationary relics in the shapes of features present in the primordial power spectrum (goal A2) and constraints or detection of non-Gaussian correlations in the primordial power spectrum (goal A3).

Goals A2 and A3 are best served by an experiment that has access to a large number of linear or quasi-linear modes. Given a sufficient density of tracers, the total number of modes scales as $V k_{\rm max}^3$, where V is the survey volume and $k_{\rm max}$ is the maximum wavenumber amenable to theoretical predictions. Going to higher redshift helps both cases. First, there is more volume per unit redshift at higher redshifts: as indicated in the left panel of Figure 6, the total volume available over $2 < z < 6$ is roughly triple the volume at $z < 2$. The effect is even more pronounced if one considers the amount of cosmic volume per unit bandwidth of the radio signal. Second, at a given comoving wavenumber k, the field is more linear at higher redshift, leading to an increase of $k_{\rm max}$. This translates into a large increase in the number of usable linear modes at higher redshift, as shown in the right panel of Figure 6 (see App. A for the details of our definition of "linear modes."). Figure 7 confirms that even low order perturbation theory calculations can accurately describe the results of hydrodynamical simulations out to a sufficiently high wavenumber. Though it is not shown in Figure 7, the cross-correlation between the observed and initial fields also remains higher to smaller scales for the 21 cm field. Finally, the bias of the 21 cm field is less scale dependent, and easier to model, than a coeval population of galaxies because the neutral hydrogen traces lower mass halos (Figure 8). This effect becomes particularly pronounced at the highest redshifts.

By a fortunate coincidence, all three science drivers naturally lead to a $z = 2 - 6$ experiment. The upper limit is set by the requirement that the universe has reionized and thus astrophysics does not limit our modeling. The lower limit is set by the fact that much more than one octave of bandwidth is difficult to achieve in realistic radio receivers. We have identified a 256×256 array of 6-m dishes operating at 200-500 MHz as a straw man configuration that would achieve the three main scientific goals specified above. Such experiment is 64 times larger than the partly funded HIRAX experiment, currently under construction in South Africa, but the total bandwidth is only ~ 40 times larger and the expectation is that with falling cost and large-scale efficiencies the experiment would be only $\sim 10 - 20$ times more expensive thus falling very comfortably in a cost profile similar to that of LSST or DESI. The total collecting area of such experiment would be around 1.8 square kilometers. While this is more than SKA, we stress that the low frequencies and in particular the non-actuating nature of the transit arrays makes such a design orders of magnitude cheaper. We assumed a 5-year on-sky integration, requiring a somewhat longer total duration of experiment, but note that compared to optical experiments the achieved observing efficiency can be considerably larger since radio telescopes can often observe during the day and through cloudy weather.

In addition to the main science goals, such experiment would enable a wide range of other science, both in the field of cosmology and fundamental physics as well as in related astrophysical sciences that could be of interest to a broad community. In the rest of this chapter we study a subset of the most interesting science that would come from such an array, with a focus on the cosmological arena.

In our forecasting we assume the existence of the DESI and LSST experiments. When relevant we also discuss and compare with the CMB-S4 survey, but we note that its final design is less certain than that of DESI and LSST. In some sections, we impose additional 2% or 5% priors on cosmic neutral hydrogen abundance, as motivated by [19] or achievable using cross-correlation with other tracers. The results presented in this chapter were derived using several forecast codes. The common assumptions used to forecast main results can be found in Appendices B, C and D, but even when slightly different assumptions are used the results are typically consistent to around 20% in accuracy over the relevant scales. We regard this as sufficient at this early stage.

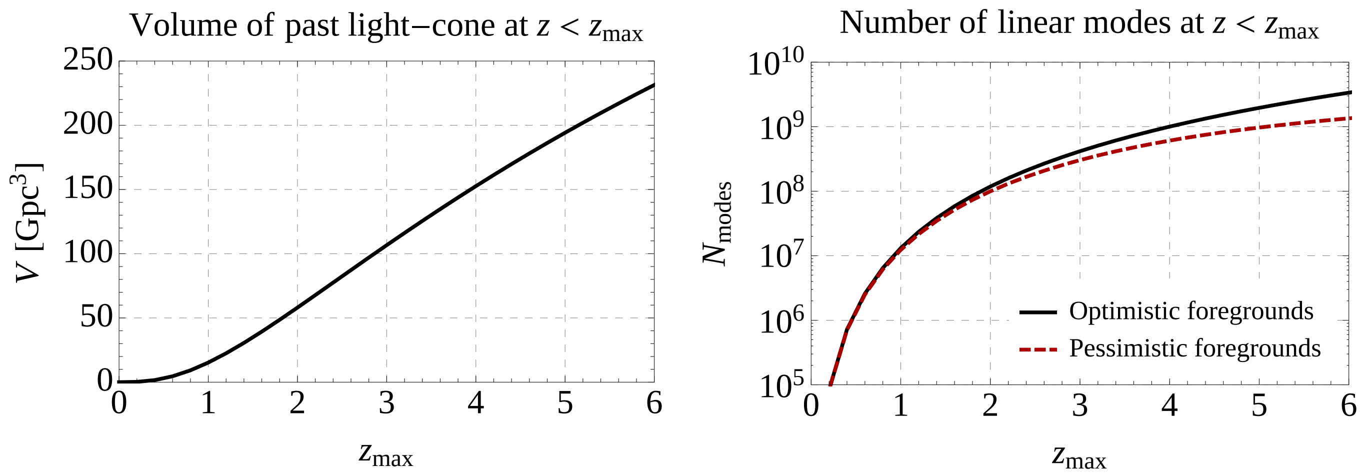

FIG. 6. *Left*: Cumulative volume observable along our past light-cone up to maximum redshift $z_{\rm max}$. *Right*: Number of linear Fourier modes of the density field observable up to $z_{\rm max}$, where "linear" refers to modes whose statistics can be predicted at the few-percent level (the precision required for many science cases in this section) by modern perturbation theories of large-scale clustering. A full-sky 21 cm survey over $2 < z < 6$ can in principle access ~ 3 times more volume and ~ 30 times more linear modes than a survey up to $z = 2$. Even under the pessimistic assumptions about foreground contamination, a Stage II 21 cm survey can still access ~ 10 times more modes than a $z < 2$ survey.

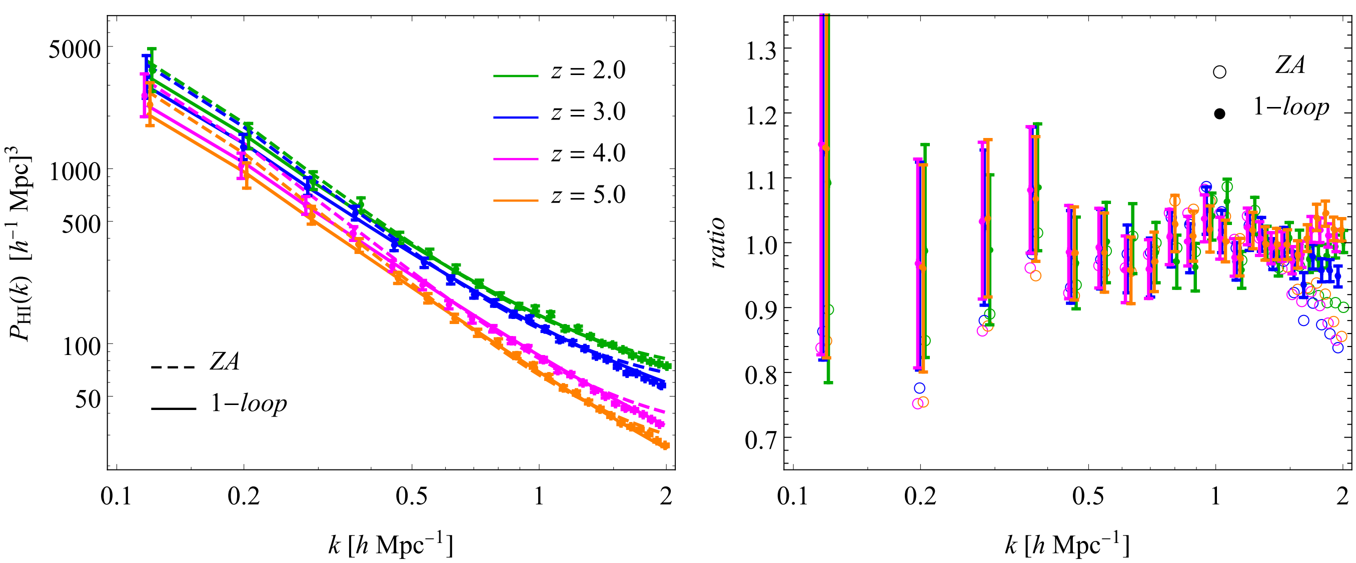

FIG. 7. Comparison of 1-loop Eulerian perturbation theory and the Zeldovich approximation (1$^{\rm st}$ order Lagrangian perturbation theory) to the Illustris simulation (from Ref. [20]). This plot demonstrates that even simple, *ab initio* theoretical models can be used to fit 21 cm data to very high $k_{\rm max}$, due to both the more linear universe at higher redshift and the greater linearity with which the neutral hydrogen gas traces these structures.

Throughout this chapter we will present forecasts for foreground optimistic and foreground pessimistic case that are likely to bracket the true value of what level of foreground cleaning is realistically achievable for the Stage II experiment.

2.2. Early dark energy and modified gravity

A concerted, community-wide effort to explain the origin of cosmic acceleration has uncovered a vast zoo of dark energy and modified gravity models. These can be broadly classified according to how they modify GR or replace the cosmological constant, Λ – for example, by adding new scalar, vector or tensor fields; adding extra spatial dimensions; introducing higher-derivative or non-local operators in the action; or introducing exotic mechanisms for mediating gravitational interactions [24–29]. A summary

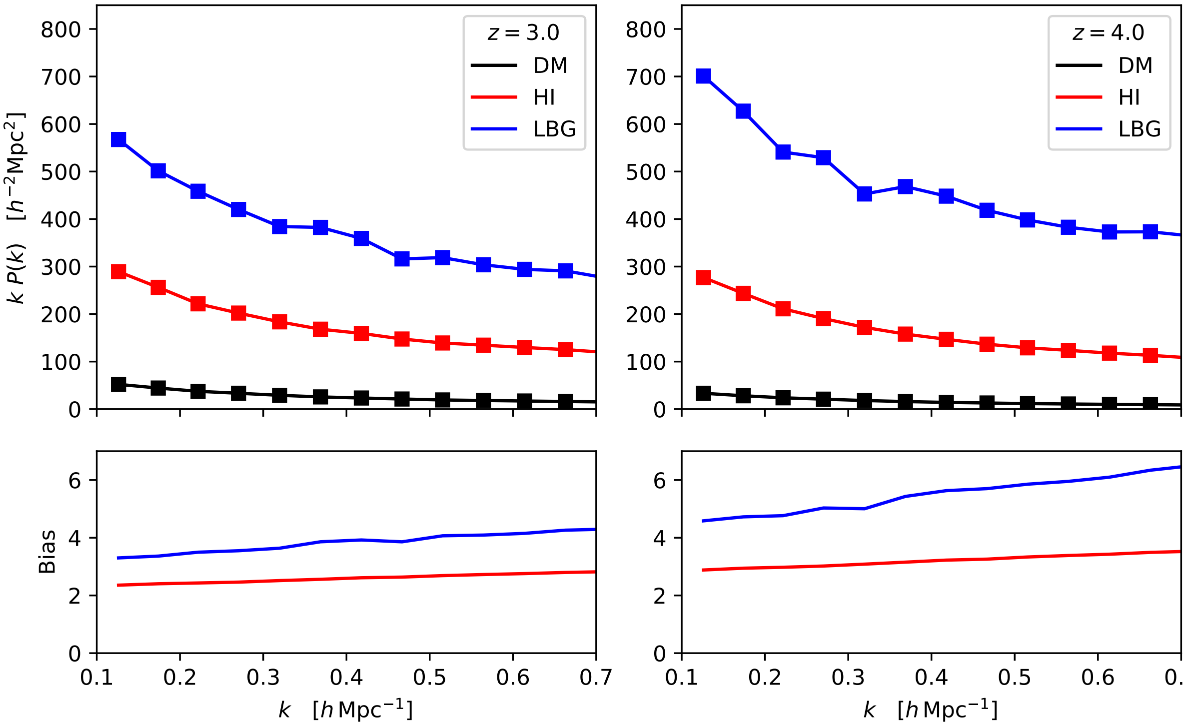

FIG. 8. (Upper) A comparison of the (real space) power spectra for dark matter, mock HI and 'dropout selected' Lyman Break Galaxies (LBGs) at $z = 3$ and 4. The power spectra are computed from an N-body simulation employing 2560^3 particles in a $256\,h^{-1}$Mpc box [21, 22]. The HI is painted into halos and subhalos of the simulation following Ref. [20] while the galaxies populate halos following Ref. [23] for $m_{UV} = 25$, close to the spectroscopic limit for large samples. (Lower) The bias, defined as $b_i = \sqrt{P_i/P_m}$, as a function of scale for the HI and LBGs. Note the LBG bias is both larger and more scale dependent than the HI bias, because LBGs populate higher mass halos.

of some possible new gravitational phenomena that can result from these modifications is included in Table III.

A systematic study of these models suggests a number of new gravitational phenomena that can arise if there are any deviations from the standard cosmological model. These include the possibility of a time-varying equation of state for the component that sources the cosmic acceleration; time- and scale-dependent variations in the gravitational constant (leading to modifications to the growth rate of large-scale structure and gravitational lensing [30–34]); and 'screening' effects, where the strength of gravity becomes dependent on the local environment [31, 35–38]. It is also the case that current constraints on possible deviations from GR are quite weak on cosmological scales, compared to the extremely precise measurements that have been obtained on Solar System and binary pulsar scales [39, 40]. The application of GR to cosmology therefore represents an extrapolation of the theory over many orders of magnitude in scale from where is has been well tested. Constraints on GR on cosmological scales are therefore a natural programmatic goal for cosmology.

Observational constraints on possible deviations from GR+Λ are only now becoming sufficiently accurate to constrain a wide variety of these scenarios. Recent theoretical work has significantly simplified the task of testing dark energy and modified gravity theories, by collecting many possibilities into a handful of broad classes, such as the Horndeski class of scalar field theories, which can then be studied in a general sense, instead of on an individual 'model-by-model' basis [41–43]. Although measurement of the speed of propagation of gravitational waves based on the gravitational wave event GW170817 and its electromagnetic counter-part GRB170817A [44] has tightly constrained a large number of possible modified gravity theories [45–50] (although see Ref. [51] for a critique that may mitigate this conclusion), large parts of parameter space remain unconstrained.

One can make predictions for observables within the context of these general classes, to see where the possibility of detecting a (potentially quite small) deviation from the standard cosmological model might be maximized. This exercise has so far been performed for a handful of theory classes and observables. In [52], for example, generic predictions were obtained for the behavior of the equation of state of dark energy $w(z)$, within the full Horndeski class. Interestingly, many of these theories predict a 'tracking' type behavior, where $w(z)$ scales along with the energy density of the dominant fluid component at any given time. This leads to the expectation that $w \simeq -1$ at low redshift, $z \lesssim 2$, where dark energy begins to dominate, but $w \to 0$ at higher redshift, deep within the matter dominated regime. This behavior is caused by couplings between the scalar field and the matter sector that generically arise in many branches of the Horndeski theories (although tracking can also be realized in

New Physics	Expansion rate/ distance	Linear clustering	Non-linear/n-point clustering	Direct expansion	Weak lensing	CMB (T/P)	Solar System/ binary pulsars	Gravitational waves
Cosmic acceleration								
Non-Λ equation of state	▲	△			▲	△		
Tracking behavior / early DE	▲	△			△	▲		
Apparent accel. / backreaction	△	△		▲	△			
Modified gravity								
Time-dependent G_N		▲	▲		▲	△	△	▲
Environment-dep. screening		△	▲				▲	△
Equivalence principle violation		△	▲				▲	▲
Lorentz symmetry violation					△			▲
Extra dimensions	△					△		△
Massive gravitons	△	△	△		△			▲
New particles								
Neutrinos (sum of masses)	△	▲	▲		△	▲		
Sterile neutrinos		△	△		△	▲		
Warm dark matter			△					
Interacting dark matter			△					
Early universe								
Primordial non-Gaussianity		△	▲			△		
Features in primordial spectrum		△	▲			△		
	Stage 2 intensity mapping				**Combined probes**		**Other experiments**	

Legend: ▲ Strongly constraining (discovery potential) △ Weakly constraining (improves current constraints)

TABLE III. Summary of some possible signatures of new physics, along with a qualitative assessment of how well each of them can be constrained by Stage II and other experiments. Empty triangles denote observables that are only expected to offer mild improvements in constraining power, e.g. improvements of at most a factor of a few over current constraints. Filled triangles denote observables that have the possibility of yielding strong, possibly decisive constraints on new physics, e.g. improvements of an order of magnitude or more. Combined probes are observations from other experiments that can be combined synergistically with Stage II measurements.

models without such couplings, e.g. freezing quintessence models [53]). The fact that this behavior is a reasonably generic prediction of a large and important class of models (most scalar field dark energy theories are included within the Horndeski class) highlights the need for precision observations in the intermediate redshift regime, $z \gtrsim 2$. If the equation of state can be reconstructed at these redshifts, possible tracking behaviors can be either definitively detected or thoroughly ruled out. Without such direct observations however, it will be difficult to tell whether a transition is occurring, or whether a possible disconnect between observations at low and high redshifts is due to some other factor (e.g. systematic effects). In Section 2.3 we discuss how the Stage II experiment will measure the expansion history at sufficiently high redshifts to constrain these models.

It is similarly important to test the growth rate of large scale structure over a range of redshifts, to ensure that possible deviations from GR on large scales have not been missed or absorbed into constraints on other parameters at late times [54–57]. As with the equation of state, the $z \gtrsim 2$ range is currently lacking in direct observational probes of the growth rate. In Section 2.5 we will discuss ability of Stage II experiment to measure the growth rate at high redshift.

2.3. Measurements of the expansion history

Baryonic Acoustic Oscillations have been a staple of survey science for the past decade. They allow measurements of the expansion history of the universe, whose relative calibration is naturally below percent level and whose absolute calibration depends only on the well understood plasma physics in the early universe.

In the early Universe, before hydrogen recombination, electrons, baryons and photons formed a tightly coupled plasma with a short mean-free path. Perturbations in this plasma, seeded at much earlier times by inflation, propagated as acoustic waves until the photons decouple from the plasma at recombination. The compressions and rarefactions in the plasma leave an imprint on the distribution of matter in the Universe at a characteristic scale of $r_d \simeq 150\,$Mpc: the speed of sound in the primordial plasma times the age of the Universe at decoupling. This scale is most commonly measured from the peak in the correlation function or, equivalently, the series of oscillations in the power spectrum known as baryon acoustic oscillations (BAOs; see Refs. [58–60] for recent reviews).

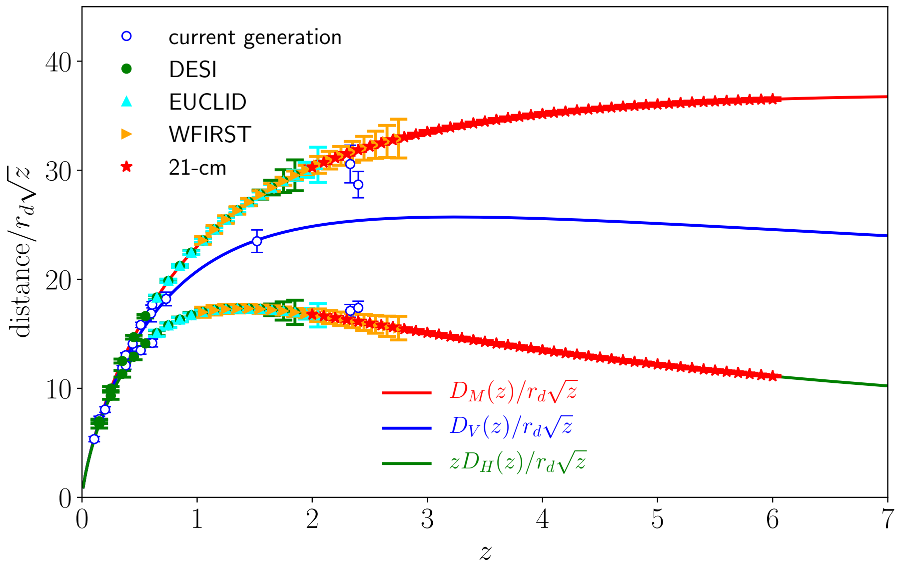

FIG. 9. Constraints on the distance-redshift relation(s) achievable with the BAO technique for some current experiments (empty symbols), some up-coming experiments (based on [69]) and our Stage II experiment (based on [70]). This Figure is an adaptation of Figure 1 from [71]. Lines from top to bottom correspond to transverse, spherically averaged and radial BAO for best-fit Planck ΛCDM model. 21 cm lines are for foreground optimistic case but with no reconstruction.

These correlations have been successfully detected using galaxies, quasars and the Lyman-α forest [61–65]. In fact, due to the large scales involved and the differential nature of the measurement (one or more peaks on top of a smooth background signal), BAOs are among the most robust measurements in cosmology. Because the physics of early universe is well known, and highly constrained by CMB observations, the BAO method provides a well-calibrated standard ruler [66]. With such a ruler BAOs can robustly measure the comoving angular diameter distance, $D_M(z)/r_d$, using transverse modes and the expansion rate, $1/H(z)r_d$, using radial modes; both as a function of redshift. For this reason current and future spectroscopic surveys (e.g. [4, 61, 67] or Table I) have BAO as a major science driver. A measurement of BAOs at $2 < z < 6$, complementary to the next generation of experiments, is one of the scientific opportunities in our proposed Stage II experiment.

In Figure 9 we estimate constraints on the distance scale from a Stage II experiment. The forecasting was done using the standard approach of Ref. [68], adapted for 21 cm measurements. In particular, at each redshift bin, we add the shot-noise and thermal noise contribution at wavenumber $k = 0.2\,h/\mathrm{Mpc}$ to power spectrum, and convert these back to an effective number density of sources. The results are largely independent of choice of fiducial k at which we do this conversion. Figure 9 shows that current and next generation optical/IR experiments lose constraining power at $z \simeq 2$, while we forecast a Stage II 21 cm experiment can map the expansion history with high precision all the way to up to the end of epoch of reionization ($z \simeq 6$).

The high precision achievable with a Stage II experiment is due in part to the very high number density of 21 cm sources, which provide sample-variance limited measurements of the relevant scales. The 21 cm signal is dominated by numerous, small galaxies with number densities greater than $10^{-2}\,h^3\mathrm{Mpc}^{-3}$. This can be compared to typical values for galaxy surveys which are around $10^{-4} - 5 \times 10^{-3}\,h^3\,\mathrm{Mpc}^{-3}$ or less. We plot these numbers in the left panel of Figure 10. The effect of the thermal noise of the system (which is not present in optical galaxy surveys) does lead to a decrease in the effective number density of sources but for our Stage II survey this is a modest change. Provided foregrounds can be controlled, we are close to saturating the information content in BAO that can be achieved over half the sky – no future BAO experiment could do significantly better as illustrated in the right panel of 10.

2.4. Cosmic inventory in the pre-acceleration era

The measurements of the cosmic expansion history and distance-redshift relation described above constrain the abundance and time evolution of the various components of the cosmic fluid. Radial BAO directly probe the expansion history, $H(z)$, while

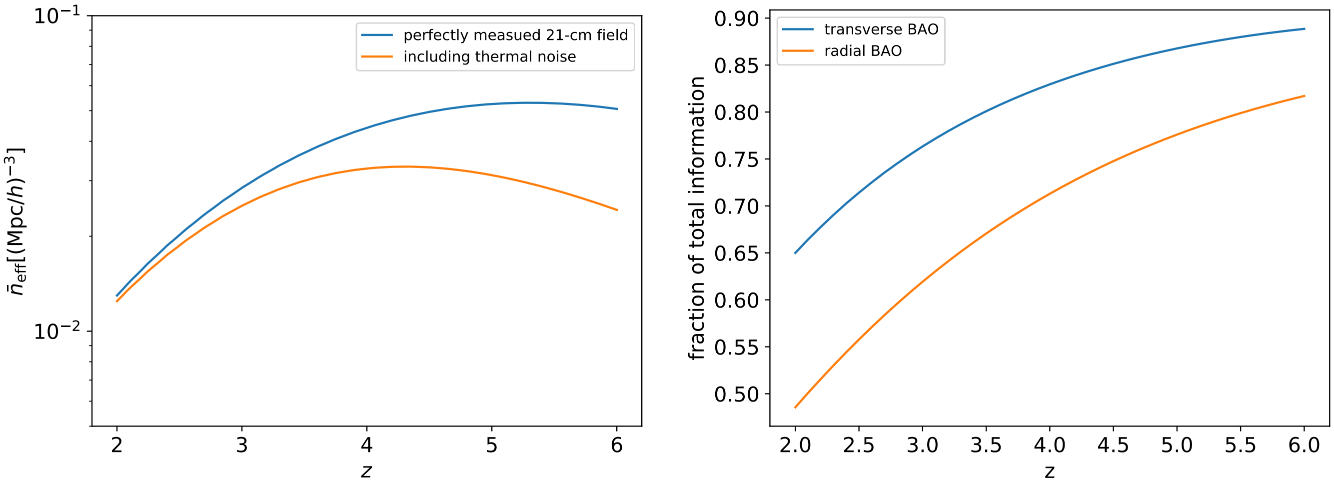

FIG. 10. Left: The effective number density of galaxies (i.e. the galaxy number density that would have an equivalent shot-noise contribution) for perfectly measured 21 cm field (blue) and effective number density for Stage II experiment after the effect of thermal noise has been accounted for (orange). Right: The fraction of total signal-to-noise obtained by Stage II experiment assuming no reconstruction compared to performing BAO measurement on perfectly measured and reconstructed field.

the angular BAO are related to the angular diameter distance,

$$D_M(z) = \frac{c}{1+z}\int \frac{1}{H(z)}dz \quad . \tag{2}$$

Within GR, both are related to the evolution of the sum of the energy densities of components in the Universe

$$H^2(z) = \frac{8\pi G}{3}\sum_i \rho_i(z) \quad . \tag{3}$$

Since the scaling of the energy density with time is known for matter, radiation, curvature, and neutrinos, the redshift dependence of $H(z)$ can be used to infer the time dependence of the dark energy density. Assuming basic thermodynamics, this is in turn determined from the dark energy equation of state, $w = p/\rho$. As discussed in previous sections, $w(z)$ is an extremely interesting quantity for studying dark energy models, and is being increasingly well constrained at relatively low redshifts, $z \lesssim 2$, where dark energy is a large fraction of the total cosmic energy density. In Section 2.2, we discussed a number of theoretical reasons why the equation of state might be near -1 at low redshift but transition to $w \approx 0$ at higher redshift, making it difficult to definitively distinguish dynamical dark energy from a Cosmological Constant using only low z measurements. Indeed, some models only show large deviations from $w = -1$ at $z \gtrsim 2$, where dark energy is already a subdominant component of the cosmic energy density [52, 72, 73]. This makes these 'early' dark energy scenarios relatively difficult to probe, as even quite large changes in equation of state only have a small effect on the total cosmic energy density [66, 74–77]. BAO measurements from a Stage II 21 cm experiment will make it possible to measure the energy density with sufficient precision to put constraints on early dark energy scenarios however, allowing us to constrain this class of (scalar field) dark energy models.

To illustrate this, Figure 11 shows current and forecast constraints on the energy density of dark energy as a function of redshift. We compare two models that allow early dark energy behaviors, while also admitting a fiducial flat ΛCDM case – 'mocker' models [53, 78], which are a particular class of quintessence models with a smooth transition to a matter-like equation of state at high redshift; and 'tracker' models, which are phenomenological models with a smooth step-like transition in the equation of state, motivated by the Horndeski model priors discussed in Section 2.2. The mocker models are minimally-coupled, and so are constrained to not cross the phantom divide (i.e. go from $w \geq -1$ to $w < -1$), while the tracker models are not subject to this restriction.

In both cases, it can be seen that current data (CMB plus BAO at $z < 0.6$) constrain any early dark energy component to be less than about 3% of the cosmic energy density at $z = 6$, with significant growth (or decay) in the energy density allowed. Adding the DESI constraints at $0.7 < z < 1.6$ would improve the upper limit to around 1% at $z = 6$, while still allowing considerable deviations from a cosmological constant – e.g. by a factor of 2 in energy density at $z = 6$ for the Mocker models. Adding a Stage II 21 cm experiment, covering $2 < z < 6$, improves the constraints by at least another factor of two, depending on the model, even in the foreground pessimistic case. This is a significant improvement considering that the dark energy density is strongly subdominant at these high redshifts.

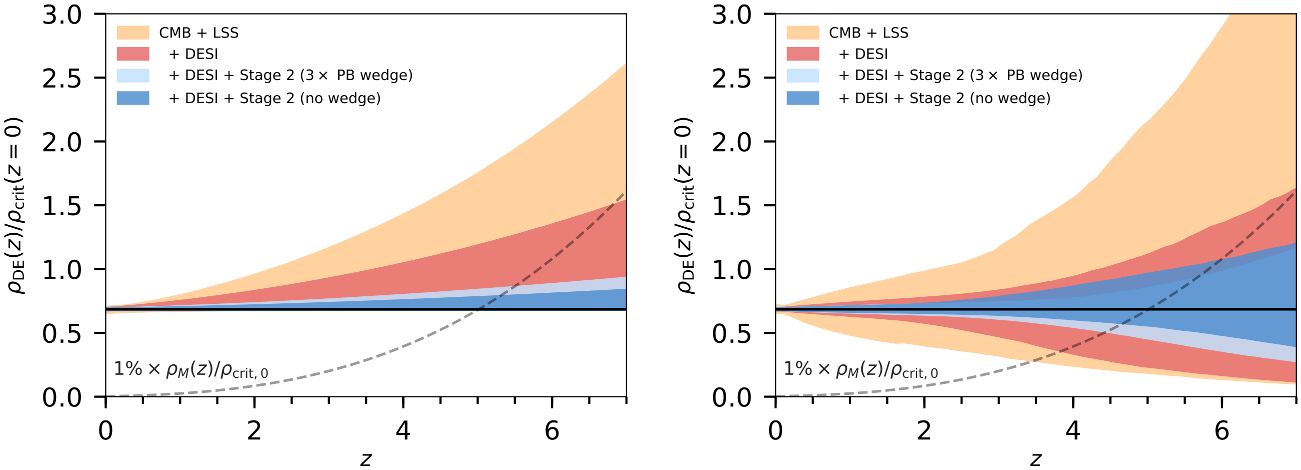

FIG. 11. Current and forecast constraints on the redshift evolution of the dark energy density out to high redshift, allowing for two types of early dark energy – 'mocker' models (left), and Horndeski-inspired tanh models (right). The colored regions show the 95% confidence intervals for several combinations of experiments: Planck CMB and existing BAO measurements from $0 < z < 0.6$; adding forecasts for DESI BAO at $0.7 < z < 1.6$; and adding forecasts for Stage II intensity mapping BAO at $2 < z < 6$ with the foreground pessimist and optimistic cases. The gray dashed line tracks 1% of the matter energy density, to give some indication of how subdominant the dark energy component is.

2.5. Growth-rate measurement in the pre-acceleration era

Redshift-space distortions are an anisotropy of the power spectrum along the line of sight caused by the peculiar velocities of sources that add to the cosmic redshift. Since these velocities are sourced by the same fluctuations in the universe, the result is a particular distortion of the power spectrum. To lowest order, these distortions multiply the standard power spectrum by $[1 + f\mu^2]^2$, where μ is the cosine of the angle to the line of sight and $f = d\log D/d\log a$ is the logarithmic derivative of the growth factor. Given that the shape of power spectrum is known to a good degree, redshift-space distortions in traditional radio surveys measure $f\sigma_8$, where σ_8 is the linear-theory value of the rms fractional fluctuations in density averaged spheres of $8\,h^{-1}$Mpc radius at $z = 0$. The ΛCDM model, constrained by current CMB observations [66, 79], predicts both $\sigma_8(z)$ and $f\sigma_8(z)$ at $2 < z < 6$ to better than 0.5% (or about 1.1% if we allow neutrino masses to vary). This provides a firm prediction which can be tested using precise observations at high z.

In 21 cm, the mean signal is unknown, so in effect redshift-space distortions instead measure the product $\Omega_{\rm HI} f\sigma_8$, with $\Omega_{\rm HI}$ being a nuisance parameter. However, there are two main ways to go around this limitation. The first is to use the method of Ref. [70], namely measure the bias from complementary data such as the Lyman-α forest, where the sources relevant for 21 cm emission appear as individually detected hydrogen systems. In Figure 12 we show constraints assuming different levels of knowledge of the neutral hydrogen abundance. Assuming the foreground contamination can be brought under control, the resulting constraints are dominated by this prior if it is weaker than $\sim 1\%$. Alternatively, it is possible to cross-correlate with other tracers at the same redshift as we discuss in Section 2.10 and Figure 16. Both methods allow redshift-space distortions to be measured with the precision of a few percent. This also happens to be the current level of theoretical uncertainty in the modeling of redshift-space distortions.

We replot the same data in Figure 13 assuming a 5% prior on $\Omega_{\rm HI}$ together with a selection of current constraints for comparison [80–85]. The theoretical models are the fiducial ΛCDM model (plotted as a solid black line) and a moderately tuned modified gravity model (plotted as a dashed black line) chosen so that the expansion is unaffected at $z > 6$ and the effects are small at low redshift. In particular, we use the Horndeski formalism of Ref. [43], with the expansion history fixed to mimic ΛCDM, $\alpha_{\rm T} = 0$ (motivated by LIGO results) and other parameters proportional to $\alpha_i(a) \propto (a/a_t)^r/[(a/a_t)^r + 1]^2$ with $a_t = 1/8$ and $r = 4$. The theoretical models are generated using the `hi_class` package [86, 87]. It is clear from the plot that the Stage II will be extremely powerful in telling departures from ΛCDM growth of fluctuations over significant portions of the evolution of the universe.

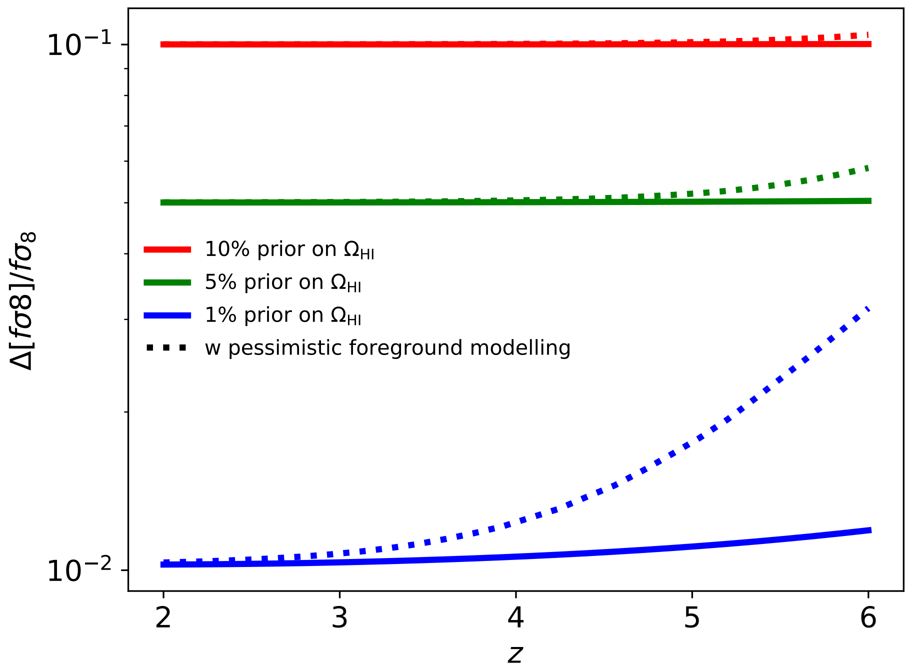

FIG. 12. Constraints on the growth rate of structure, $f\sigma_8$, for the Stage II experiment assuming priors on $\Omega_{\rm HI}$ from external data at different levels of accuracy. Solid lines are for foreground optimistic case while dotted are for foreground pessimistic case.

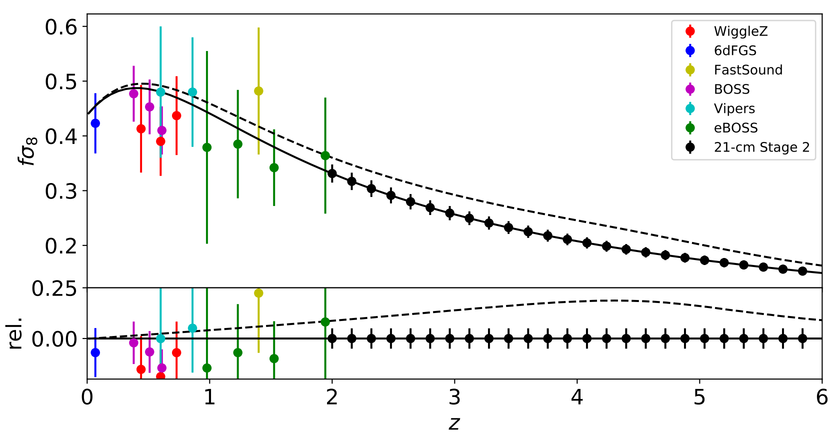

FIG. 13. Compendium of current constraints on $f\sigma_8$ (points; see text) together with forecasted errors for Stage II experiment assuming 5% priors on $\Omega_{\rm HI}$. Lines are theoretical models: ΛCDM is plotted with solid line while dashed is the modified gravity model described in the text with vanishing effects at high redshift and an expansion history equal to ΛCDM.

2.6. Features in the primordial power spectrum

BAO are well-understood features in the power spectrum introduced during the evolution of the Universe. It is also possible that there are other features in the power spectrum and we can search for them with a Stage II experiment. In linear theory the matter power spectrum at a wavenumber k and redshift z is given by

$$P_{\rm matter}(k,z) = P_{\rm primordial}(k)T^2(k,z) \quad , \tag{4}$$

where $T(k,z)$ is the 'transfer function' and $P_{\rm primordial}(k)$ is the primordial power spectrum. Assuming standard slow-roll inflation $P_{\rm primordial}(k)$ is well approximated by a power law ($A_s k^{n_s}$ with $n_s \simeq 0.96$ [66, 79]). However there are numerous

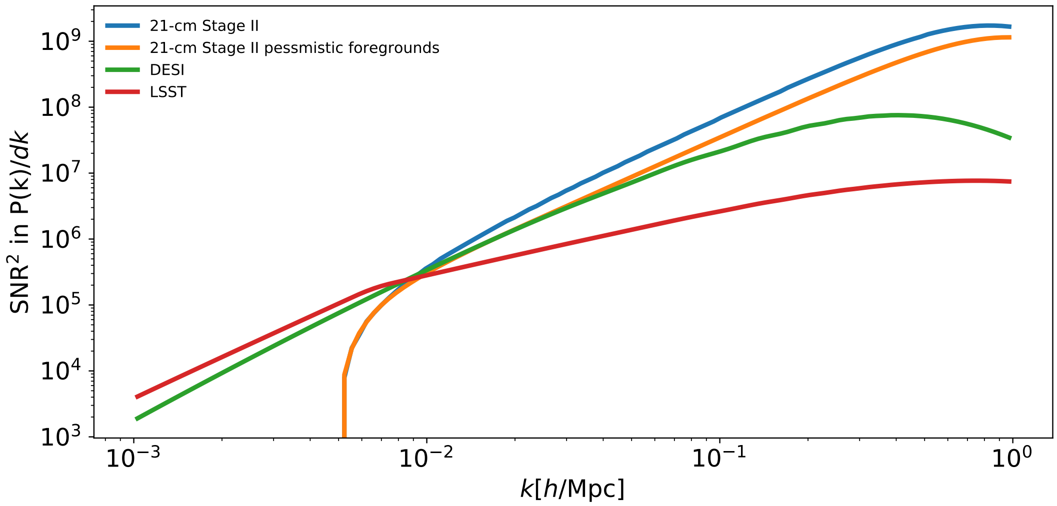

FIG. 14. Total signal-to-noise ratio (squared) in power spectrum measurements as a function of wavenumber, k. The knee in the results for the LSST (red line) corresponds to the scale at which LSST transitions from being a 3D survey to a 2D survey due to photo-z smearing. The DESI turn-over at high-k (green line) is driven by the number density of galaxies. Stage II 21 cm has the most volume and the most accurate sampling, but it looses sensitivity at low-k due to foreground contamination. Note that this plot is normalized to per linear step Δk, changing this to per $\Delta \log k$ (possibly a more natural basis) would further boost the relative usefulness of 21 cm by a factor of k.

mechanisms that could imprint features in the primordial power spectrum (see e.g. [88] for a recent review). Exotic physics in the dark sector can also add additional features to the transfer function (see e.g. [89]).

Detecting a deviation from a featureless primordial power spectrum of fluctuations would provide unique insight into the physics of the primordial Universe. These features can provide evidence particular inflation scenarios or identify the existence of new particles and forces during inflation or in the thermal plasma. The cosmic microwave background (CMB) puts stringent constraints on the amplitude of features, but no significant evidence has been found for such signals [79, 90–95]. In most cases, the amplitude of the feature is a free parameter and could be unobservably small. Furthermore, the precise characteristics of the feature can have a great impact on detectability. For example, although one can define two major classes of features (broadly defined as harmonic in k or $\log k$) the details can vary significantly, with possible runnings of the frequency [96], locality of the feature [97] and multiple features [98, 99] all possible within the vast landscape of models.

The 21 cm signal could provide both improved constraints on scales already constrained by the CMB, but also significantly extend the search for features to much smaller scales. Primordial features are easier to find in the matter power spectrum, relative to the CMB, because of the smoother shape of the transfer function.

In Figure 14 we show the total signal to noise ratio in the power spectrum measurement as a function of wave-number. This signal-to-noise can be thought of as the most model-independent proxy for comparing different surveys in their ability to constrain these models because of the broad prior model and parameter space. We see that Stage II 21 cm covers a very large k-range with exquisite signal to noise. In fact, unless there is a theoretical prior to favor looking for such signals at large scales, it is always preferable to use smaller-scales due to the scaling of the accessible number of modes.

In Figure 15 we show constraints on a primordial power spectrum feature linear in wavenumber k. For this test we modified the primoridal power spectrum of fluctuations by the addition of sine and cosine wiggles

$$\mathcal{P}(k) = A_s k^{n_s - 1} \left[1 + A_{\cos} \cos(k\omega_w) + A_{\sin} \sin(k\omega_w)\right] . \tag{5}$$

The suppression of primordial power from non-linear evolution was modeled in the Zeldovich approximation following [68]. Figure 15 shows the constraints on such inflationary wiggles using scales up to $k_{\max} = 0.5\, h\,\mathrm{Mpc}^{-1}$, marginalized over the standard BAO wiggle template amplitude and phase and six broadband fitting parameters plus an additive and multiplicative quadratic polynomial. These extra parameters were marginalized separately in $\Delta z = 0.5$ redshift bins.

How well one can detect oscillatory features depends upon how much of the non-linear 'smearing' of structure can be undone by reconstruction. Our fiducial choice is 50%, which is almost certainly conservative for a foreground optimist case. The sensitivity to this assumption is shown in the right panel of Figure 15. For low frequency features the amplitude constraints depend on the amount of broad-band marginalisation one uses, but for frequencies $\omega_w > 100$Mpc the results converge and are also the same for sine and cosine components as expected. Over the majority of the relevant parameter space we can expect measurements that are better than 3×10^{-3}.

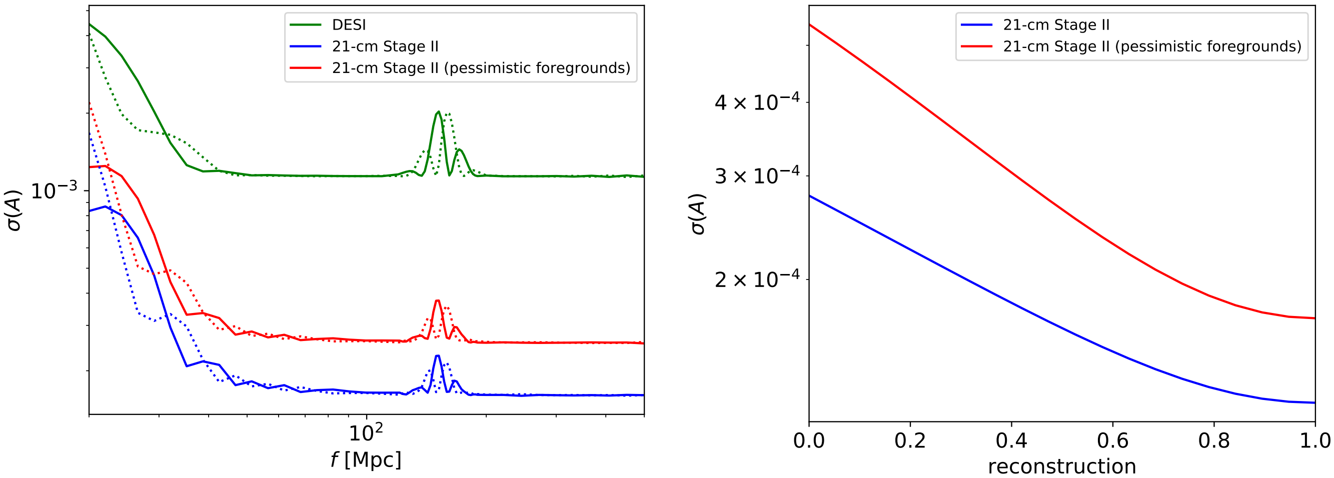

FIG. 15. Constraints on the inflationary wiggle relic. The left plot shows constraints on the amplitude of wiggle. The solid and dashed line corresponds to sine and cosine amplitude. The upturn at low ω_w is due interaction with broadband fitting parameter (and thus also depends on the same of the broadband fitting parameters). The peak at $\sim 150\mathrm{Mpc}$ is due to interaction with the BAO wiggle. The right-hand side plot shows the strong dependence on the amount of reconstruction for $\omega_w = 100\mathrm{Mpc}^{-1}$. Given the naturally more linear high-redshift universe observed by Stage II, this dependence is not very strong.

	$f_{\rm NL}^{\rm loc} \lesssim 1$	$f_{\rm NL}^{\rm loc} \gtrsim 1$
$f_{\rm NL}^{\rm eq,orth} \lesssim 1$	Single-field slow-roll	Multi-field
$f_{\rm NL}^{\rm eq,orth} \gtrsim 1$	Single-field non-slow-roll	Multi-field

TABLE IV. Physical implications for qualitatively different measurements of the shapes of primordial non-Gaussianity, adapted from [101]. For $f_{\rm NL}^{\rm loc}$ the bispectrum peaks where $k \ll k', k''$. By contrast the bispectrum for $f_{\rm NL}^{\rm eq}$ and $f_{\rm NL}^{\rm orth}$ peaks at $k \sim k' \sim k''$.

2.7. Primordial non-Gaussianity

One of the exciting targets for future large scale structure experiments is to obtain evidence for primordial non-Gaussianity (see e.g. Refs [100, 101] for reviews). In the minimal model of slow-roll, single-field inflation, the primordial density field is perfectly Gaussian. Hence, detection of non-Gaussianity in the primordial field would be immediately informative about the details of the inflationary process.

Measurable deviations from Gaussian statistics in the density field are a direct measurement of the particle spectrum and interactions relevant to the inflationary sector. As such either a detection or upper limit is testing particle physics at inflationary energy scales, which could be as high as 10^{14} GeV. These energies are unlikely to be probed in collider experiments and thus are the unique domain of cosmological surveys. Furthermore, self-interactions of the inflaton that lead to non-Gaussian signatures are often tied to the fundamental mechanism for inflation itself.

These interactions often lead to a non-zero 3-point function of fluctuations in the primordial curvature $\zeta_{\mathbf{k}}$

$$\langle \zeta_{\mathbf{k}} \zeta_{\mathbf{k}'} \zeta_{\mathbf{k}''} \rangle = \delta^{(D)}(\mathbf{k} + \mathbf{k}' + \mathbf{k}'')\, B(\mathbf{k}, \mathbf{k}', \mathbf{k}''), \tag{6}$$

where the Dirac delta-function is imposed by the translational invariance and B is the bispectrum, which is a function of the triangle configuration of the wave-vector arguments. A Gaussian field has $B = 0$. Deviations from Gaussianity lead to non-zero bispectra, whose amplitude is proportional to parameters traditionally denoted as $f_{\rm NL}$, normalized so that $f_{\rm NL} \sim 10^5$ would correspond to $\mathcal{O}(1)$ non-Gaussianity[4] [100, 101].

While the amplitude of $f_{\rm NL}$ reflects the strength of an interaction, the shape, B, carries a wealth of additional information about the nature of inflation. The local bispectrum, parameterized by $f_{\rm NL}^{\rm loc}$, is one where the shape signal to noise is dominated in the limit of one of the k modes is soft (i.e. $k \ll k', k''$). This shape is of particular interest as it cannot arise in single field inflation and would point directly to multiple light fields [102, 103]. In contrast equilateral and orthogonal shapes, with amplitudes $f_{\rm NL}^{\rm eq}$

[4] The numerical value of 10^5 comes from the fact that primordial curvature fluctuations have rms of $\sim 10^{-5}$

f_{NL}	CMB error		Stage II 21 cm error	
	Planck (current)	CMB-S4 (forecast)	FG pessimistic	FG optimistic
Squeezed (local)	5.0	2.0	0.5	0.2
Equilateral	43	21	15	5.0
Orthogonal	21	9.0	6.5	2.7

TABLE V. 1σ constraints on various types of f_{NL} parameters (see text) for Stage II 21 cm as compared with the results from CMB, both currently achieved from Planck and forecast for CMB-S4. We see that even with the foreground pessimistic case results are competitive with other experiments and would be a significant step towards a characterization of the inflationary mechanism (Table IV).

and $f_{\mathrm{NL}}^{\mathrm{orth}}$, peak in configurations where $k \sim k' \sim k''$ and are typical of non-minimal interactions of the inflaton itself [104]. The target thresholds are $f_{\mathrm{NL}} \simeq 1$ (Table IV). With sufficient signal to noise, further information can be extracted either by considering correlation functions beyond the bispectrum or by carefully exploring the scale dependence of the bispectrum [101]. In principle, from such a measurement once can extract the spectrum particles including masses [105–107] and spins [108, 109], inspiring the name *cosmological collider* physics [108].

The best current constraints come from the CMB [110, 111] and indicate no statistically significant deviations from Gaussianity. However the error bars are too large to draw any meaningful conclusions about the primordial dynamics which motivates us to explore non-Gaussianity in large scale structure. Future constraints on non-Gaussianities from the CMB are limited by the number of available modes [112] (although large improvements can still be achieved when considering bispectra involving tensors [113]). With large-scale structure we have access to a 3D volume of modes and it is expected that constraints from large-scale structure will eventually become better than those derived from the CMB [101].

In this respect the 21 cm signal has been identified as unique, because it is present throughout the Universe and could provide us with an enormous volume (the entire sky between redshift 0 and $z < 150$). While non-Gaussianity from 21 cm has been studied in the dark ages [114–116] and the epoch of reionization [117–119] in this section our focus will be on the low-redshift universe [120–124], specifically constraints coming from the our proposed Stage II experiment in the redshift range $2 \leq z \leq 6$. We follow the forecasting methodology based on [125]. In particular, our forecasts include a comprehensive list of effects, including the bias expansion for non-Gaussian initial conditions up to second order, redshift space distortions, theoretical errors and trispectrum contributions to the bispectrum. We have expanded the codes used for galaxy forecasting to take into account instrumental noise and propagating beam size effects into an effective noise in power spectrum measurements as described in Appendix D. We have further implemented various cuts to simulate the effect of low $k_{\|}$ cut and the foreground wedge to simulate our foreground pessimistic scenario. One important effect that was left out was the realistic distribution of baselines on the $u-v$ plane, which was replaced with a uniform distribution up to the maximum distance in the $u-v$ plane – we plan to correct this treatment in the next version of this document. Our results are summarized in Table V, where we see that even with conservative assumptions a Stage II 21 cm experiment could reach $f_{\mathrm{NL}}^{\mathrm{local}} = 1$ at $2\,\sigma$. This target defines a typical level of non-linearity that is inherent in many multi-field models [101]. Such a measurement would provide a valuable insight into the degrees of freedom that actively produce initial density fluctuations. For equilateral or orthogonal non-Gaussianity the reach is likely somewhere between the optimistic and pessimistic foreground scenarios. Including the wedge increases the noise but might not be necessary for constraints on these bispectra. Any measurement of $f_{\mathrm{NL}}^{\mathrm{eq,ortho}} > 1$ would be incompatible with single-field slow roll inflation [126–128]. While our forecasts cannot exclude all such possibilities, they would cut out a large fraction of the currently viable parameter space and thus represent an opportunity for a major discovery. It is also possible that Stage II data could be combined with data from a mission such as SphereX[5], leading to further improvements.

2.8. Weak lensing and tidal reconstruction

Gravitational lensing affects any map we make of the universe, with the deflection of photons by the gravitational fields of large scale structure "re-mapping" the angular coordinates we associate with a given location on the sky. This re-mapping probes the Weyl potential and is thus directly related to the projected distribution of mass between the observer and the source of the photons being measured. Therefore, a reconstruction of this re-mapping, either in terms of a deflection field or a decomposition into magnification and shearing effects, can help to address many of the science goals stated earlier, such as constraining the behavior of dark energy, measuring deviations from general relativity, or determining the masses of light neutrinos which suppress the power spectrum on small scales. A lensing map can further be cross-correlated with other maps of structure, adding redshift resolution and contributing additional constraining power by breaking degeneracies present in individual maps.

[5] http://spherex.caltech.edu/

Lensing of the CMB has been detected at high significance (e.g. [129]), and will be one of the main science deliverables of upcoming CMB projects such as the Simons Observatory [130] and CMB-S4 [112]. The joint effect of lensing on both CMB temperature and polarization allows for a robust detection in several channels, but since the CMB is effectively a single screen, it only offers access to a single projection of all matter between the observer and the surface of last scattering. Redshift information can be obtained through cross-correlation with other tracers, but this introduces additional populations have associated modeling uncertainties. Lensing can also be measured from the correlations between observed galaxy shapes in a large optical survey (see Ref. [131] for the current state of the art). By binning the galaxies in redshift, one can access multiple projections with different redshift weightings. However, there are several pernicious systematics that must be dealt with, ranging from the impact of the telescope's point-spread function on inferred galaxy ellipticities, to control over the uncertainties in photometric redshifts, to the "intrinsic alignments" of galaxies with their nearby environments (e.g. [132]).

In some sense, lensing of 21 cm fluctuations represents the "best of both worlds." 21 cm intensity maps have angular resolution and other properties that place them in roughly the same regime as CMB maps, so there is promise that the well-developed estimators and pipelines for reconstruction of CMB lensing can be adapted to 21 cm observations. However, since 21 cm maps will be intrinsically three-dimensional, they will also enable the same "tomographic" lensing studies as in galaxy lensing, but free of many of the galaxy-specific systematics mentioned above. The promise of 21 cm lensing has long been recognized in the literature (e.g. [133–137]), and work from both the simulation [138] and analytical [139] sides continues.

Of course, that is not to say that 21 cm lensing analyses will not have their own systematics to account for, and these are starting to be investigated. For example, the quadratic lensing estimators that are standard in CMB analyses rely on the Gaussianity and translation-invariance of the intrinsic statistics of the CMB, whereas 21 cm maps will have more complicated statistics that will affect any reconstruction of the lensing map. Refs. [139–141] have shown that these effects will be significant at the redshifts relevant here. Ref. [139] has also presented a technique to mitigate a portion of this impact, which will reduce the additive bias on the power spectrum of a reconstructed lensing map, but will generally increase the noise on the same quantity. In cross-correlations between lensing and other tracers, the additional bias will not be present, but the noise will remain, and this must be taken into account when performing forecasts.

However, the bias on the lensing estimator caused by nonlinear clustering is an interesting signal in its own right, being sensitive to the power spectrum of the long density modes that gravity couples to shorter modes within the 21 cm map. (Note that the long modes referred to here are in the *same* redshift range as the map; lensing also couples long density modes to short modes within the map, but those long modes are at strictly *lower* redshifts than those being directly observed.) These modes can be reconstructed in the same way as for lensing, a process often referred to as "tidal reconstruction" because it relies mainly on tidal effects [142–145]. This method can be used to reconstruct modes with low $k_\parallel$, which would be obscured by foregrounds if attempts were made to measure them directly. These modes can then be cross-correlated with the CMB to constrain possible integrated Sachs-Wolfe signatures of early dark energy or modified gravity, or cross-correlated with other measurements of lensing to probe structure growth or neutrino mass.

In Table VI, we present forecasts for the total signal to noise on the various auto or cross power spectra related to lensing and tidal reconstruction, applying the forecasting strategy of Ref. [139] to the fiducial 21 cm instrument described in Sec. 2.1. The displayed signal to noise is combined over lensing reconstruction from 10 redshift bins spanning $2 < z < 6$, while, for simplicity, we treat LSST galaxies and shear (i.e. galaxy shape correlations) non-tomographically. We also show equivalent values for CMB-S4 lensing, assuming a $1'$ beam, noise of $2\,\mu$K-arcmin, and $f_{\rm sky} = 0.4$. Even in the case of pessimistic foregrounds, we expect that cross-correlations of 21 cm lensing with LSST can be measured at a precision competitive with CMB-S4; recall that these cross-correlations will include much more tomographic information than CMB lensing.

For the 21 cm lensing auto spectrum, the "bias-hardening" method mentioned above leads to so much noise that this measurement is not competitive with CMB-S4, even if the foreground wedge can be completely cleaned. However, the power spectra of long density modes in each redshift bin can likely be accessed with very high precision, with a total signal to noise on transverse density modes alone of several hundred regardless of the foreground treatment. In terms of scales, for optimistic assumptions about foregrounds, modes transverse to the line of sight (i.e. with $k_\parallel = 0$) can be reconstructed with signal to noise greater than unity for $k_\perp \lesssim 0.04h{\rm Mpc}^{-1}$ at $z \sim 2$, and up to $k_\perp \lesssim 0.4h{\rm Mpc}^{-1}$ at $z \sim 6$. With more pessimistic foregrounds, the signal to noise degrades to less than unity above $z \sim 3$ on all scales, although cross-correlations of reconstructed modes with other tracers could still yield interesting results.

Overall, the signal-to-noise in these measurements is impressive. Following these predictions all the way to their implications for cosmological parameters or specific models of new physics goes beyond the scope of this document, because its main strength will come in particular through interaction of cross-correlations which require assumptions about the existence of other experiments. However, this is a very promising direction to pursue, and warrants further investigation.

2.9. Basic cosmological parameters: neutrino mass, radiation density, dark energy equations of state

As a natural by-product of measuring the expansion history and shape of the power spectrum, we can improve constraints on many interesting cosmological parameters. While expansion history is directly sensitive to any of the parameters discussed

Quantity / experiment	CMB-S4	Stage II FG pessimistic	Stage II FG optimistic
Lensing $\times$ LSST galaxies	367	358	676
Lensing $\times$ LSST shear	178	173	367
Lensing auto	353	8	216
Tidal reconstruction auto	—	266	2240

TABLE VI. Total signal to noise on measurements of auto or cross power spectra related to gravitational lensing of 21 cm maps. We expect cross-correlations of 21 cm lensing with LSST galaxy clustering or cosmic shear (galaxy lensing) to be measured at a precision competitive with that of cross-correlations with CMB-S4 lensing, with the advantage that the former will contain much more (tomographic) information about the growth of low-redshift structure. The lensing auto spectrum will be more challenging, due to confounding effects from nonlinear clustering in the 21 cm maps [139]. However, these same effects are sensitive to the power spectrum of long density modes at the source redshift, which can be "tidally reconstructed" using similar estimators [139, 142–145]. These measurements can be made very precisely with our fiducial 21 cm instrument, even in the presence of foregrounds. The numbers shown above correspond to reconstructed modes transverse to the line of sight (i.e. with $k_\parallel = 0$), which would ordinarily be inaccessible due to foreground contamination.

below, improvements in such measurements often additionally break degeneracies with other parameters so that results in combination with standard datasets such as Planck often improve considerably. The shape of the power spectrum depends coarsely on the matter density Ω_m and the epoch of the matter-radiation equality through their impact upon $T(k)$. Additionally, distances in the universe affect the conversion between the observed power spectrum (measured in angles and redshifts) and the comoving power spectrum (measured in inverse comoving distance units), and effect known as the Alcock-Paczynski test [146]. In practice, redshift-space distortion produce similar effects, so they must be modeled simultaneously.

In particular, a Stage II experiment would provide valuable additional information on:

Neutrino mass. Cosmology is sensitive to the sum of neutrino mass eigenstates $m_\nu = \sum m_i$. We know from neutrino oscillation experiments that $m_\nu \geq 0.06\,\mathrm{eV}$ in the normal hierarchy and $m_\nu \geq 0.1\,\mathrm{eV}$ in the inverted hierarchy [147–150]. Massive neutrinos affect the expansion history of the universe and they free-stream out of small scales density perturbations, making the field slightly smoother on scales smaller than free-streaming length. Their effect can be detected through a particular scale-dependence of the power spectrum between large and small scales, although this usual takes the form of comparing fluctuation power measured by CMB with fluctuation power measured at low redshift. The general expectation is that neutrino mass will be detected in the coming years using a number of related methods. The combination of CMB lensing with BAO, broad-band power measurements in galaxy surveys, weak gravitational lensing of galaxies all have sufficient sensitivity. We expect a Stage II 21 cm experiment could improve the signal to noise of all such measurements.

Energy density of radiation. The amount of radiation in the early universe is usually parameterized by the effective number[6] of massless neutrinos $N_{\rm eff}$. Measuring $N_{\rm eff}$ is an important discovery channel for new physics, since any light particle that was in thermal equilibrium with the Standard Model will contribute an additional $\Delta N_{\rm eff} \geq 0.027$ unless its contribution is diluted by other decays. At the high temperatures thought to be present in the early universe, even very weak interactions are sufficient for thermalization. As a result, percent level measurements of $N_{\rm eff}$ can be an extremely sensitive and broad probe of new physics (see e.g. [151, 152]). Currently the best measurements arise from CMB+BAO, but future 21 cm measurements of the matter power spectrum could help push the CMB measurement to $\Delta N_{\rm eff} = 0.027$ at more than $1\,\sigma$ [153].

Dark energy equation of state. While we stress that the main strength of the Stage II experiment lies in directly measuring the properties of dark energy at the high-redshift, it is also capable of determining low-redshift dark energy properties since these change the expansion-history and hence mapping between angles and scales to redshift $z \sim 2$. As an example, we measure the standard dark energy equation of state parameter w, but any model with dynamical dark energy at low-redshift will benefit from these observations of the universe in the pre-acceleration era.

These effects are studied though general Fisher matrix formalism, following the methodology of [70]. In Table VII we summarize these forecasts alone and in combination with some standard cosmological probes that will be available towards the end of the next decade. These parameters are the focus of the most important DOE-sponsored upcoming surveys and as such warrant further examination.

These constraints were derived assuming $k_{\rm max} = 0.4\,h\,\mathrm{Mpc}^{-1}$ for 21cm and $k_{\rm max} = 0.2\,h\,\mathrm{Mpc}^{-1}$ for DESI (LRGs+ELGs only), and for simplicity and fair comparison no BAO damping in both cases. Note that the higher $k_{\rm max}$ for 21 cm is justified given its higher redshift and less complex biasing arising from probing less massive halos. Since the non-linear damping of BAO increases with time, our neglect of BAO damping for all surveys overestimates the power of lower-redshift probes. The

[6] This nomenclature can be misleading, because any component with equation of state like radiation ($w = 1/3$) and coupled only gravitationally will contribute to this quantity.

Parameter / combination	LSST + DESI + Planck	CMB S4	Stage II+ Planck	LSST + DESI + Stage II + Planck	CMB-S4 + Stage II	Everything bagel
$\sum m_\nu$ [meV]	38	59	35 / 29	27 / 23	25 / 23	16 / 15
$\sum m_\nu$ + 3% τ prior [meV]	—	15	—	—	14 / 13	10.6 / 10.3
$\sum m_\nu$ [meV] (free w)	50	—	37 / 33	27 / 22	—	—
$N_{\rm eff}$	0.050	0.026	0.045 / 0.038	0.034 / 0.031	0.015 / 0.013	0.012 / 0.011
w (free $\sum m_\nu$)	0.017	—	0.0075 / 0.0061	0.0053 / 0.0042	—	—

TABLE VII. Combination of parameter forecasts for a compendium of future DOE experiments. All combinations include a Planck 2015 CMB prior to promote stability of the Fisher matrix, and are for a ΛCDM cosmology unless stated otherwise. For combinations involving 21 cm we state both the pessimistic and optimistic foreground removal cases respectively, separated by a slash.

LSST fisher matrices were based on the updated work of [69], while CMB-S4 Fisher matrices were provided through private communication [154]. Following [70] we used 5% priors on both $b_{\rm HI}$ and $\Omega_{\rm HI}$.

2.10. Cross-correlation studies

In the next decade we will see many different probes measure the same volume of space using different tracers and different techniques and cosmology should enter a golden era of cross-correlations. In general cross-correlations are extremely useful for three reasons: (1) any contaminating signal that is not present in both probes will not affects the signal; (2) the value of cross-correlations grows as the number of pairs, i.e. with the square of the number of probes, while the total signal-to-noise in auto-correlations grows only linearly; (3) cross-correlations allow the possibility of sample-variance-free measurements of some quantities.

Our fiducial experiment has been designed to probe volumes not well sampled by other tracers of large scale structure. Nevertheless, there will be avenues for cross-correlation. In direct cross-correlation, we should be able to obtain signals by cross-correlating with:

- **High-redshift quasars**. QSOs have been measured in larger numbers by eBOSS, but the size of the dataset will gain another considerable boost with DESI. This information will give extra BAO and RSD signal, help calibrate both 21 cm and quasar bias parameters (in conjunction with auto-correlation measurements).

  As an example of the science return enabled by the presence of 21 cm data, Figure 16 shows the forecasted 1-σ error on $f\sigma_8(z)$ from a combination of spectroscopic and intensity mapping data. DESI QSOs alone, shown as the red line, are too sparse, and their redshift error too large, to provide competitive constraints on RSD parameters. Although 21 cm auto-correlation cannot accurately determine $f\sigma_8(z)$ because of the well known degeneracy with the brightness temperature T_b, the cross-correlation of 21 cm and QSOs, shown as the blue line, could yield few % measurement of growth of structure at high redshift, and improve over QSOs alone by a factor of 5 or more.

- **Lyman-α forest**. The Lyman-α forest will have been probed by BOSS, eBOSS and DESI. This cross-correlation will go down to very small scales in the radial direction. Since both probes measure the neutral hydrogen this cross-correlation will help both probes achieve their full potential [155]. In particular, it will help with measuring the contamination of the Lyman-α forest by damped Lyman-α (DLA) and high column density (HCD) systems and thus enhance the potential of the Lyman-α forest as a probe of a small-scale physics.

- **High-redshift forests of other metals**. In addition to Lyman-α, the high redshift universe also contains other metal forests, like the SiIII, SiIV and CIV forests, whose physics and bias parameters can again be constrained by cross-correlation with 21 cm.

- **Lyman-α emitters** will be detected in large numbers in surveys like HETDEX [156]. Cross-correlations with 21 cm will allow determination of their physical parameters as well as constrain interlopers.

These cross-correlations with other tracers are particularly useful for the 21 cm experiment for a number of reasons:

- **Measure bias and enable redshift-space distortions**. Cross-correlation with even low number density tracers can, in conjuction with auto-correlations, constrain bias parameters and thus allow redshift-space distortions as measured by the intensity mapping to be used for determination of growth parameters. This will enable this crucial probe of modified gravity theories and the rate of growth of cosmic structure.

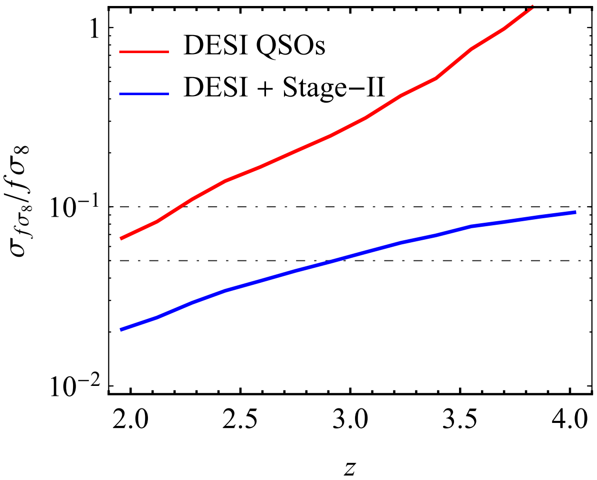

FIG. 16. Predictions for measurements of the redshift-space distortion parameter $f\sigma_8$ using Stage II experiment in combination with DESI quasars. We assumed redshift errors for the QSOs of $300 + 400(1 - z)$ km sec^{-1}, $k_{\rm max} = 0.4\,h$Mpc^{-1}, redshift bins of width $\Delta z = 0.16$, and a weak 10% prior on the brightness temperature $T_b(z)$.

- **Aid BAO reconstruction.** As discussed in [157], cross-correlation with external tracers is particularly useful to help fill in the missing modes and thus aid reconstruction, which can increase the BAO signal-to-noise.

In addition to direct cross-correlations, there will also be cross-correlations using the large-scale field recovered through tidal-mapping and the weak-lensing of the 21 cm field as discussed in Section 2.8.

2.11. Direct measurement of cosmic expansion

The measurement of the Universe's expansion in real time would be a unique confirmation of the standard cosmological model. Cosmological sources drift in redshift with the characterizing time-scale of a Hubble time. Over a 10 year time-span, this results in the redshift change of around $\delta z = 10^{-9}$. This is challenging both statistically and systematically. However, if measured, it would be one of the very few dimensional quantities that one can measure directly in cosmology[7]. Controlling absolute redshift calibration at the required level over a decade is extremely difficult, but possible in optical [158]. In radio, however, it should be considerably easier, since clock generators with sufficient accuracy are available off-the-shelf. Since in radio systems the clock-generator sets the absolute time-scale and thus frequency calibration, this (typically dominant) part of the systematic error budget is absent. There are additional subtleties to do with accurate clock transport, or subtle changes in the beam due to changes in the physical state of the reflecting material over 10 years, but while these can produce anomalous changes in the measured signal, they are unlikely to produce systematic shifts.

The basic formula for the redshift drift is given by

$$\frac{dz}{dt} = (1+z)H(0) - H(z), \tag{7}$$

where $H(z)$ is the Hubble parameter at redshift z. In Figure 17, we show a typical prediction for a total drift as a function of frequency for a 5-year experiment. We see that, in principle, the required accuracy is of the order of 10^{-2} Hz. If there existed lines whose natural width would be this small, this would have been a trivial measurement. In practice, however, the 21 cm line is velocity smeared to a few 100 km/s giving the natural smoothness of the cosmic signal of around 10^5 Hz. Thus, one really needs to rely on very precise measurements of the overall structure. On the upside, we see that there is a very definite structure to the shape of this function, so tracing the shift as a function of redshift gives another leverage on systematic control.

There are two basic approaches to this measurement. The first is to rely on the apparent radial motion of the entire field of density fluctuations. It can be shown that sensitivity of this method is given by

$$\sigma(\dot z) = \frac{1}{H(z)} \left(\frac{Vt^3}{48\pi^3} \int k_r^2 \frac{P_S(\mathbf{k})}{dP_N/d(t^{-1})(\mathbf{k})} d^3k \right)^{-1/2}, \tag{8}$$

---

[7] The other prominent examples include time-delays in gravitational lenses that allow us to measure the Hubble rate and the temperature of the CMB.

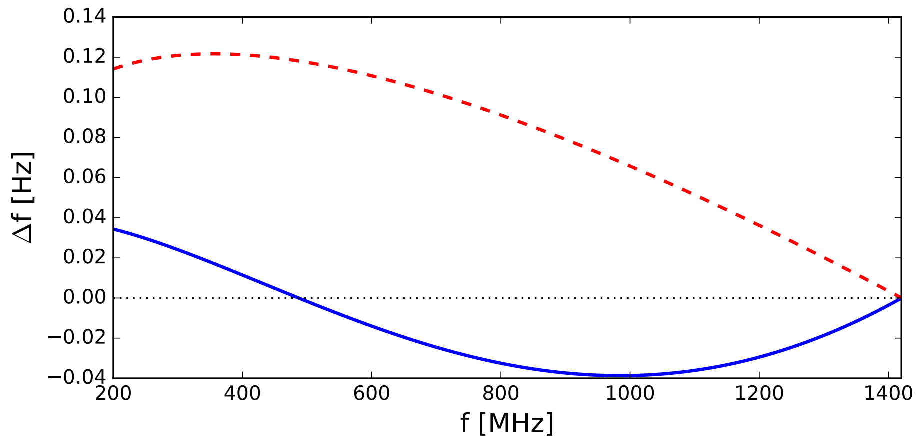

FIG. 17. Predicted drift in frequency as a function of frequency for a standard cosmological ΛCDM model (blue, solid) and flat matter dominated model ($\Lambda = 0$, red, dashed) over 5 years. We see that the required frequency precision is $\mathcal{O}(10^{-2})$ Hz in order to distinguish these two scenarios.

where V is the volume of the survey and P_S and P_N are the signal power and noise power (per inverse year of integration) in comoving space respectively and k_r is the radial wave-vector. This expression is correct even when field is non-Gaussian. We see that the majority of the signal is coming from the fine, high frequency radial modes that are suppressed by velocity dispersions in realistic cosmologies. In our numerical work we have found that this technique is not statistically promising for our straw-man configuration, but that it could be for a low redshift $z < 1$ array.

An alternative approach is to consider a finite number of cold systems observed in absorption when backlit by distant sources. This has been considered in [159], which finds a possibility of a 5σ detection over 10 years. The forecasting is highly uncertain due to poorly known redshift distribution of radio sources, which is even more poorly known in our redshift range and therefore we do not attempt it in this paper, but a simple extrapolation based on CHIME numbers shows that this measurement would most likely be possible with our Stage II proposed experiment. However, both methods would require saving data at a radial resolution that is beyond what is necessary for the standard cosmological analysis, and might increase the overall data-storage requirements by a factor of a few.

Finally, we note that in both cases, the scaling is $t^{3/2}$. This very unusually favorable scaling comes from the fact that signal increases linearly with time while noise falls as $1/\sqrt{t}$.

2.12. Ancillary science: Time-domain radio astronomy

1. *Fast Radio Bursts: A new cosmological probe*

The extremely high mapping speed that makes transit interferometers sensitive to large-scale structure also allows them to detect transients at very high rates [160–162]. Of particular interest are fast radio bursts (FRBs), a recently discovered and poorly understood class of radio transient [163, 164]. FRBs are bright, broadband, millisecond flashes, which have now been established to be of extragalactic and cosmological origin [165–167].

A defining feature of FRBs is that they are highly dispersed: their arrival times depend on spectral frequency due to the frequency-dependent refractive index of free electrons in astrophysical plasmas. This dispersion gives a precise measure of the column density of electrons to the burst source, presenting opportunities to study the distribution of plasma on cosmological scales. The large-scale distribution of plasma is poorly understood since it mostly resides at densities and temperatures where it does not significantly emit or absorb radiation. These so-called "missing baryons" have only recently been detected for the first time through stacking analyses of the thermal Sunyaev-Zel'dovich effect [168, 169]. Beyond providing a better understanding of structure formation, a precise measurement of the electron distribution would aid in the interpretation of the kinetic Sunyaev-Zel'dovich (kSZ) effect. The kSZ effect measures a degenerate combination of the electron power spectrum and of large-scale velocity flows. Independent information about the electron distribution would permit the velocity flows to be disentangled, providing a check on the theory of dark-matter structure formation, a probe of the nature of gravity on large scales, and constraints on modified gravity models.

McQuinn [170] proposed measuring the plasma distribution from a sample of FRBs by stacking their dispersion measures on foreground optically-detected galaxies. The contribution to the dispersion measure from the FRB hosts, as well as the redshift-dependent contributions from interloping plasma, can be separated from the signal using its dependence on impact parameter. Such an analysis requires relatively precise sky localizations to significantly better than an arcminute for the FRBs. This could be achieved by adding a number of low-cost outriggers to the array providing $\sim 10\,\mathrm{km}$ baselines.

A second, related method is to measure the 3D clustering of FRBs directly using dispersion, and thus electron column density, as a proxy for radial distance and redshift [171]. FRBs themselves are likely to be biased tracers of the large-scale structure, however, their measured clustering will be distorted by systematic errors in their radial distance measurements from structure in the line-of-sight plasma. These dispersion-space distortions can then be exploited to precisely measure the plasma distribution.

The proposed experiment operates at a factor of three lower frequency than most FRB discoveries to date, despite some moderately sensitive searches in this band [172]. Only very recently have FRB discoveries at 400 MHz been announced [12], and as such the rates and detectability at low frequencies are highly uncertain. At these frequencies, the effects of scattering of the burst signals by inhomogeneous plasma are expected to make them more difficult to detect (although the presence of this scattering helps in interpreting discovered bursts [165]).

To get a back-of-the-envelope event rate, we proceed as follows. We conservatively assume that, due to ISM turbulence, only the 400–500 MHz band can be used, and FRB pulse widths are scatter-broadened to 10 ms in this band. Assuming 50% surface efficiency and $T_{\rm sys} = 50$ K, this gives a 15σ detection threshold at flux 1.6 mJy, or at fluence 0.016 Jy-ms. According to [173], the all-sky FRB event rate at threshold fluence 2 Jy-ms is 2400 day^{-1}. If we speculatively use this same event rate at 450 MHz (note that fluence is preserved by ISM scattering, but the spectral index of FRBs is not well characterized), and assume that the FRB brightness distribution is Euclidean, then the event rate at the Stage II fluence threshold is (3×10^6) day^{-1} on the full sky. This gives **3000 FRB's per day** in the Stage II field of view, or approximately two every minute. Over the five year span of the experiment, this would produce around 5 million FRB detections. While this number is uncertain at a factor of a few, the reality can be better as well as worse. For example, it is likely that we will be able to get information from frequencies below 400MHz. Assuming a lower but still conservative 10σ threshold, the number of events approximately doubles.

It is clear that such large sample would be transformative for the field, as it would start to approach the number of galaxies in a typical galaxy survey (DESI will, for example, measure redshifts of some 30 million galaxies).

2. *Pulsars: alternative probe of modified gravity*

Pulsars are highly magnetized neutron stars that, due to their anisotropic emission and rapid spinning, are observed as lighthouse-like periodic sources that can be used as astrophysical clocks. The extraordinary precision of these clocks permits their use in pulsar timing arrays to search for gravitational waves with light-year wavelengths, as would be emitted by the mergers of super-massive black holes [174–176]. In addition, the extreme compactness of neutron stars permits precision tests of general relativity in the strong gravity regime by tracking the dynamics of multi-body pulsar systems using pulsar timing [177, 178]. These opportunities to test fundamental physics depend on the discovery of new highly stable millisecond pulsars or pulsars in exotic dynamical systems.

Like FRB searches, pulsar searches can benefit from the high mapping speed of transit interferometers. The proposed experiment covers the 200 to 500 MHz band, which includes part of the spectrum that has been identified as promising for finding the millisecond pulsars [179] that permit searches for gravitational waves and the most precise tests of general relativity. Current state-of-the-art surveys have searched large fractions of the sky, with a few minutes of integration time, using telescopes with order $(100\,\mathrm{m})^2$ of collecting area. Current algorithms for searching for pulsars in collected data require that data to be contiguous in time. As such, a transit interferometer can only integrate down in sensitivity for the duration of a transit which, for the proposed 6 m dishes and 70 cm wavelength, is roughly 27 minutes for a source at the equator and longer at higher declinations. It would take roughly 15 days to survey most of the sky to this depth, at which point the square kilometer of collecting area and 27 minutes of dwell time would permit the discovery of pulsars 1000 times fainter than current surveys.

In addition, recently proposed algorithms permit the coherent co-adding of observations taken on consecutive days [180], meaning the integration time on a given patch of the sky could be dramatically increased. Depending on the efficacy of these algorithms, which has not yet been demonstrated, this would permit the detection of sources fainter by a few orders of magnitude.

Compared to future surveys, the proposed experiment will be 300 times more sensitive than CHIME, 64 times more sensitive than HIRAX, and 6 times deeper than the maximum depth of FAST (even in a 10-year survey, FAST could only reach its maximum depth over a small fraction of the sky, whereas we are proposing to reach this depth over the full sky). The SKA, having a similar timeline and comparable collecting area, will have a comparable maximum depth. However, due to the non-compact configuration of the SKA antennas, it will only be able to survey a small fraction of the sky to this depth.

3. CHALLENGES AND OPPORTUNITIES

While 21 cm intensity mapping provides an efficient means of measuring large scale structure to high redshift, the instrument and analysis must be designed to overcome systematic sources of contamination: terrestrial radio signals from human-generated radio frequency interference (RFI) and the Earth's ionosphere, and extremely bright astrophysical synchrotron foregrounds from our own galaxy. The former can be addressed with suitable site locations and benefits from RFI mitigation and ionospheric characterization work from current low frequency instruments. We can address the latter by using the inherent spectral smoothness of the foregrounds to separate them from the cosmological signal. However, this places stringent requirements on frequency-dependent instrument calibration, and foreground removal becomes a key design driver for instrument characterization, stability, and uniformity. A baseline instrument configuration that can achieve foreground removal and sensitivity limits sufficient for the science goals outlined in the previous sections will require that we build a highly redundant array of order 65,000 uniformly-spaced feeds, allowing fast-Fourier transform (FFT) beamforming for data correlation and compression, operating across a redshift range of $z \sim 2-6$ (200-500 MHz), and utilizing real-time gain calibration. As noted below, storing the full correlation matrix is not practical, but beamforming this number of detectors as a method of data compression is possible with present-day computation resources, although it requires real-time calibration that has not yet been demonstrated with current instruments. This input from current experiments is critical to assess the trade-offs between raw sensitivity and ease of calibration. Achieving foreground removal requirements with a sensible analysis strategy can only occur with a concerted R&D effort along three directed paths, described in more detail throughout this section:

- *Technological:* The primary technological development paths to build and calibrate the instrument baseline design described above (with the capability to remove foregrounds and enable data compression) include **improved signal processing and digital conversion electronics**; **optimized RF analog chain design with an emphasis on uniformity**; and **gain stabilization and beam characterization instrumentation**.
- *Analysis:* The primary analysis path is to build on the foreground removal and RFI mitigation techniques from current generation experiments and develop FFT beamforming compression and associated instrument design specifications to enable analysis at an achievable computation scale.
- *Simulations:* The primary simulation path is to build synthetic data for Development and Deployment, Validation and Verification, and Uncertainty Quantification. This must include full instrument characteristics to optimize instrument design and fully explore cosmological parameter constraints, particularly for analysis involving cross-correlations and other survey data. The minimum required inputs to form a sky map for this process are mock catalogs with galactic foregrounds and point sources. By the time this project becomes reality, our understanding of the low-frequency sky will be considerably improved from Stage I and Epoch of Reionization experiments.

In Section 3.1 we review the outstanding design requirements for 21 cm cosmological mapping, heavily informed by the experience of the current generation of experiments. In Section 3.2 we summarize the main technological R&D areas to address these, and then describe specific technology advances in more detail. In Sections 3.3 and 3.4 describe the analysis and simulations challenges, respectively. Finally, in section 3.5 we relate the technical needs of a 21 cm experiment to historical DOE strengths and capabilities, as well as pointing out opportunities for growth.

3.1. Design Drivers and Requirements

Using radio surveys of galaxies to probe the BAO scale and constrain dark energy has a long history in the literature (see [189] and references therein). It was realized more than a decade ago [6, 189] that low resolution radio telescopes in an 'intensity mapping mode' could be sensitive to redshifted neutral hydrogen with enough resolution to be resolve the BAO signature and could be used to transform constraints on Dark Energy and other cosmological parameters. The first measurements were made on large, steerable dishes, choosing a survey region which overlaps with high-redshift galaxy surveys, allowing a detection of highly redshifted neutral hydrogen via cross-correlation [7, 9, 11]. Following on this success, new radio interferometers have been built that are dedicated to measuring neutral hydrogen at high redshift, in principle overcoming the limitations of a single dish measurements at higher redshifts. In this section, we outline the primary design drivers for a 21 cm cosmology survey instrument. Experience from current generations of experiments already taking data (HIRAX, CHIME, LOFAR, PAPER, HERA, MWA, and Tianlai among others – see Figure 18) has shown that the most challenging requirements come from a tackling bright astrophysical foregrounds. The experiments populate a wide space of instrument configurations, and the largest instrument on the sky in the phase-2 redshift range is CHIME [181, 190–192], which has chosen a cylindrical dish design to give the instrument a wide field of view in one direction, but which requires an intricate calibration scheme [191]. **Below we outline the design drivers for a Stage II experiment, but it should be emphasized that foreground contamination is almost always**

FIG. 18. A sample of relevant 21 cm interferometric experiments currently fielded: **(a)** 8-element HIRAX prototype array operating at 400–800 MHZ [160]; **(b)** CHIME experiment operating at 400–800 MHz [181]; **(c)** HERA [182] operating at 50–250 MHz with PAPER [183] in the background; **(d)** MWA operating at 80–300 MHz [184]; **(e)** Tianlai [185] operating at 700–800 MHz; **(f)** LOFAR [186] operating at 10–230 MHz. EDGES [187] is not included because it is targeting a global signal. LEDA is relevant but not pictured [188].

setting the requirement, and adequately removing it must include dedicated efforts across all of instrument design, data analysis, and simulation.

Astrophysical Foregrounds. Astrophysical foregrounds, primarily synchrotron emission from the galaxy and unresolved point sources, have much higher intensity than the cosmological signal of interest. These foregrounds have a smooth spectral shape and hence can in principle be distinguished from the 21 cm emission from large scale structure [183, 193–195]. However, any frequency dependence in the instrument response, for example from the instrument beam or gain fluctuations, can complicate our ability to differentiate between the smooth foreground and the essentially Gaussian cosmological signal [196, 197]. Removing these foregrounds drives design choices including element uniformity, array redundancy, assessment of instrument stability and stabilization methods; provides opportunities for new calibration techniques in both beam and gain measurements; and requires analysis and simulations to fold in calibration measurements and assess their impact on cosmological parameter estimation.

Instrument Calibration. Work in 21 cm calibration focuses on instrument gain and beam measurement for the goal of removing astrophysical foreground power. Simulations for CHIME have provided a scale to the problem: the instrument response on the sky ('beam') must be understood to 0.1%, and the time-dependent response of the instrument ('gain') must be calibrated to 1% [196, 197]. Current instruments rely primarily on sky signals for both types of calibration, however this has not yet been demonstrated to adequately remove foregrounds with these instruments. Throughout this chapter we outline design choices to meet uniformity and stability specifications that must be carefully integrated into the instrument design, verified during testing and deployment, as well as develop or advance new methods of calibration for this removal.

FFT beamforming requiring real time calibration and array redundancy. The correlation cost and data rate from the Stage II array will require implementing an FFT beamforming correlator. Such correlators use FFT-based sampling of the interferometric geometry [198] to reduce the computational correlation cost from order N^2 to $N \log N$ and output data volume from N^2 to order N. Taking advantage of this technique requires that all elements of the array be redundant (that their beams are similar), placing stringent requirements on element uniformity. In addition, this correlation will be performed in real time, and so this requires that we employ real-time calibration to account for instrumental changes (or that the instrument remains extremely stable). This technique will be attempted on current generation telescopes, and we expect work on those experiments will inform requirements and algorithms for Stage II instrument.

Environmental considerations. In addition to astrophysical foregrounds, two sources of terrestrial signal contaminants must be eliminated or otherwise mitigated: human generated radio-frequency interference (RFI) and Faraday rotation in the ionosphere.

Radio bands within the 21 cm redshift range $0.1 < z < 6$ are popular as communications frequencies. This forms a bright RFI signal at discrete frequencies within our measurement band. RFI can be reduced or eliminated by a suitable choice of radio-quiet observation site such as the middle of South Africa or western Australia [199], which are remote areas with limited communications in countries with suitable infrastructure. Even if RFI must be removed, various experiments operating in locations with high degrees of interference, notably LOFAR (located in the Netherlands), have built impressive RFI removal techniques [200] that the Stage II experiment can draw from.

The ionosphere is a plasma and acts in concert with the Earth's magnetic field to rotate the polarization vector of incoming light. The rotation is proportional to λ^2 as well as the number of free electrons present in the ionosphere, which vary across all time scales. While the cosmological signal is unpolarized, most foreground emission from the galaxy is polarized, and so this adds a time variable component to the foreground characterization and removal. The λ^2 dependence means it is not expected to impact the shorter wavelengths (frequencies above 500 MHz, $\sim z < 2$), but it will impact longer wavelengths relevant to a Stage II experiment. Work towards measuring and removing this rotation using accurate maps of the magnetic field and GPS data to infer free electron content is ongoing for experiments at long wavelengths. Because signal propagation through the ionosphere is critical for satellite telecommunications, it is well modelled and current low frequency radio telescopes are working to remove signal variability from the ionosphere [201].

Required Sensitivity. Instrument noise stems from a combination of intrinsic amplifier noise (noise temperatures for state-of-the-art radio telescopes range from 25 K cryogenic to 100 K uncooled) and sky brightness temperature (which span between 10K - 1000K depending on pointing and frequency). Because synchrotron emission increases at lower frequencies, at high redshifts (above $z \sim 3$) the system noise is dominated by the sky and no longer by the amplifier, thus improved noise must be achieved by fielding more antennas rather than better performing front-end amplifiers. In the absence of systematic effects, detecting the 21 cm signal requires fielding instruments including thousands of receivers to achieve mapping down to the mean brightness temperature of the cosmological 21 cm signal of ~0.1 - 1 mK in the redshift range $0.1 < z < 6$ within a few years.

Computing Scale. Radio astronomy has always been at the forefront of 'big data' in astronomy. Current generation 21 cm instruments produce $\gtrsim 100\,\mathrm{TB}$ of data per day without any compression, natively generating an amount of data $\propto N^2$ where N is the number of elements (currently $N \sim 10^3$), representing challenges in data reduction, transfer, storage, analysis, distribution, and simulation. Compression by a factor of $\sim N$ is achievable by exploiting redundancy within the interferometer, but requires the use of real-time, in-situ calibration and places strong constraints on the uniformity of the optics between elements. For the straw-man experiment with $N = 256^2$ (~65k) elements, this compression would reduce the data rate from $1350\,\mathrm{PB}$ per day to $100\,\mathrm{TB}$ per day, but still produce a data set that is $200\,\mathrm{PB}$ over a multi-year observation campaign. To aid in data transport, analysis, and data quality assessment, we plan to compress our data further, co-adding maps into a weekly cadence. This reduces to data size but increases pressure on real-time instrument calibration. In addition, to enable transient science we will need fast triggers, already deployed at current generation instruments.

3.2. Technologies Enabling Science

Understanding the instrument requirements illustrated above allows us to identify dedicated, targeted, and coordinated research and development areas that will enable a 21 cm Stage II experiment sufficient for the science case presented throughout this document. We propose a multi-pronged development effort: early digitization for improved stability and uniformity, optimizing the analog radio receiver elements, and new methods in beam and gain calibration.

1. Early digitization and signal processing

Most generally *gain* refers to the scaling between the incoming signal and the digitized signal, typically from the analog system (feeds, amplifiers, cables) and digitizer. Analog components are subject to gain variation, typically due to temperature changes, as the signal travels from the focus of the dish to the later digitization and correlation stages. As noted above, gain variation is one of the limiting factors in removal of astrophysical foreground power. One avenue of development is to digitize directly at the focus of the dish because signal information is "vulnerable" at all points along the analog stages, so the imperative is to digitize as early as possible, after which the signal is (nearly) "invulnerable". The resulting digital signal has more resiliency against time-variable changes in the signal chain (while some of these are simply moved from analog signal transfer into the clock distribution, the latter is inherently narrow-band), offers the possibility of more flexibility in calibration injection signal algorithms to make gain solutions more robust, and allows us to use commodity or other well-established protocols developed for timing and data transfer. However, this comes at the expense of overcoming the RFI from the digitization in the field, potentially increased cost, and will require all amplification to occur at the focus and thus we may find we need carefully designed amplifiers and thermal regulation at the focus as well.

Several technology developments make receiver electronics with integrated digitizers (early digitization) a promising technology for 21 cm projects. Critical components that are now available commercially include:

- Room temperature amplifiers with noise temperatures below sky brightness requirements from 100MHz to 1.2GHz.

- Low cost digitizers operating in the gigahertz regime with up to 14-bit resolution are readily available. This allows a trade-off: high bandwidth direct digitization provides the ability to oversample and design high performance digital band selection filters and high order frequency equalizers, but analog conditioning is simpler to implement and model. The final design will be decided by cost trade-offs while still meeting stability requirements for foreground removal.

- Low cost programmable logic devices capable of interfacing with a high-speed ADC, providing digital filtering to the frequency range of interest, and interfacing to high speed networks.

- Similarly, the availability of integrated RF / ADC / FPGA devices in the near future may provide a path to very compact high-performance receivers.

By digitizing at the focus we broaden the possibilities for instrument calibration, bandwidth, and signal processing, however there are a few additional considerations:

- As noted, one of the technical challenges for 21 cm telescopes is the need for $<1\%$ gain stability over at least 24 hours. The primary culprits of gain variation with temperature come from the amplifiers and any analog transmission (either coaxial cable loss or radio-frequency-over-fiber). By digitizing at the focus, the analog transmission is unnecessary and then any variation will be dominated purely by the amplifiers. The resulting temperature variation can be either mitigated by use of thermal regulation of the circuitry at each dish focus or removed by injecting a calibration signal, or both. Because noise diodes have a gain stability of $2 \times 10^{-3}/°\mathrm{C}$, achieving the required gain stability still requires thermal regulation of $\sim$°C. Amplifiers have roughly similar thermal regulation requirements, however they are more difficult to decouple from the environment because they are either connected or embedded in the antenna. Thus, development should be placed towards building calibration sources, digital or otherwise, to enable gain stabilization.

- We must isolate the sensitive RF input with signals in the -100dBm range from the high power digital outputs from the ADC which typically operate near 0 dBm. In addition, RF radiation from the digital processing system must be shielded from the input and from any other antennas.

- The raw data rate from the digitizer is large, a few $\times$10Gbit/second. This can be substantially reduced depending on the oversampling level, with digital filtering in the FPGA that receives the digitizer data, followed by transmitting only the bandwidth containing useful physics data. For some correlator architectures it may also be useful to transmit data separated by frequency band to an array of correlation processors. The system can trade off oversampling at a few gigahertz and digitally filtering down to the band of interest for a more complex analog system. In theory a digital filter can do significantly better than an analog filter in terms of stability and out of band rejection, and may become more cost effective on the time scale of the Stage II instrument.

- There must be a very precise clock distribution system sent out to each of the digitizers. This moves the instrument phase calibration problem from the analog system into the clock distribution system. Numerous techniques exist for synchronizing a distributed clocking system, and these must be adapted to enable a low cost calibration system. This has been found to be challenging even with the digitizers in only two locations, and so carefully designing and testing this timing system, including mitigations and estimates for cable reflections, will be a critical R&D task for any distributed digitization across the instrument.

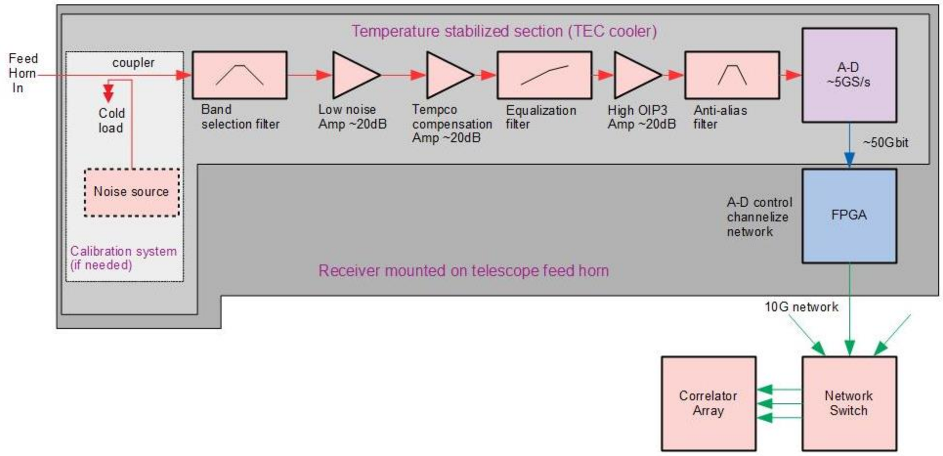

FIG. 19. Block diagram for a proposed early digitization front-end.

2. *Analog design*

Optimization of optical design. Most existing and near-future 21 cm experiments, e.g. CHIME [181], Tianlai [185], HIRAX [160], and HERA [182], all have chosen parabolic reflectors with the receivers supported at the focus with metal legs, leading to some diffraction and reflections. To illuminate the dish, they have also designed variants of dipole receivers with wide beams that have non-negligible cross-talk and frequency-dependence. These choices are typically made as a cost- and complexity savings, but make calibration more difficult. Further study for optimization, including options such as off-axis geometries (like SKA-mid and ngvLA) and possibly horn/Gregorian receivers, will be important particularly since many of those experiments will have greater experience with the parabolic reflector geometries in the near-term. These experiments also span a range of wavelength-to-size ratios and we would use these experiments along with simulations to form a specification on the dish diameter. The optimization would include keeping marginal costs low while also meeting uniformity and bandwidth flatness specifications, and exploring new dish fabrication techniques (such as using a fiberglass-based design [202], see Figure 20).

Front-end sensitivity and bandpass. When properly designed, the receiver noise temperature is dominated by loss in the analog feed as well as the noise in the first stage amplification. HIRAX has chosen to reduce the system noise by up to 30% by fabricating the first stage amplifier directly in the antenna itself, reducing the transmission loss and taking full advantage of low-noise transistors available in these bands. In addition, current generations of 21 cm experiments [182] have found that their bandpass shape is a limitation of their foreground removal, and are actively working on new feed designs that have a more carefully shaped bandpass. One development path for the active circuitry in the HIRAX feed would be to add additional RF circuitry to flatten the bandpass to remove ripple and other features, allowing an easier path for foreground removal. This introduces more stringent oscillation conditions on all amplification stages to reduce the possibility of amplifier oscillation and we will learn more about the feasibility of this technique for mass production as additional prototypes are fabricated for HIRAX.

Uniform interferometric elements for calibration and FFT correlation. Similar interferometric baselines should see the same sky signal and so differences between them can be used to assess relative instrument gains over time. This technique is known as ‘redundant baseline’ calibration and has been developed as a method of meeting the gain stability requirements [203–208]. This requires both a decision to space the interferometer dishes the same distance apart, and also have highly uniform interferometric elements. Most 21 cm instruments have chosen their baseline spacing to use this technique, however have been limited by the fact that their interferometric elements are not identical enough to achieve precision calibration. To overcome this, we would investigate dish fabrication tolerances required for this calibration as well as how we might use new dish fabrication techniques (for example, fiberglass dishes with embedded mesh conductors, currently being prototyped for SKA and HIRAX, see Figure 20) to meet these needs.

In addition, the requirements that we use FFT or similar beamforming [198, 209–211] to compress that data forces stringent requirements on the uniformity of response, beam shape, mechanical construction and alignment, gain control, etc. across what will ultimately be on the order of ∼65k detector copies. The requirements for this uniformity and how to achieve it will be part of the instrument design process.

FIG. 20. Prototype SKA fiberglass dish, located in Canada at the Dominion Radio Astrophysical Observatory

3. *Instrument Calibration*

Gain Stability. Each antenna has a characteristic response to an input sky signal, which varies with both time and frequency, known as the instrument gain. The frequency-dependent gain for each input must be known to $\sim 1\%$ on time scales between the integration period ($<$ 5s scales) and a few hours (depending on the frequency of on-sky radio calibrator sources) [196]. The two primary techniques for achieving this are to design an instrument which is inherently stable enough to meet this specification or to design a calibration plan which can ensure we meet this specification, or (ideally) both. CHIME [181, 192] is updating a classic radio noise-injection scheme which can be used to calibrate many signal chains at once. To implement such an active calibration technique for dishes will require development of stablized transmission algorithms and may be made easier with early digitization and development of calibration sources which may be independently fielded at the focus or flown on a quadcopter drone. We will also require passive models of gain and beam variation with temperature and dish pointing. This modeling is essentially standard for radio telescopes and precision modelling has been demonstrated with at least one instrument (CHIME).

Beam Characterization. Each antenna also has a characteristic response on the sky, known as the instrument beam. Because this response (main beam and sidelobes, as well as polarization) is capable of mixing frequency dependence and sky location, it is expected to be the primary source of contamination from foreground emission into the signal band, and so must be known even more accurately than the gain ($\sim$0.1%) [196]. This level of calibration is difficult for 21 cm telescopes because they are stationary and designed to have large beams for improved survey speed [212]. In addition, some instruments (such as CHIME) have large dish sizes which can be difficult to model and simulate, requiring exceedingly detailed knowledge of support structures and surface mesh. Many 21 cm instruments are beginning to use quadcopter drones to map the beam shape (HERA[213], SKA[214, 215], LOFAR[216]) and while this technique seems promising to meet the needs for 21 cm cosmology it is unlikely we will be able to measure all of the beams from all of the dishes in an instrument with 65k dishes, and so this beam calibration requirement also forces a specification on uniformity in dish fabrication.

4. *Data flow and processing*

Computing requirements for a 65k-element interferometer come from both the correlation burden and the data reduction, transfer, storage, analysis, and synthetic data production. For the correlator computation, we will need to pursue development in computing approaches which can improve the cost scaling both for equipment and power. Examples could include using

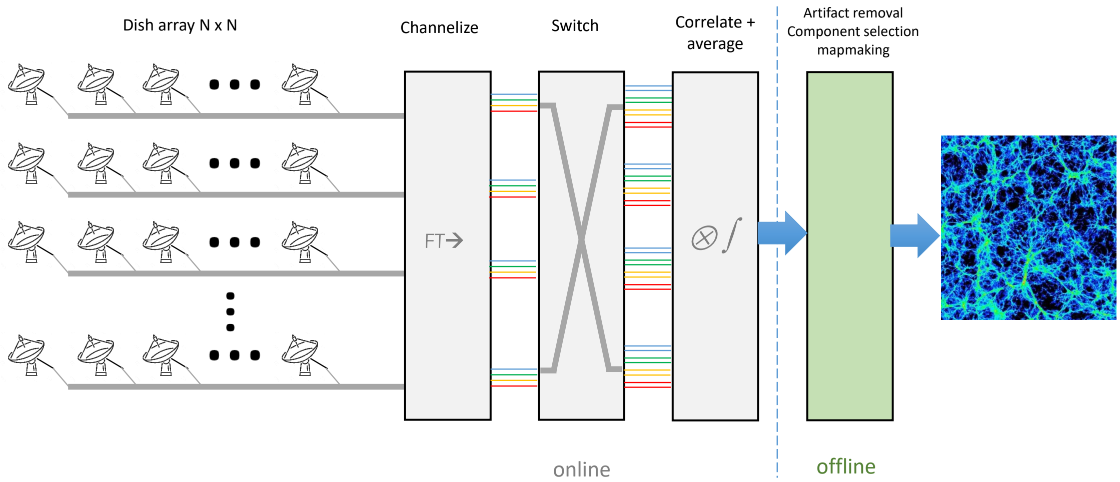

FIG. 21. Illustration of anticipated data flow in a large interferometric array. Conversion of waveform data to frequency space, e.g. channelization, is accomplished close to each receiver; coincident data for each frequency bin are collected from all stations through a cross-bar switch (also called a "corner-turn" operation); correlations are constructed for each frequency bin, which can then be time-averaged and stored, followed by physics analysis.

commodity-hosted FPGA's, using/developing dedicated ASIC's [217], or GPUs to smoothly take advantage of the fast-paced hardware updates for correlator computation.

3.3. Data Analysis

Releasing science deliverables for the community from a 21 cm experiment depends crucially on developing and deploying, including validation and verification, an analysis pipeline that can ingest vast quantities of data and transform it into well characterized frequency maps and power spectra. This is a computationally costly and varied exercise, but does not require continuous real time processing, and thus can be performed at an external high performance computing site. We can divide the analysis up into three broad areas discussed below.

Flagging, Calibration and Pre-processing at scale. In this area the data is processed to reduce the remaining systematics which may effect our ability to access the cosmological signal. Of particular importance is cleaning of any RFI by flagging times and frequency channels that have been contaminated. This is a well understood problem within radio astronomy [200], though the effects of residual RFI at the small level of the 21 cm signal is only starting to be addressed [218]. Though much of our calibration must be done in real-time (see 3.1) to enable FFT correlation, there are still degrees of freedom that must be corrected, particularly degeneracies that may not have been fully fixed (including but not limited to an overall gain scale for the entire observation, [203]), and calibration of the bandpass (the array-wide frequency dependent gain). Again these are problems that are well understood within radio astronomy.

Astrophysical Foreground Removal. Along with the sensitivity requirements for measuring a faint signal, the key analysis problem for 21 cm intensity mapping is the need to remove contaminants that are many orders of magnitude larger than the cosmological signal. Though foreground cleaning is a common problem across cosmology, the required dynamic range is unique to 21 cm intensity mapping.

In principle the foregrounds can be separated from the signal using their smooth frequency dependence [219]. However, even an ideal instrument couples anisotropy in the astrophysical foregrounds into spectral structure with an amplitude generally significantly larger than the cosmological signal. This extremely challenging problem is called mode-mixing and is exacerbated by instrumental systematics such as gain variations and optical imperfections which must be minimised (see the discussion in

Section 3.1). There exist in the literature many proposed techniques to separate the cosmological signal from the foregrounds, but these have only demonstrated success in simulations.

Foreground mitigation falls broadly into two classes: foreground avoidance and foreground cleaning. Foreground avoidance is the simplest of these two approaches, relying on the fact that contamination produced by a typical interferometer configuration is strongest in certain regions of k-space (see Appendix C). Producing cosmological results only using the cleanest modes is a simple and effective technique. This technique, however, becomes deeply unsatisfactory at low frequencies, particularly in the dark ages. Here galactic synchrotron and extragalactic point source radiation quickly becomes very bright, typically hundreds of Kelvin at $100\,\mathrm{MHz}$, even at high galactic latitudes. At the same time the window of clean modes dramatically narrows due to the relative scaling of the angular diameter distance and Hubble parameter with redshift [220]. Combined, this means that at a given threshold for contamination we exclude increasingly large regions of k-space at high redshifts, significantly degrading any cosmological result.

Foreground cleaning instead of (or in conjunction with) foreground avoidance then becomes an attractive option. A general feature of foreground cleaning methods is that they rely on detailed knowledge of the instrument response to predict and subtract the actual foreground signal. For instance, given perfect knowledge of the complex beam of each individual antenna, a tomographic map of the sky can be effectively deconvolved to remove the spectral structure induced by the instrument's beam. The residual contamination is set by both the amplitude of the raw contamination and the accuracy with which the beam has been measured. This is similar in spirit to the residual temperature-to-polarization leakage produced by mismatched beams of orthogonal polarizations in CMB B-mode searches, which can be accurately predicted and removed given beam measurements despite the fact that the CMB temperature anisotropy "foreground" is orders of magnitude larger than the B-mode signal.

Cosmological Processing. Having cleaned the foregrounds out of the data we then need to process it to quantities useful for cosmology such as power spectra and sky maps. Though this has been done within the CMB and LSS communities for many years, the fact that we are dealing with radio interferometric data after foreground cleaning brings unique challenges. The source of these is that the measured data is abstract: it is a complex, spatially and spectrally non-local measurement of the sky. This adds significant complexity in generating maps and power spectra from the data, but also tracking which modes have been measured (and which are missing) to allow us to accurately measure uncertainties. Regardless, we expect to be able to significantly draw on the conceptual frameworks used for cosmological data analysis to be able to tackle these problems [16, 196, 221].

Although we can create a broad outline of how the analysis pipeline, and we are able to draw on many mature and well understood techniques, there are several areas that will require research investment to ensure the success of a large scale 21 cm intensity mapping survey.

Scaling. While we can draw on existing techniques for all stages of the analysis, a significant challenge is scaling these to be able to work with the vast increase in data that we will generate in an energy-constrained/post-Moore's computing landscape. This will require optimizations in algorithms and implementations to reduce the computational cost of the processing, and ensuring that the techniques can scale in parallel to run on leading edge supercomputers.

Systematic Robustness. Both astrophysical uncertainties (such as the exact nature of foregrounds) and instrumental uncertainties (such as calibration and beam optics) cause foreground contamination. Developing more robust cleaning techniques will reduce systematic biases, but potentially allow us to reduce the instrumental tolerances leading to cost savings.

Improving signal recovery. Significant numbers of modes are lost to foregrounds, which reduces our constraining ability generally, but particularly affects science that needs access to the largest scales. Improved foreground removal that reduces the effect of the wedge could improve this, as would methods like tidal reconstruction [139, 144, 145], but these techniques need substantial development. Similarly, traditional reconstruction techniques [222, 223] that recover non-linear modes need work adapting them for the peculiarities of 21 cm intensity mapping.

3.4. Simulation Needs and Challenges

The challenges facing 21 cm surveys are significant but, at least to $z = 6$, well understood. However, our ability to tackle them requires a sophisticated approach to overcome them both through instrumental design and offline analysis. It is therefore essential to use simulations to close a feedback loop that allows us to predict, and thus refine, the effectiveness of a design and analysis strategy.

Producing realistic simulations of data from any instrument configuration and propagating these to final cosmological results is a conceptually straightforward prospect:

1. Produce a suite of full-sky maps of the "true" sky, with one map per frequency and at each frequency bin observed by the instrument. There are a variety of approaches to form full-sky maps of the signal and foreground, and full exploration of the data should include common sky models to include other observables (e.g. galaxy surveys) for form estimates of cross-correlations.

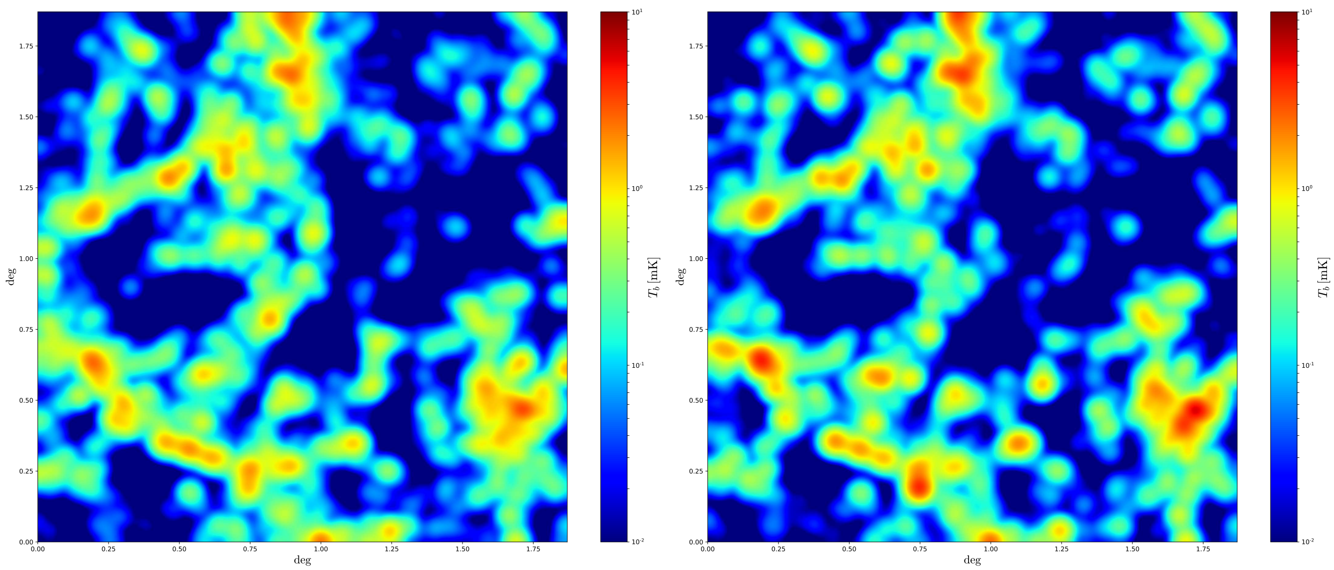

FIG. 22. 21cm maps at a frequency of 710 MHz over a channel width of 1 MHz with an angular resolution of 1.5' over an area of $\simeq 4\ \mathrm{deg}^2$. The map on the left has been created from the state-of-the-art magneto-hydrodynamic simulation IllustrisTNG with a computational cost of $\simeq$18 million cpu hours. The map on the right panel has been generated by assigning HI to dark matter halos of an N-body simulation using the a simplification of the ingredients outlined in [20]. The computational cost of the N-body simulation is much lower than that of the full hydrodynamical simulation, and allow us to model the HI field in a very precise and robust manner.

2. "Observe" these maps with a simulation pipeline that contains sufficient realism to capture any and all non-idealities that might produce contamination in the data.

3. Feed these mock observations into the data analysis pipeline discussed in the previous section, and the same pipeline that would be used on real data, and produce reduced data and cosmological analyses.

For verification of foreground removal effectiveness gaussian or pseudo-Gaussian 21 cm simulations are largely sufficient [196, 224]. However, for targeting sensitivity to specific effects (e.g. non-Gaussian initial conditions), or in cross-correlation with other probes, more accurate simulations constructed from mock-catalogues will be required. This allows us to produce correctly correlated maps for additional tracers (e.g. LSST photometric galaxies), and also for radio point source contribution to the foregrounds.

Though the relation between HI density and total matter density involves complex environment dependent processes, simulating it can be done efficiently. Recent work has shown that one can take advantage of the fact that neutral hydrogen in the post-reionization era resides almost entirely inside dark matter halos [20]. Thus, one can calibrate the relation between dark matter halos and HI using hydrodynamic simulations and create 21cm maps via less expensive methods such as N-body or fast numerical simulations like Pinocchio [225], ALPT [226], HaloGen [227], EZMock [228], PATCHY [229], COLA [230], QuickPM [231], FastPM [232], or Peak Patch [233].

As the dominant foreground contribution, simulating the galactic synchrotron must be done with care to ensure that the simulations are not artificially easy to clean. A simple approximation can be produced by proceeding from a full sky map at a radio frequency (typically the Haslam radio survey map at 408 MHz) and scaling this map to different frequencies based on the known spectral index of galactic synchrotron radiation. However this is not sufficient at the dynamic range between the foregrounds and the 21 cm signal and we must be careful to include: spectral variations about a pure power law; small scale angular fluctuations not captured in existing surveys; and polarization, including the effects of emission at a wide range of Faraday depths which generates significant spectral structure in the polarized emission [196]. More sophisticated galactic models, for example from MHD simulations, could also be developed and used here.

Regarding (2), a realistic instrument simulation pipeline would take the maps discussed and convolve them with the complex beam for each antenna in the interferometer. This can be done by direct convolution utilising the fact that for a transit telescope it is sufficient to generate a single day of data. However for wide-field transit interferometers this can be more efficiently performed in harmonic space using the m-mode formalism ($O(N \log N)$ instead of $O(N^2)$). Some of the required code would be similar and could in principle built upon similar codes used in the CMB science, such as the TOAST package[8] using fast numerical

[8] http://hpc4cmb.github.io/toast/intro.html

techniques for beam convolution [234].

For these simulations we need to generate realistic simulations of the telescope beams. Electromagnetic simulation codes such as CST, GRASP and HFSS can be used for this, but achieving the accuracy required is challenging computationally [235–237]. An alternate approach is to generate synthetic beams with sufficient complexity to capture the challenges posed by real beam, these are computationally easier to produce, but must be informed by real measurements and electromagnetic simulations to ensure their realism, and may be aided by machine learning algorithms.

Capturing non-idealities in the analog system, particularly gain variations, is mostly straightforward as these can be applied directly to the ideal timestreams. Additionally we need to include time-dependent beam convolution (including position and brightness) for temporally varying sources such as solar, jovian and lunar emission as well as the effects of RFI at low levels [218].

Including calibration uncertainties poses a particular challenge, because of the realtime calibration and compression of the instrument, simulating these effects requires either: generating data at the full uncompressed rate, applying gain variations, and then performing the calibration and compression processes; or the computationally easier alternative of generating models of the effective calibration uncertainties.

After the first two stages, mock observations are then fed to the proposed data analysis pipeline, and propagated through to final cosmological products, to assess analysis systematics, instrument design, real-time calibration, and data processing to determine whether the pipeline is sufficient to meet our science goals.

Though the simulation program is well defined, there are already many open challenges discussed below.

Understanding the HI distribution. To map the HI distribution to the cosmologically useful matter distribution requires cutting edge hydrodynamic simulations to capture the small halos that HI favours over a cosmologically interesting volume. This additionally improves the efficiency and accuracy with which we can produce mock skies.

Scale. To assess and understand a proposed design we need to be able to produce large numbers of emulators that Monte-Carlo over the experimental uncertainties. The number, size and complexity of these simulations requires a large scale effort to plan, generate and manage them.

Improving the Feedback Loop. While a straightforward version of the simulation loop above can tell us whether a proposed design does or doesn't meet our needs, it does not tell us how to improve the design to ensure that it does. For a complex instrument with many design parameters is is essential to be able to guide this process by using simulations to infer the most relevant combinations of changes.

3.5. Relation to DOE capabilities

This chapter has enumerated the technology and analysis challenges for studying cosmic acceleration by mapping the large-scale structure of the universe using 21 cm radiation. As with other large DOE-HEP experiments, it requires data from imperfect detectors to be turned into useful scientific output by application of multi-level calibration schemes that incorporate the as-built instrument characteristics and thorough end-to-end numerical simulation of the physics of the measurement process. DOE has a unique heritage in successfully constructing large experiments of this type, making it a particularly appropriate home for the development of a 21 cm intensity mapping experiment. Capabilities found in the DOE Laboratory complex in technical, computing, and management categories are discussed below.

Technical capabilities. DOE has long experience with RF systems for its hadron and electron accelerators. Hardware for manipulating RF modes to efficiently couple sources to accelerator waveguides and cavities has much in common with the matching optics used for radio telescope receivers. High channel-count, fast RF digitization and processing is also used extensively in control and beam diagnostics. Large accelerators such as LCLS-II can include over a thousand channels of RF front ends and high-performance digitizers connected to a distributed data network. Although optimization of dynamic range, bandwidth, and noise characteristics differ from those needed for the 21 cm experiment, many commonalities between the designs remain.

Data acquisition systems at large HEP and photon science experiments generate enormous volumes of digital data that must be transported over networks that may comprise tens of thousands of high-speed links. Data transport, real-time processing, and interface to commodity server farms requires DAQ developers to have specialized expertise in the most modern microelectronics families (ASICs, FPGAs, optical transceivers, etc.) and to be aware of rapidly advancing trends that open opportunities for greater performance in future projects. The Front End Link Exchange (FELIX) and global Feature Extractor (gFEX) platforms being developed for the ATLAS experiment are examples of state-of-the-art hardware coming out of the DOE labs; evolved versions of such platforms can find very direct applications in real-time 21 cm signal processing.

Table VIII shows a comparison of data rates in some current and future experiments drawn from HEP, photon science, and radio astronomy. Data rates in the 21 cm Stage II experiment proposed here, although challenging, are not out of the range of some of the more ambitious projects shown.

Experiment	Data rate [GB/s]	Year	Note	Ref.
VLA	0.3	2013	Resident Shared Risk Observing mode	[238]
ALMA	1.8	2021	Overall	[239]
LHC	25	2018	Average rate, all 4 experiments after triggering	[240]
LSST	6.4	2022	Peak rate	[241]
LCLS	10	2009	CXI instrument	[242]
LCLS-II	320	2027	High frame-rate scattering detector	[243]
XFEL	13	2017	2D area detector	[244]
SKA1	8,500	2022	Overall	[245]
CHIME	13,000	2017	Input to F-engine	[246]
21cm Stage II	**655,000**	2030	**Input to F-engine**	

TABLE VIII. Rates for current and proposed data-intensive experiments, drawn from HEP, photon science, and radio astronomy. The data rates for the Stage IIexperiment going into the F-engine are expected to be manageable within the time-frame of the experiment.

Computing capabilities. All stages of developing this experiment will require the involvement of large computing facilities. The full system simulation as well as actual data processing will require high-performance computing and efficient storage, handling and processing of data volumes in the petabyte range. This can be efficiently addressed through existing and planned infrastructure facilities within the DOE laboratory complex that will also drive new developments in network connectivity between DOE sites. DOE runs NERSC, one of the world's largest high-performance computing systems, ALCF and ORCF (limited access) and has put significant investment into exascale computing across all centers. It also hosts two CERN Tier-1 data centers.

In addition to challenges presented by the data volumes alone, there are massive algorithmic challenges that can be efficiently addressed using existing DOE structures present within Advanced Science Computer Research (ASCR) and SciDAC. On the simulation side these includes running large simulations of the universe. On the data analysis sides, the calibration problems and foreground removal problems can be recast in terms of large-scale linear solvers, error analysis, kernel estimation, machine learning, etc. These problems will benefit from developments in the current exascale initiative and work that has been done on hybrid compute architectures that can be particularly efficient ith large data rates.

Management capabilities. A 21 cm Stage II experiment will need to follow organizational models similar to those that have evolved in DOE's other recent HEP programs. These may include coordination with other agencies and/or international partners, setting up scientific collaborations and a formal structure responsible for executing the project plan, and arranging for appropriate levels of oversight. During the construction phase, test systems for quality assurance and metrology will be essential for mass-produced components to meet performance requirements. Predecessor projects such as US-ATLAS/CMS silicon detector modules, LSST focal plane raft towers, and CMB-Stage 4 detectors and readout will provide useful models and lessons. Finally, DOE has experience in organizing collaboration-wide scientific activities to generate high-fidelity simulations of system performance. The LSST Dark Energy Science Collaboration's Data Challenges are a recent example. As stated earlier, it will be absolutely essential to perform end-to-end simulations for a 21 cm Stage II experiment.

Current DOE laboratory efforts. There are currently several small path-finder efforts at various labs not directly funded by DOE HEP.

At BNL, a small test-bed experiment, BMX, has been set-up operating at 1.1-1.5GHz. It has been taking data since Fall 2017 in single dish mode and was upgraded to a 4 dish interferometer in the Summer 2019. The results are promising despite the experiment being situated at the lab site, which is an extremely poor location in terms of RFI. Early science results include characterization of out-of-band emission from global navigation satellite services that will act as a potential systematic for low-redshift 21 cm experiments. As a test-bed, the system will be used to test various approaches towards beam and gain calibration and to gather on-sky data from early digitization prototypes. It will thus continue to provide a convenient bridge between laboratory testing and a test deployment on a real radio telescope which often involves significant travel costs and limited time allocation.

The Fermilab Theoretical Astrophysics Group has been closely involved with 21 cm intensity mapping for the past decade. Early work included forecasting and technical design studies for 21 cm arrays [219] and development of analysis techniques [196, 197]. Currently, with NSF support, the group hosts the Tianlai Analysis Center (TAC), which analyzes data for the Tianlai instrument in China. The current, "Pathfinder" version of Tianlai includes an array of 16, 6-meter diameter dishes and 3, 15 m x 40 m cylinder telescopes operating in the 650-1420 MHz range and acts as a useful test-bed instrument for future efforts [247].

Near-term goals include determining the optimal design of future arrays (cylinders, dishes or both), and detecting HI at low and high redshift ($z \sim 0.15$ and 1.0). The effort includes data storage, calibration, RFI removal, data quality assessment, mapmaking, power spectrum analysis, and development and testing of the Tianlai analysis pipeline. These tasks are partly enabled by the substantial computing resources at Fermilab's Scientific Computing Division.

4. 21 CM MEASUREMENTS BEYOND REDSHIFT $z \sim 6$

In this document we have so far talked about the 21 cm intensity mapping as mapping of the aggregate emission from many unresolved galaxies. However, this is a correct picture only in the universe at redshifts lower than $z \lesssim 6$, where the universe is mostly ionized with a few pockets of neutral hydrogen residing in galaxies.

Going to earlier times and higher redshifts, we encounter two distinct regimes. The epoch between $z \sim 30$ and $z \sim 6$ is also known as the Epoch of Reionization. During these periods, first-generation stars and galaxies were formed and begun the process of reionizing the universe. This process is highly non-linear and driven by astrophysics rather than cosmology. This epoch experimentally interesting, because the signal is boosted by large region of completely ionized "bubbles" residing in sea of otherwise largely neutral hydrogen. Therefore, significant effort is dedicated to measuring this regime and we describe it in the Section 4.1.

Going even further, to redshift higher than $z \gtrsim 30$, we see the universe as it was before the formation of fist stars. The pristine hydrogen, untainted by the messy start and galaxy formation promises the ultimate frontier, but it is experimentally daunting as we discuss in Section 4.2.

4.1. Cosmic Dawn and Epoch of Reionization

21 cm techniques have been used for studying the Cosmic Dawn and the Epoch of Reionization (EoR). A number of experiments such as HERA [182], PAPER [248], LOFAR [186], MWA [249], and GMRT [250] are seeking to make the first measurements of how the first luminous objects affected the large-scale distribution and ionization state of hydrogen. While these efforts target a currently unexplored phase of galaxy formation, they do not have P5 goals as primary science and thus we are not proposing these for consideration by the DOE. However, they do have indirect relevance to the goals outlined in this roadmap, for two reasons. First, these experiments may detect signatures of exotic physics that are relevant to P5 goals, provided these signatures cannot be easily be explained by ΛCDM, even when allowing for extreme astrophysical scenarios. Second, these experiments face many of the same technical challenges as the experiments proposed in this roadmap, and thus any breakthroughs on either side in instrumentation, observation, or data analysis will be mutually beneficial.

A pruime example of possible exotic physics would be the recent results from the EDGES experiment [251]. EDGES has claimed a first detection of a large dip in spectral energy distribution of the cosmic radio monopole at around 78MHz, corresponding to $z \sim 17$ if this is due to the 21 cm line. While such an absorption feature is predicted by most theories of Cosmic Dawn, the dip measured by EDGES is anomalously large, implying hydrogen gas that is considerably cooler than is allowed by ΛCDM or an additional source of background besides the CMB [252]. This discovery has yet to be confirmed, and there are some concerns related to the foreground modeling [253]. However, if true, it would present a remarkable measurement which has already generated considerable interest within the high-energy physics community. The EDGES result, if validated, could potentially point to the first hints of interactions between baryons and the dark sector [254–260], or place constraints on the primordial power spectrum [261], relic neutrino decays [262], dark energy [263, 264], axions [265–267], interactions between dark matter and dark energy [268], dark matter annihilations [269–271], decaying dark matter [272], primordial black holes [272, 273], fuzzy dark matter [274], and warm dark matter [257, 275, 276].

Fundamentally, a 21 cm experiment aims to make large, three-dimensional maps of the distribution of hydrogen, regardless of the epoch it is probing. Thus, breakthroughs with Cosmic Dawn and EoR experiments also represent breakthroughs for any experiment described within this roadmap. In this respect, discoveries like the EDGES result could potentially be significant steps forward. A confirmed EDGES detection would be analogous to the first measurements of the CMB blackbody spectrum, while follow-up measurements of the spatial fluctuations of the 21 cm line would be analogous to the first measurements of CMB anisotropies. Just as with the CMB, such measurements would herald the beginning of a new standard probe of cosmology.

4.2. Dark Ages

After recombination[9] of hydrogen, when the Cosmic Microwave Background (CMB) was created at redshifts around $z \sim 1150$, the universe was completely neutral, with neutral hydrogen the dominant component. As matter continued to cluster in the post-recombination universe, peaks in the matter density were enhanced and eventually led to the formation of the first generation of stars and galaxies, which emitted radiation capable of reionizing the ambient neutral hydrogen. Between recombination and the formation of the first stars, there is a high-redshift epoch that is ideal for the cosmological mapping of density fluctuations

[9] Recombination is really a misnomer for this epoch since protons and electrons were never combined before. Primordial combination might be a more appropriate phrase.

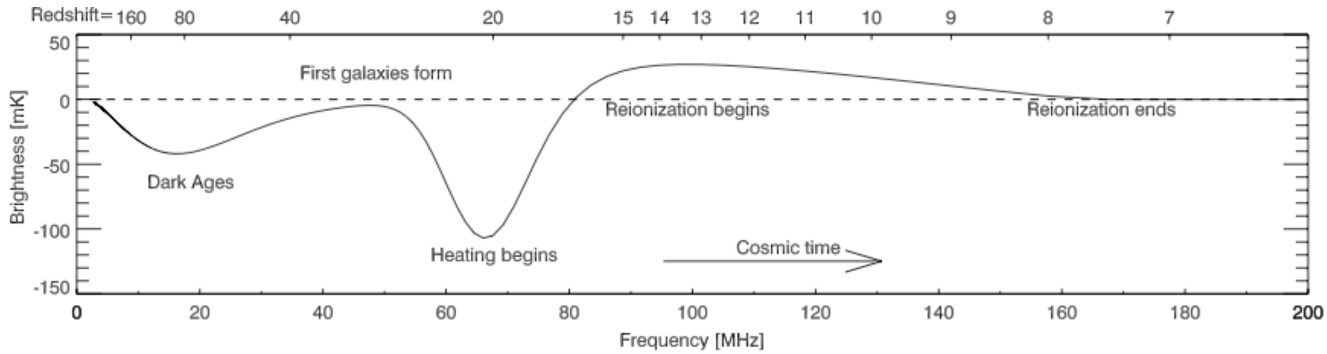

FIG. 23. The 21 cm monopole intensity through cosmic times (plot adapted from [277]).

through 21 cm intensity mapping, during which hydrogen is neutral and and traces the overall matter distribution. This epoch is generally referred to as the Dark Ages.

Several physical details prevent the mapping of density fluctuations over the entire redshift range from recombination and reionization. For instance, when $z \gtrsim 150$, residual free electrons from recombination provide a coupling between the CMB and the temperature of the hydrogen gas through Compton scattering. In turn, collisions drive the spin temperature (which quantifies the relative number of hydrogen atoms in the ground versus the excited hyperfine state) to the gas temperature. With the CMB temperature in equilibrium with the spin temperature, there is no net absorption or emission from the 21 cm line, and therefore no signal to observe. At $z \sim 150$, Compton scattering becomes inefficient. The spin temperature and the gas temperature remain coupled to one another, but together decouple from the CMB temperature. The gas then cools adiabatically as $(1+z)^{-2}$, in contrast with the CMB's cooling as a $(1+z)^{-1}$, which results in a net absorption signal. This continues until $z \sim 30$, at which point the neutral hydrogen is sufficiently dilute that the collisional coupling between the gas temperature and the spin temperature become ineffective. Direct absorption of emission of 21 cm photons then couples the CMB temperature to the spin temperature once again, and the signal disappears. The observed brightness temperature of the 21 cm signal as a function of redshift is shown in Figure 23.

A redshift window in the range $30 \lesssim z \lesssim 150$ could potentially be used for 21 cm intensity mapping and would provide large-scale maps of pristine density fluctuations. There are several advantages to doing so. First, the regime is too high in redshift for the first luminous objects to have formed yet, and therefore the signal is driven by cosmology rather than astrophysics. Second, the signal is not Silk damped, and thus density perturbations can in principle be mapped to extremely small scales (with perhaps the Jeans scale being the only limitation). Third, these small-scale structures are still in the linear regime at such redshifts, making theoretical modeling efforts considerably simpler than analogous efforts for $z \sim 0$ galaxy surveys. Finally, the volume of our observable Universe that falls in the range $30 \lesssim z \lesssim 150$ is substantial, leading to exquisite statistical errors on parameters.

1. *A new window into the Universe*

In the CMB, well-understood linear processes are sufficient to relate observed anisotropies in temperature and polarization to energy density perturbations generated during the early universe. This is what makes the CMB such a powerful probe of fundamental physics, limited mainly by diffusion damping [278] that erases anisotropies (and therefore primordial information) on small scales. On the other hand, lower-redshift large scale structure in principle offers many more accessible modes, but a large portion of these modes is affected by nonlinear processes that are difficult to model. These nonlinearities are less severe at higher redshift: in particular, before the first collapsed objects formed at $z \sim 30$, the limiting scale is the Jeans scale, $k_\mathrm{J} \sim 300$ Mpc^{-1} [279]. Since the number of linear modes scales as the cube of the maximum linear wavenumber, observations at this epoch hold great promise for increasing our knowledge of fundamental physics.

The only observable available to us during this epoch is the 21 cm hyperfine transition of neutral hydrogen.[10] The theory of the high-redshift 21 cm signal is very well understood [281, 282], and for most purposes is well described by linear perturbation theory [279]. From a practical standpoint, the signal, which is in absorption against the CMB back-light, will be very hard to observe for many reasons that are similar to those that hinder the detection of 21 cm emission at lower redshifts. In addition, a

[10] There is also a hyperfine transition in deuterium nuclei, corresponding to photons with wavelength 92 cm. In principle, this is observable with the same interferometers designed for 21 cm, and would yield a pristine measurement of the primordial deuterium abundance, but will be a much more challenging observation than 21 cm [280].

21 cm photon originating at these very high redshifts will redshift into the low MHz wavebands, which will be hard to observe from the ground due to reflection by the ionosphere. It is estimated that this limitation becomes significant for $z \gtrsim 45$ ($\nu \lesssim$ 30MHz [283]), and any signal beyond that would require an experiment outside of the ionosphere, such as in space, or, as has been proposed in Refs. [283–285], on the far side of the moon.

This certainly implies that any measurement will be very far in the future. For this reason, we will not suggest a specific experiment (which would come with a unique set of limitations), but instead remark upon the general potential of an experiment targeting these observations, that would inevitably build on the progress made with lower-redshift detections. Simply put, the high-redshift 21 cm signal will provide a three dimensional window into the linear Universe, providing access to of order 10^{10} more modes than the CMB[11]. This tremendous amount of statistical power makes 21 cm measurements from the Dark Ages the ultimate probe of the conditions in the early Universe. Exquisite constraints could be expected on many quantities of interest [281], such as the scalar spectral index [286] and primordial non-Gaussianities [115, 116, 287].

Before we present a unique science target, let us briefly highlight two observables discussed earlier, namely primordial features (Section 2.6) and non-Gaussianties (Section 2.7), that a probe of the Dark Ages could significantly improve.

The detectability of features at high reshifts depends critically on the amplitude, frequency and scale-location of the features, as well as the angular and redshift resolution of the experiment. Forecasts show [288] that a cosmic variance limited 21 cm experiment measuring fluctuations in the redshift range $30 \leq z \leq 100$ with a 0.01-MHz bandwidth and sub-arcminute angular resolution could potentially improve bounds by several orders of magnitude for most features compared to current Planck bounds. At the same time, 21 cm tomography also opens up a unique window into features that are located on very small scales ($k \gg 1$ Mpc^{-1}).

Besides features in the power spectrum, the same physics generally produces features in all primordial correlation functions. The 21 cm field as a probe of non-Gaussianities, and the bispectrum in particular, has been explored in Ref. [120]. Of particular interest is the possible detection of massive particles in the early Universe. Heavy particles with higher spin can leave distinct features on higher-order correlation function [109, 289]. The signal is predicted to be very small, but a detection would present the first evidence for a mass hierarchy as predicted by string theory [108]. Because of the smallness of the signal, 21 cm has been suggested [116] to provide the only realistic observable to constrain the presence of these particles. We refer to Ref. [116] for details of the models that could potentially be observed with 21 cm.

Now, we will present a single example that is rather unique, concerning the potential signatures of primordial gravitational waves in fluctuations of the observed 21 cm intensity. We describe these signatures below, and provide estimates for their constraining power on the amplitude of gravitational wave power left over from the early Universe.

2. *Gravitational tensor modes*

One of the holiest grails in our attempt to understand the physics of the early Universe is the possible detection of primordial gravitational waves. These can be generated by the same early-universe process that generates the seeds for the (scalar) density fluctuations that we observe in the CMB and large scale structure. Within the paradigm of inflation, the expected level of primordial gravitational waves generated during inflation is measured with respect to the production of scalar fluctuations by a relation of the two primordial power spectra:

$$P_\zeta = A_s k^{-3} \left(\frac{k}{k_*}\right)^{n_s - 1}, \tag{9}$$

$$P_h = r A_s k^{-3} \left(\frac{k}{k_*}\right)^{n_t}. \tag{10}$$

In single-field slow-roll inflation, some of the parameters above are related by $n_s = 1 - 2\eta - 6\epsilon$, $r = 16\epsilon$, and $n_t = -r/8$. Here η and ϵ are two slow-roll parameters, which are proportional to the second and first derivative of the scalar potential, respectively, and are required to be much less than unity for inflation to last a sufficient time to solve the horizon and flatness problems [290]. In more complicated models, including those with multiple fields, deviations from slow-roll, and non-canonical kinetics, these relations will be altered, pick up additional degrees of freedom, or break altogether. The relation between the scale dependence and the amplitude of primordial waves is particularly interesting. A deviation from a red spectrum would indicate a violation of the null energy condition, and suggest the spectrum was not generated from the vacuum (see e.g. [291, 292]), or could rule out inflation as the source of gravitational waves [293].

Current attempts using the B-mode polarization signal in the CMB aim to detect r as low as 10^{-3} [112], providing an interesting science target in terms of the field excursion during inflation [294]. Unfortunately, it is quite possible given the

---

[11] Assuming 10^4 independent redshift slices in this redshift range, each with for $\ell_{\max} = 10^6 \simeq \ell_{\rm Jeans}$ [281].

nature of r, which effectively describes the energy scale of inflation, that the actual level of primordial gravitational waves is orders of magnitude below 10^{-3}. Measurements beyond this level will be difficult using CMB B-modes, mostly due to B-modes generated through lensing of E-modes, which obscure primordial B-modes at the level of 10^{-2} for ground-based observations. Delensing methods can mitigate a large fraction, but this becomes increasingly hard for smaller values of r. Furthermore, for very low values of r, patchy screening and scattering of CMB photons around reionization can generate B-modes which will be hard to disentangle (although the maps could in principle be de-screened [295]) from primary B-modes. Many other probes of primordial gravitational waves face significant challenges. For example, direct detection using interferometers (e.g. LIGO and (E)LISA) is unlikely given the relatively small scales probed by such experiments [296], and methods utilizing the polarized Sunyaev-Zel'dovich effect require very low noise levels in the CMB and an exquisite measurement of free electrons in the Universe [297].

Measurements of large-scale structure during the Dark Ages will be affected by a gravitational wave background in several ways, and observations over a large enough volume have the potential to see these effects at high significance. We will highlight two such effects here:

1. **Tidal fossils**: After a large-scale tensor mode enters the horizon, it will induce a specific kind of inhomogeneity into the statistics of the density field, similar to what happens with the tidal field generated by scalar perturbations at second order. While the original tensor mode will decay with time, its imprint on large-scale structure will not, leaving behind a "fossil" that can be detected at later times using an appropriate estimator [143, 298, 299]. The power spectrum of this estimator is directly connected to the primordial tensor power spectrum, and therefore to the tensor-to-scalar ratio, with constraining power scaling with the inverse of the number of observed modes. Ref. [298] has argued that a Dark Ages survey could use this effect to constrain r to the 10^{-6} level.

2. **Curl lensing**: Like density fluctuations, gravitational waves can affect the paths of photons as they travel through the universe. Unlike density fluctuations, however, gravitational waves generate a curl component of a reconstructed deflection field. The potential of these curl modes as a probe of gravitational waves has been studied e.g. in Refs. [300–304]. The constraining power of this method also scales with the inverse of the number of modes, and in Ref. [302] it was argued that in principle a measurement of curl lensing from the Dark Ages could provide a constraint as low as $r = 10^{-9}$.

A full treatment of all effects induced due to the presence of large-scale tensor perturbations, including the two effects above, was performed in Refs. [143, 305]. Observationally, it is not evident that all of these effects can be easily separated. In our forecast below, we will assume that tidal fossils and curl lensing can be distinguished. We hope to report in the near future to what extent these effects can indeed be separated (for example, through bias-hardened estimators, as recently explored in Ref. [139] for the case of scalar lensing).

We consider a Dark Ages 21 cm survey over $30 < z < 150$, corresponding to a comoving volume of roughly $900\,(h^{-1}\mathrm{Gpc})^3$. The number of modes is set by the maximum observable wavenumbers along and perpendicular to the line of sight, $k_{\parallel\mathrm{max}}$ and $k_{\perp\mathrm{max}}$, and we assume that the statistics of these modes are amenable to theoretical predictions at the necessary precision. We assume sufficient frequency resolution to access the Jeans scale in the line-of-sight direction, $k_{\parallel\mathrm{max}} \sim 300\mathrm{Mpc}^{-1}$. In the transverse direction, we map $k_{\perp\mathrm{max}}$ into the corresponding baseline b that can observe that wavenumber. This mapping is redshift-dependent; for the tidal fossil forecast, we evaluate it at $z = 30$ since this is where the signal to noise peaks. For the curl lensing forecast, we split the survey into four equal redshift bins, evaluate the mapping (and any other relevant redshift-dependent quantities) at the midpoint of each bin, and combine the separate forecasts from the different bins. Note that b is not necessarily the longest baseline present in the instrument, but rather the maximum baseline at which all shorter modes are signal-dominated.

For tidal fossils, we adopt the quadratic estimator from Ref. [299], using their expression for the estimator noise with the survey properties given above. For curl lensing, we use a modification of the formalism from Ref. [139], which simply amounts to a change in filters applied to the observed 21 cm fluctuations. We ignore nonlinearities in the 21 cm field, which will slightly degrade the signal to noise at the longest baselines we consider. The ability to detect lensing is affected by shearing of coordinates at the source redshift by gravitational waves present at that redshift; we incorporate this "metric shear" in our forecasts, following Ref. [300].[12] The curl lensing power spectrum is computed using a modified version of CAMB [306], and we compute the 21 cm brightness temperature power spectrum following Ref. [287].

In Fig. 24, we plot the minimum value of r detectable at 3σ by either method, assuming that primordial gravitational waves are the dominant signal in each case. We have also indicated the levels at which other effects begin to dominate the primordial signal. For curl lensing, vector perturbations generated at second order by primordial scalar perturbations produce the dominant signal if $r \lesssim 10^{-5}$ [307, 308]. Contaminants in the tidal fossil estimator have not been extensively investigated, but tensor

[12] Important differences between our forecast and that of Ref. [302] include the incorporation of metric shear, which degrades the signal to noise, and the use of a fully 3-dimensional formalism that accounts for correlations caused by long modes along the line of sight.

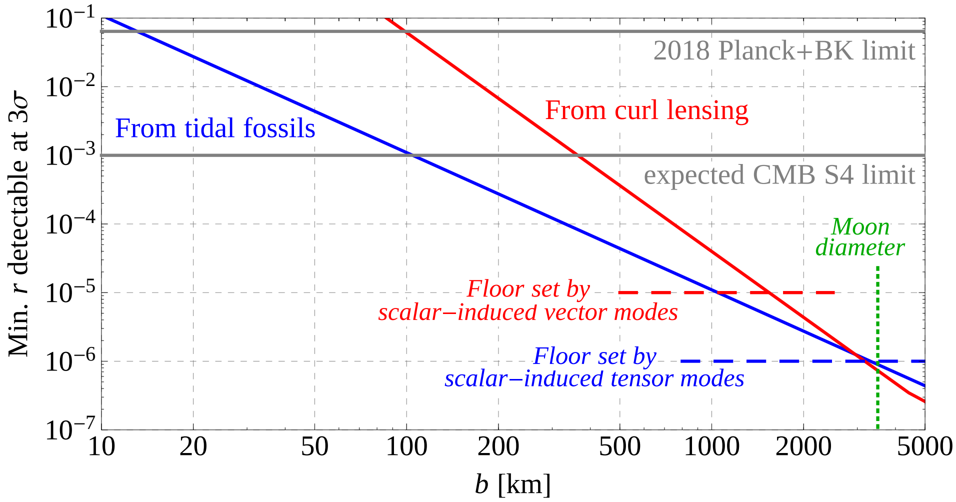

FIG. 24. The minimum value of the tensor-to-scalar ratio r detectable with a Dark Ages 21 cm survey, as a function of the maximum baseline b for which 21 cm observations are signal-dominated. Blue and red curves correspond to the tidal fossil and curl lensing methods discussed in the main text. The corresponding dashed lines indicate floors at which the primordial GW signal becomes dominated by the next-strongest signal in each method. The horizontal grey lines show the current upper limit, $r \leq 0.064$ (95% CL), from a combination of Planck 2018 and BICEP2/Keck 2014 data [95], and the expected limit from CMB-S4 ($r \lesssim 10^{-3}$ [151]). We find that for $b \gtrsim \mathcal{O}(100\text{km})$, r can be detected at a lower level than with CMB-S4, while an interferometer covering a large portion of the moon can detect r as low as 10^{-6}. Achieving even a fraction of this precision would be challenging for any other known probe of primordial GWs.

perturbations generated by second-order scalar couplings have been found to enter other observables at the level of $r \sim 10^{-6}$ (e.g. [309]), so we take this to be the relevant floor.[13]

We find that an interferometer with baselines of at least a few hundred kilometers would be able to constrain r to the level of 10^{-3}, equivalent to the target for CMB-S4, with even larger arrays being able to beat this target. Such arrays are clearly a highly ambitious notion, but currently represent the only feasible way to detect primordial gravitational waves at a lower level than CMB-S4. At the extreme limit of feasibility, an array covering a large fraction of the Moon's surface (corresponding to a maximal baseline of 3500 km, the Moon's diameter), could in principle detect r as low as 10^{-6}. Achieving even a fraction of this goal would result in a large scientific payoff, which motivates further research and development in this direction.

[13] These second-order contributions can be exactly computed once the amplitude of scalar perturbations is known, and could then be subtracted from a measurement of tidal fossils or curl lensing to access values of r smaller than the floors we have quoted. However, cosmic variance will prevent us from obtaining sufficiently precise measurements for this procedure to work. Our forecasts do not include cosmic variance; in other words, for each maximum baseline, we have computed maximum values of r for which the null hypotheses of "no tidal fossils" or "no curl lensing" could be rejected at 3σ. If r is below either of the quoted floors, a rejection of these null hypothesis will not inform us about the value of r.

5. CONCLUSIONS

In this white paper, we have provided an overview of 21 cm cosmology, and argued that there is a unique opportunity for the US cosmology community to take a leading role in this field by beginning to plan for a second-generation experiment. We reiterate three main reasons for doing so:

- **The experiment will address pressing science questions.** There have been no major discoveries revealing new physics in the past two decades. Collider experiments, while achieving important milestones such as direct detection of the Higgs boson, have not detected supersymmetry or other signatures that would directly indicate new physics beyond the standard model. In cosmology, the minimal $w = -1$ ΛCDM model has avoided any definitive observational challenge, while minimal progress has been made to uncover the physics of the early Universe. We are proposing a Stage II 21 cm experiment that could advance three possible avenues for finding new physics: deviations from the standard expansion history at high redshift, features in the primordial power spectrum, and measurements of primordial non-Gaussianity. The first item has the potential to directly address some pressing dark energy questions, such as the timing of dark energy domination, while the second and third items are theoretically well-motivated searches that a large 21 cm array is particularly suited to address, and if detected, would present groundbreaking discoveries. In addition to these cornerstone measurements, the experiment will open up a trove of new scientific capabilities, such as providing a unique source screen for gravitational lensing and tidal reconstruction, real-time measurements of the cosmic expansion, and identifying or characterizing exotic transient phenomena in the radio. Finally, a Stage II experiment would constitute a pivotal test ground towards the ultimate goal of opening up the cosmic Dark Ages for direct observations.
- **Now is time to do it.** After the current generation flagship dark energy experiments LSST and DESI, there is not an obvious path to continue following in optical dark energy studies. Pivoting to 21 cm would allow US to become a leader in a fundamentally new and different cosmological observable. Moore's law improvements in the corresponding technology will continue to make this possibility attractive and cost-effective in the foreseeable future.
- **The DOE HEP program is the natural home for this experiment.** As argued in the text, the success of such Stage II experiment lies in a tightly integrated instrument design, calibration and data analysis. The traditional radio astronomy projects are designed to be multi-purpose observatories on which time is allocated though a PI-drive process and are therefore not appropriate for achieving the science goals presented here. On the other hand, DOE has a long pedigree in building and managing large production programs and scientific communities in large HEP-style collaborations. This makes the DOE a natural home for an experiment like this. As argued in Section 2, the science case naturally extends beyond dark energy and here other agencies will probably join the effort in a mode similar to how LSST is being built and operated.
- **The US national lab complex has the right expertise.** A Stage II 21 cm experiment will be a large experiment requiring significant R&D and a large analysis collaboration, and will have significant infrastructural and production components. Traditionally, such experiments were done under auspices of the DOE, as the main mission-driven high energy physics agency. In particular, the DOE brings know-how in RF technology from accelerator and light-source facilities, as well as considerable expertise in high-performance computing (which is crucial, given the potentially enormous data volumes of a Stage II experiment).

In the core of this white paper, Chapters 2 and 3, we have made a case for a concrete experimental design that is an order of magnitude larger than the current generation of 21 cm experiments. We have made forecasts and listed the numerous technical challenges. These first steps elucidate the works that lies ahead. The work should progress on three main fronts:

- **Strengthen the science case.** More work needs to be done to strengthen the science case. All science forecasts should be done with the same forecasting code that will use concrete observing strategy and baseline distributions rather than idealized approximations. Special emphasis must be paid to the modelling of instrumental *systematics* to push beyond forecasts that assume all measurements are thermal noise limited beyond some simple (though conservative) data cuts to deal with foregrounds. These detailed forecasts should be used to optimize the design and understand the pros and cons of different choices for array parameters. The full scientific implications of specific measurements, such as lensing and tidal reconstruction, as well as synergies with other probes and planned surveys, should be better understood. Alternative avenues for recovering information lost to foreground should be explored.
- **Research and develop hardware and calibration systems.** In Chapter 3, we have outlined a number of developments that must occur before a Stage II experiment. Some of them will improve the systematics, and some of them simply control the cost and reliability of such a large experiment. Some of these developments can be designed and tested in laboratory environments, but some will have to employ either 21 cm test-beds such as the BMX experiment at BNL or actual Stage I experiments. These development need to start as soon as possible in order to to be able to converge on an actual design in time.

- **Fully understand implications of Stage I experiments.** Stage I experiments will provide invaluable experience that should be absorbed. Have they achieved not just the primary scientific goals, but also the expected noise performance and systematics control? What were the dominant issues? On this front, one should take advantage of the considerable US presence in 21 cm experiments targeting Cosmic Dawn and reionization. While the scientific output of these experiments lies beyond the DOE purview, the resulting lessons in hardware and data analysis are directly transferable to our proposed Stage II experiment.

- **Ensure that programmatic aspects are solid.** The writing of this white paper helped to generate a kernel collaboration and identify core issues. The next steps are submission to the Astronomy and Astrophysics Decadal Survey and later to the Snowmass and P5 processes.

This whitepaper if the first step on a path towards harnessing the considerable power of 21 cm cosmology. We hope you have enjoyed reading it as much as we have enjoyed writing it.

ACKNOWLEDGMENTS

We thank Chris Carilli, Kyle Dawson and Matt Dobbs for reviewing a draft document and providing many useful comments. We thank Joel Meyers for providing the CMB-S4 noise computation used in Section 2.8. BNL scientists acknowledge generous support of BNL LDRD program which enabled work presented in this whitepaper. DM acknowledges support from the Senior Kavli Institute Fellowships at the University of Cambridge and from the Netherlands organization for scientific research (NWO) VIDI grant (dossier 639.042.730). AO acknowledges support from the INFN grant PD 51 INDARK.

APPENDICES

Appendix A: Counting linear modes

A mode of the density field is classified as "linear" if its wavenumber k falls below some (redshift-dependent) "nonlinear scale" $k_{\rm NL}(z)$, typically defined as the scale at which the variance of the density field becomes order unity. In this document, we use a rather stricter definition, taking $k_{\rm NL}(z)$ to be the scale below which we expect to be able to predict the measured clustering statistics *at the few-percent level*. A conservative estimate of this scale can be obtained from the rms displacement Σ in the Zel'dovich approximation:

$$k_{\rm NL}(z) \approx \Sigma(z)^{-1} = \left[\frac{1}{6\pi^2}\int_0^\infty dk\, P_{\rm lin}(k,z)\right]^{-1/2} . \tag{A1}$$

We show the associated $k_{\rm NL}(z)$ curve in Figure 25. Note that this is the scale we estimate for the validity of one-loop perturbation theory; calculations carried out to higher order (e.g. [310]) indicate that higher values of $k_{\rm NL}(z)$ may be achievable, which would imply a substantial increase in the number of linear modes, but further work will be required before these calculations are ready to apply to data.

The cumulative number of linear modes below redshift $z_{\rm max}$ is given by (e.g. [311])

$$N_{\rm modes} = \frac{1}{(2\pi)^3}\int_0^{z_{\rm max}} dz \frac{dV}{dz}\int_{k_{\rm min}}^{k_{\rm NL}(z)} d^3\boldsymbol{k} \approx \frac{2}{3\pi}\int_0^{z_{\rm max}} dz\, \chi(z)^2 \frac{d\chi}{dz} k_{\rm NL}(z)^3 . \tag{A2}$$

In the second equality, we have taken $k_{\rm min} = 0$ (which has a negligible effect on the results) and used $dV/dz = 4\pi\chi(z)^2 d\chi/dz$, where $\chi(z)$ is the comoving distance to redshift z. In the presence of a foreground wedge (Appendix C), we multiply the integrand above by the factor

$$\Theta\left(k^2\mu^2 - k^2(1-\mu)^2\left[\frac{\chi(z)H(z)}{c(1+z)}\sin(\theta_w)\right]^2\right) , \tag{A3}$$

where $\Theta(\cdot)$ is the Heaviside function and $\mu = \hat{k}\cdot\hat{z}$.

Appendix B: Assumptions about 21 cm signal

The 21 cm brightness temperature is assumed to be

$$T_{\rm b} = 180{\rm mK}(1+z)^2\left(H(z)/H_0(z)\right)^{-1} \times \left(4\times10^{-4}(1+z)^{0.6}\right) , \tag{B1}$$

where the expression in the last bracket approximates the cosmic evolution of $\Omega_{\rm HI}$. This is consistent with [70] and other recent literature. For derivation of the brightness temperature, see e.g. [312]. We have in addition assumed evolution of cosmic $\Omega_{\rm HI}$ from [313].

The total power-spectrum signal observed by the radio interferometer is given by

$$P(\mathbf{k}) = T_{\rm b}^2[(b+f\mu^2)^2 P(k) + P_{\rm SN}] + P_{\rm N}, \tag{B2}$$

where the first term is the large-scale power spectrum modeled using linear biasing and redshift-space distortions, $P_{\rm SN}$ is the shot-noise contribution from halos making up the neutral hydrogen signal (and usually irrelevant) and $P_{\rm N}$ is the noise coming from the finite system temperature of the instrument (see App. D).

At the high redshifts considered here, the linear biasing assumption should be a decent approximation down to considerably smaller scales than for galaxies at lower redshift. Following [69], we assume an *effective* maximum wave-number $k_{\rm max,eff} = 0.4\,h\,{\rm Mpc}^{-1}$. The idea is that in practice one will fit the data to somewhat larger k, which would allow one to constrain and marginalise beyond-linear order bias parameters. For neutral hydrogen large-scale bias and shot-noise, we used results from [19]. While the shot-noise term is highly uncertain, it is also very sub-dominant and does not significantly affect results. We assume a Planck 2015 best-fit cosmology, an assumption that should not affect the results in any significant way.

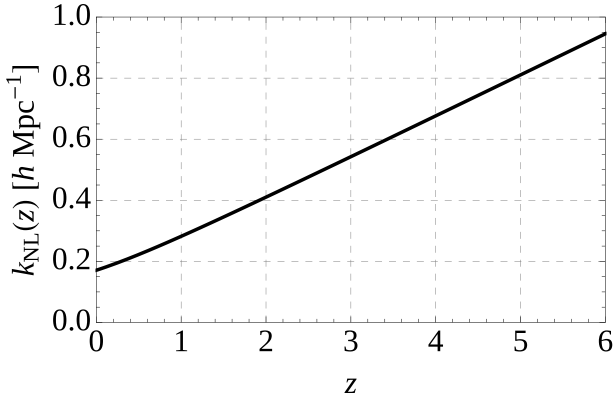

FIG. 25. Numerical results based on our definition of the nonlinear scale $k_{\rm NL}(z)$ (see main text), which is an estimate for where the statistics of modes with $k < k_{\rm NL}(z)$ can be predicted with few-percent precision.

Appendix C: Foreground filtering and foreground wedge considerations

Foregrounds present a major calibration issue for 21 cm cosmology. At a minimum, one loses low $k_\parallel$ modes due to filtering of smooth foregrounds. Many foregrounds on the sky are (within a crude approximation) slowly varying functions of frequency [314–316], so a perfectly calibrated instrument will have a minimum accessible (i.e., not foreground contaminated) value of $k_\parallel$ corresponding to the fundamental mode that fits in the radial range under consideration. In practice, however, amplifier gain stability and beam response changes due to changing environmental factors (e.g. temperature affecting the shape of the reflector), mean that the lowest accessible $k_\parallel$ will be somewhat higher. It is useful to parameterize this in terms of the fractional bandwidth over which we consider the instrument can be perfectly calibrated, since both mechanical and analog electronic drivers scale with $\Delta f/f$. In Figure 26 we plot the minimum value of $k_\parallel$ (and thus total $k = \sqrt{k_\parallel^2 + k_\perp^2}$) accessible as a function of fractional bandwidth. We find that it is only a weak function of redshift. For 20% fractional bandwidth we find that $k_{\rm min} \simeq 10^{-2}\,h\,{\rm Mpc}^{-1}$ is appropriate over a wide range of redshifts. We shall assume this $k_{\rm min}$ in our forecasts.

A different issue, first discovered in the context of the epoch of reionization experiments is the the foreground wedge [15–17, 220, 317–331] (see also Section 1.5). It has mainly been studied for interferometric 21 cm experiments, although a related issue also exists for single-dish experiments. The foreground wedge results from the fact that a given interferometric baseline has a fixed physical length, which implies that it probes different angular scales at different frequencies ($\theta \propto \lambda^{-1}$). Interferometers are therefore inherently chromatic, and intrinsically smooth-spectrum foregrounds can appear to have significantly more complicated spectra. This effect can be reduced by careful inter-baseline calibration, which could in principle be achieved by a carefully designed array with a sufficient density of baselines. Achieving such calibration requirements in existing experiments, however, has proven elusive.

We model the 'wedge' as a cut on μ, the cosine of the angle along the line of sight, assuming all signal modes with $\mu < \mu_w$ are lost. The wedge is particularly acute at higher redshifts, since the value of μ_w increases with redshift (Eq. C1). In general, the wedge effects can be thought of as being caused by sources from different parts of the sky, with sources away from phase center being particularly affected. The most pessimistic case (known as the "horizon wedge") assumes all sources above the horizon can contaminate the signal. We take a less pessimistic assumption, and only consider contamination from sources that are no further than N_w times the size of the primary beam away from the beam center. In Figure 6, we show the effective loss of observed volume and number of linear modes for these cases for an experiment with 6-m dishes. We see that the effect is dramatic for the horizon wedge, but even in this case our fiducial experiment achieves a fifty-fold increase in the number of measured linear modes compared to an optical survey at $z < 2$.

We take the position that this systematic will have to be overcome to fully exploit the possibilities offered by the 21 cm technique. We reiterate that it is a technical rather than fundamental problem. Instrumental design choices are vital to support this – for example, dishes result in a characteristic 'pitchfork'-shaped region of foreground contamination within the wedge, which leaves modes between the pure radial ($k_\parallel \sim 0$) and horizon boundary of the wedge relatively uncontaminated, while dipoles have strong contamination throughout the entire wedge region in Fourier space (i.e., it results in the loss of all modes with $\mu < \mu_w$). Other design choices, such as reducing sidelobes and generally improving the stability of the primary beam response with frequency will also be valuable for allowing modes inside the wedge to be recovered. There have also been promising methodological advances that render full wedge calibration realistic in the future [18]. Therefore, when forecasting, we use two possibilities: we either assume that the wedge has been completely calibrated out (optimistic) or that calibration allows us to cut at $N_w = 3$ times the position of the primary beam (pessimistic). This is motivated by the notion that for a typical

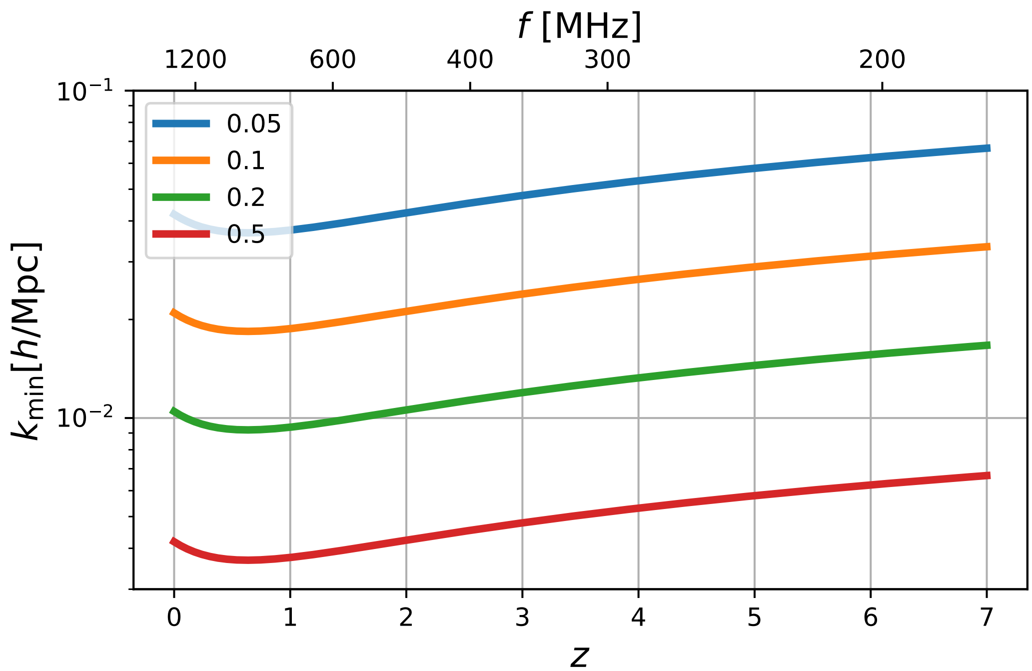

FIG. 26. The minimum $k_\parallel$ accessible as a function of redshift for different choices of fractional bandwidth. Note that the curves are quite flat as a function of redshift. For $\Delta f/f = 0.2$, $k_{\rm min} \simeq 10^{-2}\, h\, {\rm Mpc}^{-1}$ which we shall assume for our forecasts.

antenna design, the beam response is suppressed at the signal/foreground level at those distances.

The $N_w = 3\times$ primary-beam wedge assumption was realised by only considering modes that satisfy

$$k_\parallel > k_\perp \frac{\chi(z)H(z)}{c(1+z)} \sin(\theta_w), \tag{C1}$$

where θ_w is the maximum angle at which fringes from a monochromatic point source can enter the measurement and be confused with a non-monochromatic source at phase center. Given that the beam shape is idealised in our experiment, we take $\theta_w = N_w 1.22\lambda/2D$[14], although other choices can be found in the literature, e.g. $\theta_w = N_w 1.06\lambda/2D$ [332].

Appendix D: Instrumental noise of Stage II experiment

The Stage II experiment was assumed to be a compact array of $D =$ 6-m fully illuminated dishes in a square array with side of $N_s = 256$ (so that there are $N_s \times N_s$ total receivers). We assumed an integration time of 5 years (at 100% efficiency) over half the sky ($f_{\rm sky} = 0.5$) with a system noise temperature of $T_{\rm sys} = 50$K.

At these frequencies, the system temperature is eclipsed by the sky temperature, which we take to be

$$T_{\rm sky}(f) = \left(\frac{f}{400{\rm MHz}}\right)^{-2.75} 25{\rm K} + 2.7{\rm K}. \tag{D1}$$

This approximation is consistent with assumptions made in the SKA forecasting exercise [333, 334] and also with effective temperature derived by averaging T^{-2} over the Haslam 408 MHz galaxy map [335] (i.e. approximately taking into account the inverse variance weighting one might do in practice)

For the system noise, we assumed the limit of uniform coverage in the $u - v$ plane, namely

$$P_N = T_{\rm sys}^2 r^2 \left(\frac{\lambda(1+z)}{H(z)}\right) \left(\frac{\lambda^2}{A_e}\right)^2 \left(\frac{1}{2n_b(u)t}\right) \left(\frac{S_{\rm Area}}{\rm FOV}\right), \tag{D2}$$

[14] We note that the factor of 2 in the denominator here is ad-hoc, for an airy disk, the first null as measured from the center is at $1.22\lambda/D$ and we then take this distance to represent an effective full width.

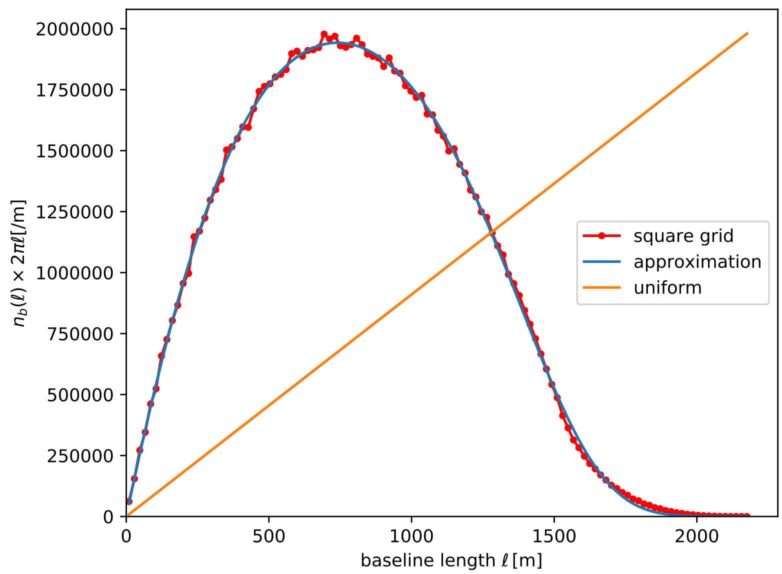

FIG. 27. The number of baselines per unit radial distance (i.e. the integral under the above curve equals to the total number of baselines) for the Stage II experiment. We plot the exact numerical results in red, our fitting formula in blue and the approximation of constant $n_b(u)$ in orange.

where r is the comoving distance to the observed slice, $\lambda_0 \sim 21$cm is the transition rest-frame frequency, $\lambda = \lambda_0(1+z)$ is the observing wavelength, $n_b(u)$ is the number density of baselines, $S_{\rm area}$ is the total survey area and FOV is the field of view of each receiver. The quantity $A_e = 3/4\pi D^2\eta$ is the area per feed where we for simplicity assume unit efficiency $\eta = 1$.

Many results in the literature rely on the approximation that the baseline density is independent of u up to some maximum baseline length $u_{\rm max}$:

$$n_b(u) = \frac{N_r^2/2}{\pi u_{\rm max}^2}. \tag{D3}$$

We have found that this is a surprisingly poor approximation (see Figure 27 also discussed below). Instead we use the following fitting formula for the number of baselines as a function of physical distance of antennas

$$n_b(l) = n_0 \frac{a + b(l/L)}{1 + c(l/L)^d} e^{-(l/L)^e}, \tag{D4}$$

where $n_0 = (N_s/D)^2$ and $L = N_s D$ with $n_b(u) = n_b(l = u\lambda)\lambda^2$. This formula has been fitted to our fiducial case and calibrated so that $\int n_b(u) d^2u = N_s^2/2$. The fitting parameters are $a = 0.4847, b = -0.3300, c = 1.3157, d = 1.5974, e = 6.8390$. It works well down to a very small value of N_s; even with $N_s = 8$ the total number of baselines is correct to 1.5%. Figure 27 shows the numerical result together with the fitting formula. The shown formula is only true for an observing field at zenith, but we ignore this effect in our forecasting.

Appendix E: Figures 4 and 5

Figures 4 and 5 were made as follows. A numerical simulation with 3072^3 particles in a box of size 300 Mpc/h has been run using the L-PICOLA code [336]. Halos were identified using the Friends-of-Friends algorithm [337], with a value of the linking length parameter $b = 0.2$. Neutral hydrogen was then assigned to halos according to [20].

For LSST we assumed a photometric error of $\sigma_z = 0.032(1+z)$ and number density according to the fitting formula from the Appendix of [338].

For dropout survey we assumed number densities of $1.6\times10^{-4}/({\rm Mpc}/h)^3$ ($m_{\rm UV} < 24$) and $6.0\times10^{-4}/({\rm Mpc}/h)^3$ ($m_{\rm UV} < 24.5$) at $z = 3$ and $5\times10^{-6}/({\rm Mpc}/h)^3$ ($m_{\rm UV} < 24$) and $4\times10^{-5}/({\rm Mpc}/h)^3$ ($m_{\rm UV} < 24.5$) at $z = 5$ respectively, following [339].

For Stage 2 we have assumed foreground filtering of modes with $k_{\parallel} < 0.01h$/Mpc, which for the simulation size of this box filters just modes with $k_{\parallel} = 0$ and $k_{\perp} \geq 0$. For beam filtering we have applied a simple Gaussian filtering with variance given by the linear size of the array.

Appendix F: Tabulated forecasts

Redshift	Bias	Effective $\bar{n}$	$\alpha_\perp$ S-2	$\alpha_\parallel$ S-2	$\alpha_\perp$ SVL	$\alpha_\parallel$ SVL
2.0	1.88	12	0.41	0.90	0.27	0.44
2.1	1.92	14	0.40	0.87	0.27	0.43
2.2	1.96	15	0.39	0.84	0.26	0.43
2.3	2.00	16	0.38	0.81	0.26	0.43
2.4	2.04	17	0.38	0.79	0.26	0.43
2.5	2.08	19	0.37	0.77	0.26	0.43
2.6	2.12	20	0.36	0.76	0.26	0.43
2.7	2.17	21	0.36	0.74	0.26	0.43
2.8	2.21	22	0.36	0.73	0.26	0.43
2.9	2.26	23	0.35	0.71	0.27	0.43
3.0	2.30	24	0.35	0.70	0.27	0.43
3.1	2.35	25	0.35	0.69	0.27	0.44
3.2	2.40	26	0.34	0.68	0.27	0.44
3.3	2.45	27	0.34	0.68	0.27	0.44
3.4	2.50	28	0.34	0.67	0.27	0.44
3.5	2.55	28	0.34	0.66	0.27	0.44
3.6	2.60	29	0.34	0.66	0.27	0.44
3.7	2.65	29	0.34	0.65	0.27	0.45
3.8	2.71	29	0.34	0.65	0.27	0.45
3.9	2.76	29	0.34	0.64	0.28	0.45
4.0	2.82	29	0.34	0.64	0.28	0.45
4.1	2.88	29	0.34	0.64	0.28	0.46
4.2	2.93	29	0.34	0.63	0.28	0.46
4.3	2.99	29	0.34	0.63	0.28	0.46
4.4	3.05	28	0.34	0.63	0.28	0.46
4.5	3.11	28	0.34	0.63	0.28	0.47
4.6	3.17	27	0.34	0.63	0.29	0.47
4.7	3.23	27	0.34	0.63	0.29	0.47
4.8	3.30	26	0.34	0.62	0.29	0.47
4.9	3.36	25	0.34	0.62	0.29	0.48
5.0	3.43	25	0.34	0.62	0.29	0.48
5.1	3.49	24	0.34	0.62	0.29	0.48
5.2	3.56	23	0.35	0.62	0.30	0.48
5.3	3.63	22	0.35	0.62	0.30	0.49
5.4	3.70	22	0.35	0.63	0.30	0.49
5.5	3.77	21	0.35	0.63	0.30	0.49
5.6	3.84	20	0.35	0.63	0.30	0.49
5.7	3.91	19	0.35	0.63	0.30	0.50
5.8	3.98	18	0.36	0.63	0.31	0.50
5.9	4.06	18	0.36	0.63	0.31	0.50
6.0	4.13	17	0.36	0.63	0.31	0.51

TABLE IX. The BAO constraints derived in Section 2.3 are as shown in the following table, together with effective number density (i.e the number density at a galaxy survey would have the same errorbars on power spectrum as the radio intensity mapping experiment) at $k = 0.2h/\mathrm{Mpc}$. Errors in expressed in percent. The last two columns show errors for a sample variance limited experiment over half the sky.

	Optimistic foregrounds			Pessimistic foregrounds		
Redshift	10% prior	5% prior	1% prior	10% prior	5% prior	1% prior
2.0	0.100	0.050	0.010	0.100	0.050	0.010
2.2	0.100	0.050	0.010	0.100	0.050	0.010
2.3	0.100	0.050	0.010	0.100	0.050	0.010
2.5	0.100	0.050	0.010	0.100	0.050	0.010
2.6	0.100	0.050	0.010	0.100	0.050	0.011
2.8	0.100	0.050	0.010	0.100	0.050	0.011
3.0	0.100	0.050	0.010	0.100	0.050	0.011
3.1	0.100	0.050	0.010	0.100	0.050	0.011
3.3	0.100	0.050	0.010	0.100	0.050	0.011
3.4	0.100	0.050	0.010	0.100	0.050	0.011
3.6	0.100	0.050	0.010	0.100	0.050	0.011
3.8	0.100	0.050	0.011	0.100	0.050	0.012
3.9	0.100	0.050	0.011	0.100	0.050	0.012
4.1	0.100	0.050	0.011	0.100	0.051	0.013
4.2	0.100	0.050	0.011	0.100	0.051	0.013
4.4	0.100	0.050	0.011	0.100	0.051	0.014
4.6	0.100	0.050	0.011	0.101	0.051	0.015
4.7	0.100	0.050	0.011	0.101	0.051	0.015
4.9	0.100	0.050	0.011	0.101	0.052	0.017
5.0	0.100	0.050	0.011	0.101	0.052	0.018
5.2	0.100	0.050	0.011	0.101	0.053	0.019
5.4	0.100	0.050	0.011	0.102	0.053	0.021
5.5	0.100	0.050	0.011	0.102	0.054	0.023
5.7	0.100	0.050	0.012	0.103	0.055	0.026
5.8	0.100	0.050	0.012	0.103	0.057	0.028
6.0	0.100	0.050	0.012	0.104	0.058	0.032

TABLE X. The RSD constraints plotted in Figure 12. The first three columns after redshift column are relative errors on $f\sigma_8$ for optimistic foreground modeling with 10%, 5% and 1% prior on $\Omega_{\rm HI}$, while that remaining three are the same for pessimistic foreground modeling.

[1] S. Dodelson, K. Heitmann, C. Hirata, K. Honscheid, A. Roodman, U. Seljak, A. Slosar, and M. Trodden, ArXiv e-prints (2016), arXiv:1604.07626.
[2] S. Dodelson, K. Heitmann, C. Hirata, K. Honscheid, A. Roodman, U. Seljak, A. Slosar, and M. Trodden, ArXiv e-prints (2016), arXiv:1604.07821 [astro-ph.IM].
[3] K. Dawson, J. Frieman, K. Heitmann, B. Jain, S. Kahn, R. Mandelbaum, S. Perlmutter, and A. Slosar, ArXiv e-prints (2018), arXiv:1802.07216.
[4] DESI Collaboration, A. Aghamousa, J. Aguilar, S. Ahlen, S. Alam, L. E. Allen, C. Allende Prieto, J. Annis, S. Bailey, C. Balland, and et al., ArXiv e-prints (2016), arXiv:1611.00036 [astro-ph.IM].
[5] LSST Science Collaboration, P. A. Abell, J. Allison, S. F. Anderson, J. R. Andrew, J. R. P. Angel, L. Armus, D. Arnett, S. J. Asztalos, T. S. Axelrod, and et al., ArXiv e-prints (2009), arXiv:0912.0201 [astro-ph.IM].
[6] J. B. Peterson, K. Bandura, and U. L. Pen, ArXiv Astrophysics e-prints (2006), arXiv:astro-ph/0606104.
[7] T.-C. Chang, U.-L. Pen, K. Bandura, and J. B. Peterson, Nature **466**, 463 (2010).
[8] M. Davis, J. A. Newman, S. M. Faber, and A. C. Phillips, in *Deep Fields*, edited by S. Cristiani, A. Renzini, and R. E. Williams (2001) p. 241, astro-ph/0012189.
[9] K. W. Masui, E. R. Switzer, N. Banavar, K. Bandura, C. Blake, L.-M. Calin, T.-C. Chang, X. Chen, Y.-C. Li, Y.-W. Liao, A. Natarajan, U.-L. Pen, J. B. Peterson, J. R. Shaw, and T. C. Voytek, ApJ **763**, L20 (2013), arXiv:1208.0331 [astro-ph.CO].
[10] M. J. Drinkwater, R. J. Jurek, C. Blake, D. Woods, K. A. Pimbblet, K. Glazebrook, R. Sharp, M. B. Pracy, S. Brough, M. Colless, W. J. Couch, S. M. Croom, T. M. Davis, D. Forbes, K. Forster, D. G. Gilbank, M. Gladders, B. Jelliffe, N. Jones, I.-H. Li, B. Madore, D. C. Martin, G. B. Poole, T. Small, E. Wisnioski, T. Wyder, and H. K. C. Yee, MNRAS **401**, 1429 (2010), arXiv:0911.4246.
[11] E. R. Switzer, K. W. Masui, K. Bandura, L.-M. Calin, T.-C. Chang, X.-L. Chen, Y.-C. Li, Y.-W. Liao, A. Natarajan, U.-L. Pen, J. B. Peterson, J. R. Shaw, and T. C. Voytek, MNRAS **434**, L46 (2013), arXiv:1304.3712 [astro-ph.CO].
[12] P. C. Boyle and Chime/Frb Collaboration, The Astronomer's Telegram **11901** (2018).
[13] F. Villaescusa-Navarro, D. Alonso, and M. Viel, Mon. Not. Roy. Astron. Soc. **466**, 2736 (2017), arXiv:1609.00019 [astro-ph.CO].
[14] P. Bull, ApJ **817**, 26 (2016), arXiv:1509.07562.
[15] A. R. Parsons, J. C. Pober, J. E. Aguirre, C. L. Carilli, D. C. Jacobs, and D. F. Moore, ApJ **756**, 165 (2012), arXiv:1204.4749 [astro-ph.IM].
[16] A. Liu, A. R. Parsons, and C. M. Trott, Phys. Rev. D **90**, 023018 (2014), arXiv:1404.2596.
[17] A. Liu, A. R. Parsons, and C. M. Trott, Phys. Rev. D **90**, 023019 (2014), arXiv:1404.4372.
[18] A. Ghosh, F. Mertens, and L. V. E. Koopmans, Mon. Not. Roy. Astron. Soc. **474**, 4552 (2018), arXiv:1709.06752 [astro-ph.CO].
[19] E. Castorina and F. Villaescusa-Navarro, MNRAS **471**, 1788 (2017), arXiv:1609.05157.
[20] F. Villaescusa-Navarro, S. Genel, E. Castorina, A. Obuljen, D. N. Spergel, L. Hernquist, D. Nelson, I. P. Carucci, A. Pillepich, F. Marinacci, B. Diemer, M. Vogelsberger, R. Weinberger, and R. Pakmor, ArXiv e-prints (2018), arXiv:1804.09180.
[21] C. W. Stark, M. White, K.-G. Lee, and J. F. Hennawi, MNRAS **453**, 311 (2015), arXiv:1412.1507.
[22] C. W. Stark, A. Font-Ribera, M. White, and K.-G. Lee, MNRAS **453**, 4311 (2015), arXiv:1504.03290.
[23] Y. Harikane, M. Ouchi, Y. Ono, S. Saito, P. Behroozi, S. More, K. Shimasaku, J. Toshikawa, Y.-T. Lin, M. Akiyama, J. Coupon, Y. Komiyama, A. Konno, S.-C. Lin, S. Miyazaki, A. J. Nishizawa, T. Shibuya, and J. Silverman, PASJ **70**, S11 (2018), arXiv:1704.06535.
[24] B. Jain and J. Khoury, Annals of Physics **325**, 1479 (2010), arXiv:1004.3294.
[25] T. Clifton, P. G. Ferreira, A. Padilla, and C. Skordis, Phys. Rept. **513**, 1 (2012), arXiv:1106.2476 [astro-ph.CO].
[26] D. H. Weinberg, M. J. Mortonson, D. J. Eisenstein, C. Hirata, A. G. Riess, and E. Rozo, Phys. Rep. **530**, 87 (2013), arXiv:1201.2434.
[27] A. Joyce, B. Jain, J. Khoury, and M. Trodden, Phys. Rep. **568**, 1 (2015), arXiv:1407.0059.
[28] A. Joyce, L. Lombriser, and F. Schmidt, Annual Review of Nuclear and Particle Science **66**, 95 (2016), arXiv:1601.06133.
[29] L. Amendola, S. Appleby, A. Avgoustidis, D. Bacon, T. Baker, M. Baldi, N. Bartolo, A. Blanchard, C. Bonvin, S. Borgani, E. Branchini, C. Burrage, S. Camera, C. Carbone, L. Casarini, M. Cropper, C. de Rham, J. P. Dietrich, C. Di Porto, R. Durrer, A. Ealet, P. G. Ferreira, F. Finelli, J. García-Bellido, T. Giannantonio, L. Guzzo, A. Heavens, L. Heisenberg, C. Heymans, H. Hoekstra, L. Hollenstein, R. Holmes, Z. Hwang, K. Jahnke, T. D. Kitching, T. Koivisto, M. Kunz, G. La Vacca, E. Linder, M. March, V. Marra, C. Martins, E. Majerotto, D. Markovic, D. Marsh, F. Marulli, R. Massey, Y. Mellier, F. Montanari, D. F. Mota, N. J. Nunes, W. Percival, V. Pettorino, C. Porciani, C. Quercellini, J. Read, M. Rinaldi, D. Sapone, I. Sawicki, R. Scaramella, C. Skordis, F. Simpson, A. Taylor, S. Thomas, R. Trotta, L. Verde, F. Vernizzi, A. Vollmer, Y. Wang, J. Weller, and T. Zlosnik, Living Reviews in Relativity **21**, 2 (2018).
[30] L. Amendola, S. Appleby, D. Bacon, T. Baker, M. Baldi, N. Bartolo, A. Blanchard, C. Bonvin, S. Borgani, E. Branchini, C. Burrage, S. Camera, C. Carbone, L. Casarini, M. Cropper, C. de Rham, C. Di Porto, A. Ealet, P. G. Ferreira, F. Finelli, J. García-Bellido, T. Giannantonio, L. Guzzo, A. Heavens, L. Heisenberg, C. Heymans, H. Hoekstra, L. Hollenstein, R. Holmes, O. Horst, K. Jahnke, T. D. Kitching, T. Koivisto, M. Kunz, G. La Vacca, M. March, E. Majerotto, K. Markovic, D. Marsh, F. Marulli, R. Massey, Y. Mellier, D. F. Mota, N. J. Nunes, W. Percival, V. Pettorino, C. Porciani, C. Quercellini, J. Read, M. Rinaldi, D. Sapone, R. Scaramella, C. Skordis, F. Simpson, A. Taylor, S. Thomas, R. Trotta, L. Verde, F. Vernizzi, A. Vollmer, Y. Wang, J. Weller, and T. Zlosnik, Living Reviews in Relativity **16**, 6 (2013), arXiv:1206.1225.
[31] B. Jain, A. Joyce, R. Thompson, A. Upadhye, J. Battat, P. Brax, A.-C. Davis, C. de Rham, S. Dodelson, A. Erickcek, G. Gabadadze, W. Hu, L. Hui, D. Huterer, M. Kamionkowski, J. Khoury, K. Koyama, B. Li, E. Linder, F. Schmidt, R. Scoccimarro, G. Starkman, C. Stubbs, M. Takada, A. Tolley, M. Trodden, J.-P. Uzan, V. Vikram, A. Weltman, M. Wyman, D. Zaritsky, and G. Zhao, ArXiv e-prints (2013), arXiv:1309.5389 [astro-ph.CO].
[32] L. Amendola, M. Kunz, M. Motta, I. D. Saltas, and I. Sawicki, Phys. Rev. D **87**, 023501 (2013), arXiv:1210.0439 [astro-ph.CO].

[33] T. Baker, P. G. Ferreira, C. D. Leonard, and M. Motta, Phys. Rev. D **90**, 124030 (2014), arXiv:1409.8284.
[34] C. D. Leonard, T. Baker, and P. G. Ferreira, Phys. Rev. D **91**, 083504 (2015), arXiv:1501.03509.
[35] J. Khoury and A. Weltman, Phys. Rev. **D69**, 044026 (2004), arXiv:astro-ph/0309411 [astro-ph].
[36] K. Hinterbichler and J. Khoury, Physical Review Letters **104**, 231301 (2010), arXiv:1001.4525 [hep-th].
[37] P. Brax, A.-C. Davis, B. Li, and H. A. Winther, Phys. Rev. D **86**, 044015 (2012), arXiv:1203.4812 [astro-ph.CO].
[38] K. Koyama, Reports on Progress in Physics **79**, 046902 (2016), arXiv:1504.04623.
[39] T. Baker, D. Psaltis, and C. Skordis, ApJ **802**, 63 (2015), arXiv:1412.3455.
[40] E. Berti, E. Barausse, V. Cardoso, L. Gualtieri, P. Pani, U. Sperhake, L. C. Stein, N. Wex, K. Yagi, T. Baker, C. P. Burgess, F. S. Coelho, D. Doneva, A. De Felice, P. G. Ferreira, P. C. C. Freire, J. Healy, C. Herdeiro, M. Horbatsch, B. Kleihaus, A. Klein, K. Kokkotas, J. Kunz, P. Laguna, R. N. Lang, T. G. F. Li, T. Littenberg, A. Matas, S. Mirshekari, H. Okawa, E. Radu, R. O'Shaughnessy, B. S. Sathyaprakash, C. Van Den Broeck, H. A. Winther, H. Witek, M. Emad Aghili, J. Alsing, B. Bolen, L. Bombelli, S. Caudill, L. Chen, J. C. Degollado, R. Fujita, C. Gao, D. Gerosa, S. Kamali, H. O. Silva, J. G. Rosa, L. Sadeghian, M. Sampaio, H. Sotani, and M. Zilhao, Classical and Quantum Gravity **32**, 243001 (2015), arXiv:1501.07274 [gr-qc].
[41] G. Gubitosi, F. Piazza, and F. Vernizzi, J. Cosmology Astropart. Phys. **2**, 032 (2013), arXiv:1210.0201 [hep-th].
[42] J. Bloomfield, É. É. Flanagan, M. Park, and S. Watson, J. Cosmology Astropart. Phys. **8**, 010 (2013), arXiv:1211.7054 [astro-ph.CO].
[43] E. Bellini and I. Sawicki, J. Cosmology Astropart. Phys. **7**, 050 (2014), arXiv:1404.3713.
[44] B. P. Abbott, R. Abbott, T. D. Abbott, F. Acernese, K. Ackley, C. Adams, T. Adams, P. Addesso, R. X. Adhikari, V. B. Adya, and et al., ApJ **848**, L13 (2017), arXiv:1710.05834 [astro-ph.HE].
[45] L. Lombriser and A. Taylor, J. Cosmology Astropart. Phys. **3**, 031 (2016), arXiv:1509.08458.
[46] P. Creminelli and F. Vernizzi, Physical Review Letters **119**, 251302 (2017), arXiv:1710.05877.
[47] J. Sakstein and B. Jain, Physical Review Letters **119**, 251303 (2017), arXiv:1710.05893.
[48] J. M. Ezquiaga and M. Zumalacárregui, Physical Review Letters **119**, 251304 (2017), arXiv:1710.05901.
[49] T. Baker, E. Bellini, P. G. Ferreira, M. Lagos, J. Noller, and I. Sawicki, Physical Review Letters **119**, 251301 (2017), arXiv:1710.06394.
[50] L. Amendola, M. Kunz, I. D. Saltas, and I. Sawicki, Physical Review Letters **120**, 131101 (2018), arXiv:1711.04825.
[51] C. de Rham and S. Melville, (2018), arXiv:1806.09417 [hep-th].
[52] M. Raveri, P. Bull, A. Silvestri, and L. Pogosian, Phys. Rev. D **96**, 083509 (2017), arXiv:1703.05297.
[53] E. V. Linder, Phys. Rev. D **73**, 063010 (2006), astro-ph/0601052.
[54] C. di Porto and L. Amendola, Phys. Rev. D **77**, 083508 (2008), arXiv:0707.2686.
[55] F. Simpson and J. A. Peacock, Phys. Rev. D **81**, 043512 (2010), arXiv:0910.3834 [astro-ph.CO].
[56] T. Baker, P. Ferreira, and C. Skordis, Phys. Rev. D **89**, 024026 (2014), arXiv:1310.1086.
[57] L. Perenon, F. Piazza, C. Marinoni, and L. Hui, JCAP **1511**, 029 (2015), arXiv:1506.03047 [astro-ph.CO].
[58] D. H. Weinberg, M. J. Mortonson, D. J. Eisenstein, C. Hirata, A. G. Riess, and E. Rozo, Phys. Rep. **530**, 87 (2013), arXiv:1201.2434.
[59] W. Percival, Physics Today **70**, 32 (2017).
[60] M. Tanabashi, K. Hagiwara, K. Hikasa, K. Nakamura, Y. Sumino, F. Takahashi, J. Tanaka, K. Agashe, G. Aielli, C. Amsler, M. Antonelli, D. M. Asner, H. Baer, S. Banerjee, R. M. Barnett, T. Basaglia, C. W. Bauer, J. J. Beatty, V. I. Belousov, J. Beringer, S. Bethke, A. Bettini, H. Bichsel, O. Biebel, K. M. Black, E. Blucher, O. Buchmuller, V. Burkert, M. A. Bychkov, R. N. Cahn, M. Carena, A. Ceccucci, A. Cerri, D. Chakraborty, M.-C. Chen, R. S. Chivukula, G. Cowan, O. Dahl, G. D'Ambrosio, T. Damour, D. de Florian, A. de Gouvêa, T. DeGrand, P. de Jong, G. Dissertori, B. A. Dobrescu, M. D'Onofrio, M. Doser, M. Drees, H. K. Dreiner, D. A. Dwyer, P. Eerola, S. Eidelman, J. Ellis, J. Erler, V. V. Ezhela, W. Fetscher, B. D. Fields, R. Firestone, B. Foster, A. Freitas, H. Gallagher, L. Garren, H.-J. Gerber, G. Gerbier, T. Gershon, Y. Gershtein, T. Gherghetta, A. A. Godizov, M. Goodman, C. Grab, A. V. Gritsan, C. Grojean, D. E. Groom, M. Grünewald, A. Gurtu, T. Gutsche, H. E. Haber, C. Hanhart, S. Hashimoto, Y. Hayato, K. G. Hayes, A. Hebecker, S. Heinemeyer, B. Heltsley, J. J. Hernández-Rey, J. Hisano, A. Höcker, J. Holder, A. Holtkamp, T. Hyodo, K. D. Irwin, K. F. Johnson, M. Kado, M. Karliner, U. F. Katz, S. R. Klein, E. Klempt, R. V. Kowalewski, F. Krauss, M. Kreps, B. Krusche, Y. V. Kuyanov, Y. Kwon, O. Lahav, J. Laiho, J. Lesgourgues, A. Liddle, Z. Ligeti, C.-J. Lin, C. Lippmann, T. M. Liss, L. Littenberg, K. S. Lugovsky, S. B. Lugovsky, A. Lusiani, Y. Makida, F. Maltoni, T. Mannel, A. V. Manohar, W. J. Marciano, A. D. Martin, A. Masoni, J. Matthews, U.-G. Meißner, D. Milstead, R. E. Mitchell, K. Mönig, P. Molaro, F. Moortgat, M. Moskovic, H. Murayama, M. Narain, P. Nason, S. Navas, M. Neubert, P. Nevski, Y. Nir, K. A. Olive, S. Pagan Griso, J. Parsons, C. Patrignani, J. A. Peacock, M. Pennington, S. T. Petcov, V. A. Petrov, E. Pianori, A. Piepke, A. Pomarol, A. Quadt, J. Rademacker, G. Raffelt, B. N. Ratcliff, P. Richardson, A. Ringwald, S. Roesler, S. Rolli, A. Romaniouk, L. J. Rosenberg, J. L. Rosner, G. Rybka, R. A. Ryutin, C. T. Sachrajda, Y. Sakai, G. P. Salam, S. Sarkar, F. Sauli, O. Schneider, K. Scholberg, A. J. Schwartz, D. Scott, V. Sharma, S. R. Sharpe, T. Shutt, M. Silari, T. Sjöstrand, P. Skands, T. Skwarnicki, J. G. Smith, G. F. Smoot, S. Spanier, H. Spieler, C. Spiering, A. Stahl, S. L. Stone, T. Sumiyoshi, M. J. Syphers, K. Terashi, J. Terning, U. Thoma, R. S. Thorne, L. Tiator, M. Titov, N. P. Tkachenko, N. A. Törnqvist, D. R. Tovey, G. Valencia, R. Van de Water, N. Varelas, G. Venanzoni, L. Verde, M. G. Vincter, P. Vogel, A. Vogt, S. P. Wakely, W. Walkowiak, C. W. Walter, D. Wands, D. R. Ward, M. O. Wascko, G. Weiglein, D. H. Weinberg, E. J. Weinberg, M. White, L. R. Wiencke, S. Willocq, C. G. Wohl, J. Womersley, C. L. Woody, R. L. Workman, W.-M. Yao, G. P. Zeller, O. V. Zenin, R.-Y. Zhu, S.-L. Zhu, F. Zimmermann, P. A. Zyla, J. Anderson, L. Fuller, V. S. Lugovsky, and P. Schaffner (Particle Data Group), Phys. Rev. D **98**, 030001 (2018).
[61] S. Alam, M. Ata, S. Bailey, F. Beutler, D. Bizyaev, J. A. Blazek, A. S. Bolton, J. R. Brownstein, A. Burden, C.-H. Chuang, J. Comparat, A. J. Cuesta, K. S. Dawson, D. J. Eisenstein, S. Escoffier, H. Gil-Marín, J. N. Grieb, N. Hand, S. Ho, K. Kinemuchi, D. Kirkby, F. Kitaura, E. Malanushenko, V. Malanushenko, C. Maraston, C. K. McBride, R. C. Nichol, M. D. Olmstead, D. Oravetz, N. Padmanabhan, N. Palanque-Delabrouille, K. Pan, M. Pellejero-Ibanez, W. J. Percival, P. Petitjean, F. Prada, A. M. Price-Whelan, B. A. Reid, S. A. Rodríguez-Torres, N. A. Roe, A. J. Ross, N. P. Ross, G. Rossi, J. A. Rubiño-Martín, S. Saito, S. Salazar-Albornoz, L. Samushia, A. G. Sánchez, S. Satpathy, D. J. Schlegel, D. P. Schneider, C. G. Scóccola, H.-J. Seo, E. S. Sheldon, A. Simmons, A. Slosar, M. A. Strauss, M. E. C. Swanson, D. Thomas, J. L. Tinker, R. Tojeiro, M. V. Magaña, J. A. Vazquez, L. Verde, D. A. Wake, Y. Wang, D. H. Weinberg, M. White, W. M. Wood-Vasey, C. Yèche, I. Zehavi, Z. Zhai, and G.-B. Zhao, MNRAS **470**, 2617 (2017), arXiv:1607.03155.

[62] H. du Mas des Bourboux, J.-M. Le Goff, M. Blomqvist, N. G. Busca, J. Guy, J. Rich, C. Yèche, J. E. Bautista, É. Burtin, K. S. Dawson, D. J. Eisenstein, A. Font-Ribera, D. Kirkby, J. Miralda-Escudé, P. Noterdaeme, N. Palanque-Delabrouille, I. Pâris, P. Petitjean, I. Pérez-Ràfols, M. M. Pieri, N. P. Ross, D. J. Schlegel, D. P. Schneider, A. Slosar, D. H. Weinberg, and P. Zarrouk, A&A **608**, A130 (2017), arXiv:1708.02225.

[63] A. Slosar, V. Iršič, D. Kirkby, S. Bailey, N. G. Busca, T. Delubac, J. Rich, É. Aubourg, J. E. Bautista, V. Bhardwaj, M. Blomqvist, A. S. Bolton, J. Bovy, J. Brownstein, B. Carithers, R. A. C. Croft, K. S. Dawson, A. Font-Ribera, J.-M. Le Goff, S. Ho, K. Honscheid, K.-G. Lee, D. Margala, P. McDonald, B. Medolin, J. Miralda-Escudé, A. D. Myers, R. C. Nichol, P. Noterdaeme, N. Palanque-Delabrouille, I. Pâris, P. Petitjean, M. M. Pieri, Y. Piškur, N. A. Roe, N. P. Ross, G. Rossi, D. J. Schlegel, D. P. Schneider, N. Suzuki, E. S. Sheldon, U. Seljak, M. Viel, D. H. Weinberg, and C. Yèche, J. Cosmology Astropart. Phys. **4**, 026 (2013), arXiv:1301.3459.

[64] M. Ata, F. Baumgarten, J. Bautista, F. Beutler, D. Bizyaev, M. R. Blanton, J. A. Blazek, A. S. Bolton, J. Brinkmann, J. R. Brownstein, E. Burtin, C.-H. Chuang, J. Comparat, K. S. Dawson, A. de la Macorra, W. Du, H. du Mas des Bourboux, D. J. Eisenstein, H. Gil-Marín, K. Grabowski, J. Guy, N. Hand, S. Ho, T. A. Hutchinson, M. M. Ivanov, F.-S. Kitaura, J.-P. Kneib, P. Laurent, J.-M. Le Goff, J. E. McEwen, E.-M. Mueller, A. D. Myers, J. A. Newman, N. Palanque-Delabrouille, K. Pan, I. Pâris, M. Pellejero-Ibanez, W. J. Percival, P. Petitjean, F. Prada, A. Prakash, S. A. Rodríguez-Torres, A. J. Ross, G. Rossi, R. Ruggeri, A. G. Sánchez, S. Satpathy, D. J. Schlegel, D. P. Schneider, H.-J. Seo, A. Slosar, A. Streblyanska, J. L. Tinker, R. Tojeiro, M. Vargas Magaña, M. Vivek, Y. Wang, C. Yèche, L. Yu, P. Zarrouk, C. Zhao, G.-B. Zhao, and F. Zhu, MNRAS **473**, 4773 (2018), arXiv:1705.06373.

[65] E. A. Kazin, J. Koda, C. Blake, N. Padmanabhan, S. Brough, M. Colless, C. Contreras, W. Couch, S. Croom, D. J. Croton, T. M. Davis, M. J. Drinkwater, K. Forster, D. Gilbank, M. Gladders, K. Glazebrook, B. Jelliffe, R. J. Jurek, I.-h. Li, B. Madore, D. C. Martin, K. Pimbblet, G. B. Poole, M. Pracy, R. Sharp, E. Wisnioski, D. Woods, T. K. Wyder, and H. K. C. Yee, MNRAS **441**, 3524 (2014), arXiv:1401.0358.

[66] Planck Collaboration, N. Aghanim, Y. Akrami, M. Ashdown, J. Aumont, C. Baccigalupi, M. Ballardini, A. J. Banday, R. B. Barreiro, N. Bartolo, S. Basak, R. Battye, K. Benabed, J.-P. Bernard, M. Bersanelli, P. Bielewicz, J. J. Bock, J. R. Bond, J. Borrill, F. R. Bouchet, F. Boulanger, M. Bucher, C. Burigana, R. C. Butler, E. Calabrese, J.-F. Cardoso, J. Carron, A. Challinor, H. C. Chiang, J. Chluba, L. P. L. Colombo, C. Combet, D. Contreras, B. P. Crill, F. Cuttaia, P. de Bernardis, G. de Zotti, J. Delabrouille, J.-M. Delouis, E. Di Valentino, J. M. Diego, O. Doré, M. Douspis, A. Ducout, X. Dupac, S. Dusini, G. Efstathiou, F. Elsner, T. A. Enßlin, H. K. Eriksen, Y. Fantaye, M. Farhang, J. Fergusson, R. Fernandez-Cobos, F. Finelli, F. Forastieri, M. Frailis, E. Franceschi, A. Frolov, S. Galeotta, S. Galli, K. Ganga, R. T. Génova-Santos, M. Gerbino, T. Ghosh, J. González-Nuevo, K. M. Górski, S. Gratton, A. Gruppuso, J. E. Gudmundsson, J. Hamann, W. Handley, D. Herranz, E. Hivon, Z. Huang, A. H. Jaffe, W. C. Jones, A. Karakci, E. Keihänen, R. Keskitalo, K. Kiiveri, J. Kim, T. S. Kisner, L. Knox, N. Krachmalnicoff, M. Kunz, H. Kurki-Suonio, G. Lagache, J.-M. Lamarre, A. Lasenby, M. Lattanzi, C. R. Lawrence, M. Le Jeune, P. Lemos, J. Lesgourgues, F. Levrier, A. Lewis, M. Liguori, P. B. Lilje, M. Lilley, V. Lindholm, M. López-Caniego, P. M. Lubin, Y.-Z. Ma, J. F. Macías-Pérez, G. Maggio, D. Maino, N. Mandolesi, A. Mangilli, A. Marcos-Caballero, M. Maris, P. G. Martin, M. Martinelli, E. Martínez-González, S. Matarrese, N. Mauri, J. D. McEwen, P. R. Meinhold, A. Melchiorri, A. Mennella, M. Migliaccio, M. Millea, S. Mitra, M.-A. Miville-Deschênes, D. Molinari, L. Montier, G. Morgante, A. Moss, P. Natoli, H. U. Nørgaard-Nielsen, L. Pagano, D. Paoletti, B. Partridge, G. Patanchon, H. V. Peiris, F. Perrotta, V. Pettorino, F. Piacentini, L. Polastri, G. Polenta, J.-L. Puget, J. P. Rachen, M. Reinecke, M. Remazeilles, A. Renzi, G. Rocha, C. Rosset, G. Roudier, J. A. Rubiño-Martín, B. Ruiz-Granados, L. Salvati, M. Sandri, M. Savelainen, D. Scott, E. P. S. Shellard, C. Sirignano, G. Sirri, L. D. Spencer, R. Sunyaev, A.-S. Suur-Uski, J. A. Tauber, D. Tavagnacco, M. Tenti, L. Toffolatti, M. Tomasi, T. Trombetti, L. Valenziano, J. Valiviita, B. Van Tent, L. Vibert, P. Vielva, F. Villa, N. Vittorio, B. D. Wandelt, I. K. Wehus, M. White, S. D. M. White, A. Zacchei, and A. Zonca, ArXiv e-prints (2018), arXiv:1807.06209.

[67] R. Laureijs, J. Amiaux, S. Arduini, J. . Augueres, J. Brinchmann, R. Cole, M. Cropper, C. Dabin, L. Duvet, A. Ealet, and et al., ArXiv e-prints (2011), arXiv:1110.3193 [astro-ph.CO].

[68] H.-J. Seo and D. J. Eisenstein, ApJ **598**, 720 (2003), astro-ph/0307460.

[69] A. Font-Ribera, P. McDonald, N. Mostek, B. A. Reid, H.-J. Seo, and A. Slosar, J. Cosmology Astropart. Phys. **5**, 023 (2014), arXiv:1308.4164.

[70] A. Obuljen, E. Castorina, F. Villaescusa-Navarro, and M. Viel, ArXiv e-prints (2017), arXiv:1709.07893.

[71] É. Aubourg, S. Bailey, J. E. Bautista, F. Beutler, V. Bhardwaj, D. Bizyaev, M. Blanton, M. Blomqvist, A. S. Bolton, J. Bovy, H. Brewington, J. Brinkmann, J. R. Brownstein, A. Burden, N. G. Busca, W. Carithers, C.-H. Chuang, J. Comparat, R. A. C. Croft, A. J. Cuesta, K. S. Dawson, T. Delubac, D. J. Eisenstein, A. Font-Ribera, J. Ge, J.-M. Le Goff, S. G. A. Gontcho, J. R. Gott, J. E. Gunn, H. Guo, J. Guy, J.-C. Hamilton, S. Ho, K. Honscheid, C. Howlett, D. Kirkby, F. S. Kitaura, J.-P. Kneib, K.-G. Lee, D. Long, R. H. Lupton, M. V. Magaña, V. Malanushenko, E. Malanushenko, M. Manera, C. Maraston, D. Margala, C. K. McBride, J. Miralda-Escudé, A. D. Myers, R. C. Nichol, P. Noterdaeme, S. E. Nuza, M. D. Olmstead, D. Oravetz, I. Pâris, N. Padmanabhan, N. Palanque-Delabrouille, K. Pan, M. Pellejero-Ibanez, W. J. Percival, P. Petitjean, M. M. Pieri, F. Prada, B. Reid, J. Rich, N. A. Roe, A. J. Ross, N. P. Ross, G. Rossi, J. A. Rubiño-Martín, A. G. Sánchez, L. Samushia, R. T. Génova-Santos, C. G. Scóccola, D. J. Schlegel, D. P. Schneider, H.-J. Seo, E. Sheldon, A. Simmons, R. A. Skibba, A. Slosar, M. A. Strauss, D. Thomas, J. L. Tinker, R. Tojeiro, J. A. Vazquez, M. Viel, D. A. Wake, B. A. Weaver, D. H. Weinberg, W. M. Wood-Vasey, C. Yèche, I. Zehavi, G.-B. Zhao, and BOSS Collaboration, Phys. Rev. D **92**, 123516 (2015), arXiv:1411.1074.

[72] M. Doran and G. Robbers, J. Cosmology Astropart. Phys. **6**, 026 (2006), astro-ph/0601544.

[73] T. Karwal and M. Kamionkowski, Phys. Rev. D **94**, 103523 (2016), arXiv:1608.01309.

[74] R. Bean, S. H. Hansen, and A. Melchiorri, Phys. Rev. D **64**, 103508 (2001), astro-ph/0104162.

[75] J.-Q. Xia and M. Viel, J. Cosmology Astropart. Phys. **4**, 002 (2009), arXiv:0901.0605 [astro-ph.CO].

[76] E. Calabrese, D. Huterer, E. V. Linder, A. Melchiorri, and L. Pagano, Phys. Rev. D **83**, 123504 (2011), arXiv:1103.4132 [astro-ph.CO].

[77] V. Pettorino, L. Amendola, and C. Wetterich, Phys. Rev. D **87**, 083009 (2013), arXiv:1301.5279 [astro-ph.CO].

[78] E. V. Linder, Astroparticle Physics **26**, 16 (2006), astro-ph/0603584.

[79] Planck Collaboration, Y. Akrami, F. Arroja, M. Ashdown, J. Aumont, C. Baccigalupi, M. Ballardini, A. J. Banday, R. B. Barreiro,

N. Bartolo, S. Basak, R. Battye, K. Benabed, J.-P. Bernard, M. Bersanelli, P. Bielewicz, J. J. Bock, J. R. Bond, J. Borrill, F. R. Bouchet, F. Boulanger, M. Bucher, C. Burigana, R. C. Butler, E. Calabrese, J.-F. Cardoso, J. Carron, B. Casaponsa, A. Challinor, H. C. Chiang, L. P. L. Colombo, C. Combet, D. Contreras, B. P. Crill, F. Cuttaia, P. de Bernardis, G. de Zotti, J. Delabrouille, J.-M. Delouis, F.-X. Désert, E. Di Valentino, C. Dickinson, J. M. Diego, S. Donzelli, O. Doré, M. Douspis, A. Ducout, X. Dupac, G. Efstathiou, F. Elsner, T. A. Enßlin, H. K. Eriksen, E. Falgarone, Y. Fantaye, J. Fergusson, R. Fernandez-Cobos, F. Finelli, F. Forastieri, M. Frailis, E. Franceschi, A. Frolov, S. Galeotta, S. Galli, K. Ganga, R. T. Génova-Santos, M. Gerbino, T. Ghosh, J. González-Nuevo, K. M. Górski, S. Gratton, A. Gruppuso, J. E. Gudmundsson, J. Hamann, W. Handley, F. K. Hansen, G. Helou, D. Herranz, E. Hivon, Z. Huang, A. H. Jaffe, W. C. Jones, A. Karakci, E. Keihänen, R. Keskitalo, K. Kiiveri, J. Kim, T. S. Kisner, L. Knox, N. Krachmalnicoff, M. Kunz, H. Kurki-Suonio, G. Lagache, J.-M. Lamarre, M. Langer, A. Lasenby, M. Lattanzi, C. R. Lawrence, M. Le Jeune, J. P. Leahy, J. Lesgourgues, F. Levrier, A. Lewis, M. Liguori, P. B. Lilje, M. Lilley, V. Lindholm, M. López-Caniego, P. M. Lubin, Y.-Z. Ma, J. F. Macías-Pérez, G. Maggio, D. Maino, N. Mandolesi, A. Mangilli, A. Marcos-Caballero, M. Maris, P. G. Martin, E. Martínez-González, S. Matarrese, N. Mauri, J. D. McEwen, P. D. Meerburg, P. R. Meinhold, A. Melchiorri, A. Mennella, M. Migliaccio, M. Millea, S. Mitra, M.-A. Miville-Deschênes, D. Molinari, A. Moneti, L. Montier, G. Morgante, A. Moss, S. Mottet, M. Münchmeyer, P. Natoli, H. U. Nørgaard-Nielsen, C. A. Oxborrow, L. Pagano, D. Paoletti, B. Partridge, G. Patanchon, T. J. Pearson, M. Peel, H. V. Peiris, F. Perrotta, V. Pettorino, F. Piacentini, L. Polastri, G. Polenta, J.-L. Puget, J. P. Rachen, M. Reinecke, M. Remazeilles, A. Renzi, G. Rocha, C. Rosset, G. Roudier, J. A. Rubiño-Martín, B. Ruiz-Granados, L. Salvati, M. Sandri, M. Savelainen, D. Scott, E. P. S. Shellard, M. Shiraishi, C. Sirignano, G. Sirri, L. D. Spencer, R. Sunyaev, A.-S. Suur-Uski, J. A. Tauber, D. Tavagnacco, M. Tenti, L. Terenzi, L. Toffolatti, M. Tomasi, T. Trombetti, J. Valiviita, B. Van Tent, L. Vibert, P. Vielva, F. Villa, N. Vittorio, B. D. Wandelt, I. K. Wehus, M. White, S. D. M. White, A. Zacchei, and A. Zonca, ArXiv e-prints (2018), arXiv:1807.06205.

[80] C. Blake, S. Brough, M. Colless, C. Contreras, W. Couch, S. Croom, D. Croton, T. M. Davis, M. J. Drinkwater, K. Forster, D. Gilbank, M. Gladders, K. Glazebrook, B. Jelliffe, R. J. Jurek, I.-h. Li, B. Madore, D. C. Martin, K. Pimbblet, G. B. Poole, M. Pracy, R. Sharp, E. Wisnioski, D. Woods, T. K. Wyder, and H. K. C. Yee, MNRAS **425**, 405 (2012), arXiv:1204.3674.

[81] F. Beutler, C. Blake, M. Colless, D. H. Jones, L. Staveley-Smith, G. B. Poole, L. Campbell, Q. Parker, W. Saunders, and F. Watson, MNRAS **423**, 3430 (2012), arXiv:1204.4725.

[82] T. Okumura, C. Hikage, T. Totani, M. Tonegawa, H. Okada, K. Glazebrook, C. Blake, P. G. Ferreira, S. More, A. Taruya, S. Tsujikawa, M. Akiyama, G. Dalton, T. Goto, T. Ishikawa, F. Iwamuro, T. Matsubara, T. Nishimichi, K. Ohta, I. Shimizu, R. Takahashi, N. Takato, N. Tamura, K. Yabe, and N. Yoshida, PASJ **68**, 38 (2016), arXiv:1511.08083.

[83] F. Beutler, H.-J. Seo, S. Saito, C.-H. Chuang, A. J. Cuesta, D. J. Eisenstein, H. Gil-Marín, J. N. Grieb, N. Hand, F.-S. Kitaura, C. Modi, R. C. Nichol, M. D. Olmstead, W. J. Percival, F. Prada, A. G. Sánchez, S. Rodriguez-Torres, A. J. Ross, N. P. Ross, D. P. Schneider, J. Tinker, R. Tojeiro, and M. Vargas-Magaña, MNRAS **466**, 2242 (2017), arXiv:1607.03150.

[84] S. de la Torre, E. Jullo, C. Giocoli, A. Pezzotta, J. Bel, B. R. Granett, L. Guzzo, B. Garilli, M. Scodeggio, M. Bolzonella, U. Abbas, C. Adami, D. Bottini, A. Cappi, O. Cucciati, I. Davidzon, P. Franzetti, A. Fritz, A. Iovino, J. Krywult, V. Le Brun, O. Le Fèvre, D. Maccagni, K. Małek, F. Marulli, M. Polletta, A. Pollo, L. A. M. Tasca, R. Tojeiro, D. Vergani, A. Zanichelli, S. Arnouts, E. Branchini, J. Coupon, G. De Lucia, O. Ilbert, T. Moutard, L. Moscardini, J. A. Peacock, R. B. Metcalf, F. Prada, and G. Yepes, A&A **608**, A44 (2017), arXiv:1612.05647.

[85] G.-B. Zhao, Y. Wang, S. Saito, H. Gil-Marín, W. J. Percival, D. Wang, C.-H. Chuang, R. Ruggeri, E.-M. Mueller, F. Zhu, A. J. Ross, R. Tojeiro, I. Pâris, A. D. Myers, J. L. Tinker, E. Burtin, P. Zarrouk, F. Beutler, F. Baumgarten, J. E. Bautista, J. R. Brownstein, K. S. Dawson, J. Hou, A. de la Macorra, G. Rossi, J. A. Peacock, A. G. Sánchez, A. Shafieloo, D. P. Schneider, and C. Zhao, ArXiv e-prints (2018), arXiv:1801.03043.

[86] M. Zumalacárregui, E. Bellini, I. Sawicki, J. Lesgourgues, and P. G. Ferreira, J. Cosmology Astropart. Phys. **8**, 019 (2017), arXiv:1605.06102.

[87] D. Blas, J. Lesgourgues, and T. Tram, J. Cosmology Astropart. Phys. **7**, 034 (2011), arXiv:1104.2933.

[88] J. Chluba, J. Hamann, and S. P. Patil, Int. J. Mod. Phys. **D24**, 1530023 (2015), arXiv:1505.01834 [astro-ph.CO].

[89] F.-Y. Cyr-Racine, R. de Putter, A. Raccanelli, and K. Sigurdson, Phys. Rev. **D89**, 063517 (2014), arXiv:1310.3278 [astro-ph.CO].

[90] P. D. Meerburg, R. A. M. J. Wijers, and J. P. van der Schaar, MNRAS **421**, 369 (2012), arXiv:1109.5264 [astro-ph.CO].

[91] H. Peiris, R. Easther, and R. Flauger, JCAP **1309**, 018 (2013), arXiv:1303.2616 [astro-ph.CO].

[92] P. D. Meerburg and D. N. Spergel, Phys. Rev. **D89**, 063537 (2014), arXiv:1308.3705 [astro-ph.CO].

[93] R. Easther and R. Flauger, JCAP **1402**, 037 (2014), arXiv:1308.3736 [astro-ph.CO].

[94] P. A. R. Ade *et al.* (Planck), Astron. Astrophys. **594**, A20 (2016), arXiv:1502.02114 [astro-ph.CO].

[95] Y. Akrami *et al.* (Planck), (2018), arXiv:1807.06211 [astro-ph.CO].

[96] R. Flauger, L. McAllister, E. Silverstein, and A. Westphal, (2014), arXiv:1412.1814 [hep-th].

[97] A. Achúcarro, V. Atal, P. Ortiz, and J. Torrado, Phys. Rev. **D89**, 103006 (2014), arXiv:1311.2552 [astro-ph.CO].

[98] X. Chen and M. H. Namjoo, Phys. Lett. **B739**, 285 (2014), arXiv:1404.1536 [astro-ph.CO].

[99] X. Chen, M. H. Namjoo, and Y. Wang, JCAP **1502**, 027 (2015), arXiv:1411.2349 [astro-ph.CO].

[100] X. Chen, Advances in Astronomy **2010**, 638979 (2010), arXiv:1002.1416 [astro-ph.CO].

[101] M. Alvarez, T. Baldauf, J. R. Bond, N. Dalal, R. de Putter, O. Doré, D. Green, C. Hirata, Z. Huang, D. Huterer, D. Jeong, M. C. Johnson, E. Krause, M. Loverde, J. Meyers, P. D. Meerburg, L. Senatore, S. Shandera, E. Silverstein, A. Slosar, K. Smith, M. Zaldarriaga, V. Assassi, J. Braden, A. Hajian, T. Kobayashi, G. Stein, and A. van Engelen, ArXiv e-prints (2014), arXiv:1412.4671.

[102] J. M. Maldacena, JHEP **05**, 013 (2003), arXiv:astro-ph/0210603 [astro-ph].

[103] P. Creminelli and M. Zaldarriaga, JCAP **0410**, 006 (2004), arXiv:astro-ph/0407059 [astro-ph].

[104] E. Komatsu, N. Afshordi, N. Bartolo, D. Baumann, J. R. Bond, E. I. Buchbinder, C. T. Byrnes, X. Chen, D. J. H. Chung, A. Cooray, P. Creminelli, N. Dalal, O. Dore, R. Easther, A. V. Frolov, J. Khoury, W. H. Kinney, L. Kofman, K. Koyama, L. Leblond, J.-L. Lehners, J. E. Lidsey, M. Liguori, E. A. Lim, A. Linde, D. H. Lyth, J. Maldacena, S. Matarrese, L. McAllister, P. McDonald, S. Mukohyama, B. Ovrut, H. V. Peiris, A. Riotto, Y. Rodrigues, M. Sasaki, R. Scoccimarro, D. Seery, A. Sefusatti, K. M. Smith, A. A. Starobinsky,

P. J. Steinhardt, F. Takahashi, M. Tegmark, A. J. Tolley, L. Verde, B. D. Wandelt, D. Wands, S. Weinberg, M. Wyman, A. P. S. Yadav, and M. Zaldarriaga, in *astro2010: The Astronomy and Astrophysics Decadal Survey*, Astronomy, Vol. 2010 (2009) arXiv:0902.4759 [astro-ph.CO].

[105] X. Chen and Y. Wang, JCAP **1004**, 027 (2010), arXiv:0911.3380 [hep-th].

[106] D. Baumann and D. Green, Phys. Rev. **D85**, 103520 (2012), arXiv:1109.0292 [hep-th].

[107] T. Noumi, M. Yamaguchi, and D. Yokoyama, JHEP **06**, 051 (2013), arXiv:1211.1624 [hep-th].

[108] N. Arkani-Hamed and J. Maldacena, (2015), arXiv:1503.08043 [hep-th].

[109] H. Lee, D. Baumann, and G. L. Pimentel, JHEP **12**, 040 (2016), arXiv:1607.03735 [hep-th].

[110] Planck Collaboration, P. A. R. Ade, N. Aghanim, C. Armitage-Caplan, M. Arnaud, M. Ashdown, F. Atrio-Barandela, J. Aumont, C. Baccigalupi, A. J. Banday, and et al., A&A **571**, A24 (2014), arXiv:1303.5084.

[111] Planck Collaboration, P. A. R. Ade, N. Aghanim, M. Arnaud, F. Arroja, M. Ashdown, J. Aumont, C. Baccigalupi, M. Ballardini, A. J. Banday, and et al., A&A **594**, A17 (2016), arXiv:1502.01592.

[112] K. N. Abazajian, P. Adshead, Z. Ahmed, S. W. Allen, D. Alonso, K. S. Arnold, C. Baccigalupi, J. G. Bartlett, N. Battaglia, B. A. Benson, C. A. Bischoff, J. Borrill, V. Buza, E. Calabrese, R. Caldwell, J. E. Carlstrom, C. L. Chang, T. M. Crawford, F.-Y. Cyr-Racine, F. De Bernardis, T. de Haan, S. di Serego Alighieri, J. Dunkley, C. Dvorkin, J. Errard, G. Fabbian, S. Feeney, S. Ferraro, J. P. Filippini, R. Flauger, G. M. Fuller, V. Gluscevic, D. Green, D. Grin, E. Grohs, J. W. Henning, J. C. Hill, R. Hlozek, G. Holder, W. Holzapfel, W. Hu, K. M. Huffenberger, R. Keskitalo, L. Knox, A. Kosowsky, J. Kovac, E. D. Kovetz, C.-L. Kuo, A. Kusaka, M. Le Jeune, A. T. Lee, M. Lilley, M. Loverde, M. S. Madhavacheril, A. Mantz, D. J. E. Marsh, J. McMahon, P. D. Meerburg, J. Meyers, A. D. Miller, J. B. Munoz, H. N. Nguyen, M. D. Niemack, M. Peloso, J. Peloton, L. Pogosian, C. Pryke, M. Raveri, C. L. Reichardt, G. Rocha, A. Rotti, E. Schaan, M. M. Schmittfull, D. Scott, N. Sehgal, S. Shandera, B. D. Sherwin, T. L. Smith, L. Sorbo, G. D. Starkman, K. T. Story, A. van Engelen, J. D. Vieira, S. Watson, N. Whitehorn, and W. L. Kimmy Wu, ArXiv e-prints (2016), arXiv:1610.02743.

[113] P. D. Meerburg, J. Meyers, A. van Engelen, and Y. Ali-Haïmoud, Phys. Rev. D **93**, 123511 (2016), arXiv:1603.02243.

[114] A. Cooray, Physical Review Letters **97**, 261301 (2006), astro-ph/0610257.

[115] A. Pillepich, C. Porciani, and S. Matarrese, ApJ **662**, 1 (2007), astro-ph/0611126.

[116] P. D. Meerburg, M. Münchmeyer, J. B. Muñoz, and X. Chen, J. Cosmology Astropart. Phys. **3**, 050 (2017), arXiv:1610.06559.

[117] A. Lidz, E. J. Baxter, P. Adshead, and S. Dodelson, Phys. Rev. D **88**, 023534 (2013), arXiv:1304.8049 [astro-ph.CO].

[118] Y. Mao, A. D'Aloisio, J. Zhang, and P. R. Shapiro, Phys. Rev. D **88**, 081303 (2013), arXiv:1305.0313.

[119] D. Crociani, L. Moscardini, M. Viel, and S. Matarrese, MNRAS **394**, 133 (2009), arXiv:0809.3909.

[120] Y. Xu, J. Hamann, and X. Chen, Phys. Rev. D **94**, 123518 (2016), arXiv:1607.00817.

[121] H. Tashiro and S. Ho, MNRAS **431**, 2017 (2013), arXiv:1205.0563.

[122] A. D'Aloisio, J. Zhang, P. R. Shapiro, and Y. Mao, MNRAS **433**, 2900 (2013), arXiv:1304.6411.

[123] S. Camera, M. G. Santos, and R. Maartens, MNRAS **448**, 1035 (2015), arXiv:1409.8286.

[124] Y.-C. Li and Y.-Z. Ma, Phys. Rev. D **96**, 063525 (2017), arXiv:1701.00221.

[125] D. Karagiannis, A. Lazanu, M. Liguori, A. Raccanelli, N. Bartolo, and L. Verde, ArXiv e-prints (2018), arXiv:1801.09280.

[126] P. Creminelli, J. Cosmology Astropart. Phys. **10**, 003 (2003), astro-ph/0306122.

[127] D. Baumann, D. Green, and R. A. Porto, J. Cosmology Astropart. Phys. **1**, 016 (2015), arXiv:1407.2621 [hep-th].

[128] D. Baumann, D. Green, H. Lee, and R. A. Porto, Phys. Rev. D **93**, 023523 (2016), arXiv:1502.07304 [hep-th].

[129] Planck Collaboration, N. Aghanim, Y. Akrami, M. Ashdown, J. Aumont, C. Baccigalupi, M. Ballardini, A. J. Banday, R. B. Barreiro, N. Bartolo, S. Basak, K. Benabed, J.-P. Bernard, M. Bersanelli, P. Bielewicz, J. J. Bock, J. R. Bond, J. Borrill, F. R. Bouchet, F. Boulanger, M. Bucher, C. Burigana, E. Calabrese, J.-F. Cardoso, J. Carron, A. Challinor, H. C. Chiang, L. P. L. Colombo, C. Combet, B. P. Crill, F. Cuttaia, P. de Bernardis, G. de Zotti, J. Delabrouille, E. Di Valentino, J. M. Diego, O. Doré, M. Douspis, A. Ducout, X. Dupac, G. Efstathiou, F. Elsner, T. A. Enßlin, H. K. Eriksen, Y. Fantaye, R. Fernandez-Cobos, F. Forastieri, M. Frailis, A. A. Fraisse, E. Franceschi, A. Frolov, S. Galeotta, S. Galli, K. Ganga, R. T. Génova-Santos, M. Gerbino, T. Ghosh, J. González-Nuevo, K. M. Górski, S. Gratton, A. Gruppuso, J. E. Gudmundsson, J. Hamann, W. Handley, F. K. Hansen, D. Herranz, E. Hivon, Z. Huang, A. H. Jaffe, W. C. Jones, A. Karakci, E. Keihänen, R. Keskitalo, K. Kiiveri, J. Kim, L. Knox, N. Krachmalnicoff, M. Kunz, H. Kurki-Suonio, G. Lagache, J.-M. Lamarre, A. Lasenby, M. Lattanzi, C. R. Lawrence, M. Le Jeune, F. Levrier, A. Lewis, M. Liguori, P. B. Lilje, V. Lindholm, M. López-Caniego, P. M. Lubin, Y.-Z. Ma, J. F. Macías-Pérez, G. Maggio, D. Maino, N. Mandolesi, A. Mangilli, A. Marcos-Caballero, M. Maris, P. G. Martin, E. Martínez-González, S. Matarrese, N. Mauri, J. D. McEwen, A. Melchiorri, A. Mennella, M. Migliaccio, M.-A. Miville-Deschênes, D. Molinari, A. Moneti, L. Montier, G. Morgante, A. Moss, P. Natoli, L. Pagano, D. Paoletti, B. Partridge, G. Patanchon, F. Perrotta, V. Pettorino, F. Piacentini, L. Polastri, G. Polenta, J.-L. Puget, J. P. Rachen, M. Reinecke, M. Remazeilles, A. Renzi, G. Rocha, C. Rosset, G. Roudier, J. A. Rubiño-Martín, B. Ruiz-Granados, L. Salvati, M. Sandri, M. Savelainen, D. Scott, C. Sirignano, R. Sunyaev, A.-S. Suur-Uski, J. A. Tauber, D. Tavagnacco, M. Tenti, L. Toffolatti, M. Tomasi, T. Trombetti, J. Valiviita, B. Van Tent, P. Vielva, F. Villa, N. Vittorio, B. D. Wandelt, I. K. Wehus, M. White, S. D. M. White, A. Zacchei, and A. Zonca, ArXiv e-prints (2018), arXiv:1807.06210.

[130] N. Galitzki, A. Ali, K. S. Arnold, P. C. Ashton, J. E. Austermann, C. Baccigalupi, T. Baildon, D. Barron, J. A. Beall\, S. Beckman, S. M. M. Bruno, S. Bryan, P. G. Calisse, G. E. Chesmore, Y. Chinone, S. K. Choi, G. Coppi, K. D. Crowley, K. T. Crowley, A. Cukierman, M. J. Devlin, S. Dicker, B. Dober, S. M. Duff, J. Dunkley, G. Fabbian, P. A. Gallardo, M. Gerbino, N. Goeckner-Wald, J. E. Golec, J. E. Gudmundsson, E. E. Healy, S. Henderson, C. A. Hill, G. C. Hilton, S.-P. P. Ho, L. A. Howe, J. Hubmayr, O. Jeong, B. Keating, B. J. Koopman, K. Kuichi, A. Kusaka, J. Lashner, A. T. Lee, Y. Li, M. Limon, M. Lungu, F. Matsuda, P. D. Mauskopf, A. J. May, N. McCallum, J. McMahon, F. Nati, M. D. Niemack, J. L. Orlowski-Scherer, S. C. Parshley, L. Piccirillo, M. Sathyanarayana Rao, C. Raum, M. Salatino, J. S. Seibert, C. Sierra, M. Silva-Feaver, S. M. Simon, S. T. Staggs, J. R. Stevens, A. Suzuki\, G. Teply, R. Thornton, C. Tsai, J. N. Ullom, E. M. Vavagiakis, M. R. Vissers, B. Westbrook, E. J. Wollack, Z. Xu\, and N. Zhu, ArXiv e-prints (2018), arXiv:1808.04493 [astro-ph.IM].

[131] M. A. Troxel *et al.* (DES), (2017), arXiv:1708.01538 [astro-ph.CO].

[132] R. Mandelbaum, (2017), arXiv:1710.03235 [astro-ph.CO].
[133] A. R. Cooray, New Astron. **9**, 173 (2004), arXiv:astro-ph/0309301 [astro-ph].
[134] U.-L. Pen, New Astron. **9**, 417 (2004), arXiv:astro-ph/0305387 [astro-ph].
[135] O. Zahn and M. Zaldarriaga, Astrophys. J. **653**, 922 (2006), arXiv:astro-ph/0511547 [astro-ph].
[136] R. B. Metcalf and S. D. M. White, Mon. Not. Roy. Astron. Soc. (2006), 10.1111/j.1365-2966.2007.12212.x, [Mon. Not. Roy. Astron. Soc.381,447(2007)], arXiv:astro-ph/0611862 [astro-ph].
[137] A. Pourtsidou and R. B. Metcalf, Mon. Not. Roy. Astron. Soc. **439**, L36 (2014), arXiv:1311.4484 [astro-ph.CO].
[138] A. Romeo, R. B. Metcalf, and A. Pourtsidou, (2017), 10.1093/mnras/stx2733, arXiv:1708.01235 [astro-ph.CO].
[139] S. Foreman, P. D. Meerburg, A. van Engelen, and J. Meyers, JCAP **1807**, 046 (2018), arXiv:1803.04975 [astro-ph.CO].
[140] T. Lu and U.-L. Pen, Mon. Not. Roy. Astron. Soc. **388**, 1819 (2008), arXiv:0710.1108 [astro-ph].
[141] T. Lu, U.-L. Pen, and O. Dore, Phys. Rev. **D81**, 123015 (2010), arXiv:0905.0499 [astro-ph.CO].
[142] U.-L. Pen, R. Sheth, J. Harnois-Deraps, X. Chen, and Z. Li, (2012), arXiv:1202.5804 [astro-ph.CO].
[143] F. Schmidt, E. Pajer, and M. Zaldarriaga, Phys. Rev. **D89**, 083507 (2014), arXiv:1312.5616 [astro-ph.CO].
[144] H.-M. Zhu, U.-L. Pen, Y. Yu, X. Er, and X. Chen, Phys. Rev. **D93**, 103504 (2016), arXiv:1511.04680 [astro-ph.CO].
[145] H.-M. Zhu, U.-L. Pen, Y. Yu, and X. Chen, (2016), arXiv:1610.07062 [astro-ph.CO].
[146] C. Alcock and B. Paczynski, Nature **281**, 358 (1979).
[147] J. Lesgourgues, G. Mangano, G. Miele, and S. Pastor, *Neutrino Cosmology, by Julien Lesgourgues , Gianpiero Mangano , Gennaro Miele , Sergio Pastor, Cambridge, UK: Cambridge University Press, 2013* (Cambridge University Press, 2013).
[148] R. B. Patterson, Annual Review of Nuclear and Particle Science **65**, 177 (2015), arXiv:1506.07917 [hep-ex].
[149] M. Archidiacono, T. Brinckmann, J. Lesgourgues, and V. Poulin, J. Cosmology Astropart. Phys. **2**, 052 (2017), arXiv:1610.09852.
[150] M. Lattanzi and M. Gerbino, ArXiv e-prints (2017), arXiv:1712.07109.
[151] K. N. Abazajian *et al.* (CMB-S4), (2016), arXiv:1610.02743 [astro-ph.CO].
[152] D. Baumann, D. Green, and B. Wallisch, Phys. Rev. Lett. **117**, 171301 (2016), arXiv:1604.08614 [astro-ph.CO].
[153] D. Baumann, D. Green, and B. Wallisch, (2017), arXiv:1712.08067 [astro-ph.CO].
[154] J. Meyers, private communication (2015).
[155] I. P. Carucci, F. Villaescusa-Navarro, and M. Viel, J. Cosmology Astropart. Phys. **4**, 001 (2017), arXiv:1611.07527.
[156] G. J. Hill, K. Gebhardt, E. Komatsu, N. Drory, P. J. MacQueen, J. Adams, G. A. Blanc, R. Koehler, M. Rafal, M. M. Roth, A. Kelz, C. Gronwall, R. Ciardullo, and D. P. Schneider, in *Panoramic Views of Galaxy Formation and Evolution*, Astronomical Society of the Pacific Conference Series, Vol. 399, edited by T. Kodama, T. Yamada, and K. Aoki (2008) p. 115, arXiv:0806.0183.
[157] J. D. Cohn, M. White, T.-C. Chang, G. Holder, N. Padmanabhan, and O. Doré, MNRAS **457**, 2068 (2016), arXiv:1511.07377.
[158] A. G. Kim, E. V. Linder, J. Edelstein, and D. Erskine, Astroparticle Physics **62**, 195 (2015), arXiv:1402.6614.
[159] H.-R. Yu, T.-J. Zhang, and U.-L. Pen, Physical Review Letters **113**, 041303 (2014), arXiv:1311.2363.
[160] L. B. Newburgh, K. Bandura, M. A. Bucher, T.-C. Chang, H. C. Chiang, J. F. Cliche, R. Davé, M. Dobbs, C. Clarkson, K. M. Ganga, T. Gogo, A. Gumba, N. Gupta, M. Hilton, B. Johnstone, A. Karastergiou, M. Kunz, D. Lokhorst, R. Maartens, S. Macpherson, M. Mdlalose, K. Moodley, L. Ngwenya, J. M. Parra, J. Peterson, O. Recnik, B. Saliwanchik, M. G. Santos, J. L. Sievers, O. Smirnov, P. Stronkhorst, R. Taylor, K. Vanderlinde, G. Van Vuuren, A. Weltman, and A. Witzemann, in *Ground-based and Airborne Telescopes VI*, Proc. SPIE, Vol. 9906 (2016) p. 99065X, arXiv:1607.02059 [astro-ph.IM].
[161] M. Bailes, A. Jameson, C. Flynn, T. Bateman, E. D. Barr, S. Bhandari, J. D. Bunton, M. Caleb, D. Campbell-Wilson, W. Farah, B. Gaensler, A. J. Green, R. W. Hunstead, F. Jankowski, E. F. Keane, V. V. Krishnan, T. Murphy, M. O'Neill, S. Osłowski, A. Parthasarathy, V. Ravi, P. Rosado, and D. Temby, PASA **34**, e045 (2017), arXiv:1708.09619 [astro-ph.IM].
[162] M. Amiri, K. Bandura, P. Berger, M. Bhardwaj, M. M. Boyce, P. J. Boyle, C. Brar, M. Burhanpurkar, P. Chawla, J. Chowdhury, J. F. Cliche, M. D. Cranmer, D. Cubranic, M. Deng, N. Denman, M. Dobbs, M. Fandino, E. Fonseca, B. M. Gaensler, U. Giri, A. J. Gilbert, D. C. Good, S. Guliani, M. Halpern, G. Hinshaw, C. Hofer, A. Josephy, V. M. Kaspi, T. L. Landecker, D. Lang, H. Liao, K. W. Masui, J. Mena-Parra, A. Naidu, L. B. Newburgh, C. Ng, C. Patel, U.-L. Pen, T. Pinsonneault-Marotte, Z. Pleunis, M. Rafiei Ravandi, S. M. Ransom, A. Renard, P. Scholz, K. Sigurdson, S. R. Siegel, K. M. Smith, I. H. Stairs, S. P. Tendulkar, K. Vanderlinde, and D. V. Wiebe, ArXiv e-prints (2018), arXiv:1803.11235 [astro-ph.IM].
[163] D. R. Lorimer, M. Bailes, M. A. McLaughlin, D. J. Narkevic, and F. Crawford, Science **318**, 777 (2007), arXiv:0709.4301.
[164] D. Thornton, B. Stappers, M. Bailes, B. Barsdell, S. Bates, N. D. R. Bhat, M. Burgay, S. Burke-Spolaor, D. J. Champion, P. Coster, N. D'Amico, A. Jameson, S. Johnston, M. Keith, M. Kramer, L. Levin, S. Milia, C. Ng, A. Possenti, and W. van Straten, Science **341**, 53 (2013), arXiv:1307.1628 [astro-ph.HE].
[165] K. Masui, H.-H. Lin, J. Sievers, C. J. Anderson, T.-C. Chang, X. Chen, A. Ganguly, M. Jarvis, C.-Y. Kuo, Y.-C. Li, Y.-W. Liao, M. McLaughlin, U.-L. Pen, J. B. Peterson, A. Roman, P. T. Timbie, T. Voytek, and J. K. Yadav, Nature **528**, 523 (2015), arXiv:1512.00529 [astro-ph.HE].
[166] S. Chatterjee, C. J. Law, R. S. Wharton, S. Burke-Spolaor, J. W. T. Hessels, G. C. Bower, J. M. Cordes, S. P. Tendulkar, C. G. Bassa, P. Demorest, B. J. Butler, A. Seymour, P. Scholz, M. W. Abruzzo, S. Bogdanov, V. M. Kaspi, A. Keimpema, T. J. W. Lazio, B. Marcote, M. A. McLaughlin, Z. Paragi, S. M. Ransom, M. Rupen, L. G. Spitler, and H. J. van Langevelde, Nature **541**, 58 (2017), arXiv:1701.01098 [astro-ph.HE].
[167] S. P. Tendulkar, C. G. Bassa, J. M. Cordes, G. C. Bower, C. J. Law, S. Chatterjee, E. A. K. Adams, S. Bogdanov, S. Burke-Spolaor, B. J. Butler, P. Demorest, J. W. T. Hessels, V. M. Kaspi, T. J. W. Lazio, N. Maddox, B. Marcote, M. A. McLaughlin, Z. Paragi, S. M. Ransom, P. Scholz, A. Seymour, L. G. Spitler, H. J. van Langevelde, and R. S. Wharton, ApJ **834**, L7 (2017), arXiv:1701.01100 [astro-ph.HE].
[168] H. Tanimura, G. Hinshaw, I. G. McCarthy, L. Van Waerbeke, Y.-Z. Ma, A. Mead, A. Hojjati, and T. Tröster, ArXiv e-prints (2017), arXiv:1709.05024.
[169] A. de Graaff, Y.-C. Cai, C. Heymans, and J. A. Peacock, ArXiv e-prints (2017), arXiv:1709.10378.
[170] M. McQuinn, ApJ **780**, L33 (2014), arXiv:1309.4451.

[171] K. W. Masui and K. Sigurdson, Physical Review Letters **115**, 121301 (2015), arXiv:1506.01704.

[172] P. Chawla, V. M. Kaspi, A. Josephy, K. M. Rajwade, D. R. Lorimer, A. M. Archibald, M. E. DeCesar, J. W. T. Hessels, D. L. Kaplan, C. Karako-Argaman, V. I. Kondratiev, L. Levin, R. S. Lynch, M. A. McLaughlin, S. M. Ransom, M. S. E. Roberts, I. H. Stairs, K. Stovall, J. K. Swiggum, and J. van Leeuwen, ApJ **844**, 140 (2017), arXiv:1701.07457 [astro-ph.HE].

[173] S. Vander Wiel, S. Burke-Spolaor, E. Lawrence, C. J. Law, and G. C. Bower, ArXiv e-prints (2016), arXiv:1612.00896 [astro-ph.IM].

[174] Z. Arzoumanian, A. Brazier, S. Burke-Spolaor, S. Chamberlin, S. Chatterjee, B. Christy, J. M. Cordes, N. J. Cornish, F. Crawford, H. Thankful Cromartie, K. Crowter, M. E. DeCesar, P. B. Demorest, T. Dolch, J. A. Ellis, R. D. Ferdman, E. C. Ferrara, E. Fonseca, N. Garver-Daniels, P. A. Gentile, D. Halmrast, E. A. Huerta, F. A. Jenet, C. Jessup, G. Jones, M. L. Jones, D. L. Kaplan, M. T. Lam, T. J. W. Lazio, L. Levin, A. Lommen, D. R. Lorimer, J. Luo, R. S. Lynch, D. Madison, A. M. Matthews, M. A. McLaughlin, S. T. McWilliams, C. Mingarelli, C. Ng, D. J. Nice, T. T. Pennucci, S. M. Ransom, P. S. Ray, X. Siemens, J. Simon, R. Spiewak, I. H. Stairs, D. R. Stinebring, K. Stovall, J. K. Swiggum, S. R. Taylor, M. Vallisneri, R. van Haasteren, S. J. Vigeland, W. Zhu, and The NANOGrav Collaboration, ApJS **235**, 37 (2018), arXiv:1801.01837 [astro-ph.HE].

[175] S. R. Taylor, C. M. F. Mingarelli, J. R. Gair, A. Sesana, G. Theureau, S. Babak, C. G. Bassa, P. Brem, M. Burgay, R. N. Caballero, D. J. Champion, I. Cognard, G. Desvignes, L. Guillemot, J. W. T. Hessels, G. H. Janssen, R. Karuppusamy, M. Kramer, A. Lassus, P. Lazarus, L. Lentati, K. Liu, S. Osłowski, D. Perrodin, A. Petiteau, A. Possenti, M. B. Purver, P. A. Rosado, S. A. Sanidas, R. Smits, B. Stappers, C. Tiburzi, R. van Haasteren, A. Vecchio, J. P. W. Verbiest, and EPTA Collaboration, Physical Review Letters **115**, 041101 (2015), arXiv:1506.08817 [astro-ph.HE].

[176] R. M. Shannon, V. Ravi, W. A. Coles, G. Hobbs, M. J. Keith, R. N. Manchester, J. S. B. Wyithe, M. Bailes, N. D. R. Bhat, S. Burke-Spolaor, J. Khoo, Y. Levin, S. Oslowski, J. M. Sarkissian, W. van Straten, J. P. W. Verbiest, and J.-B. Wang, Science **342**, 334 (2013), arXiv:1310.4569.

[177] J. H. Taylor and J. M. Weisberg, ApJ **345**, 434 (1989).

[178] M. Kramer, I. H. Stairs, R. N. Manchester, M. A. McLaughlin, A. G. Lyne, R. D. Ferdman, M. Burgay, D. R. Lorimer, A. Possenti, N. D'Amico, J. M. Sarkissian, G. B. Hobbs, J. E. Reynolds, P. C. C. Freire, and F. Camilo, Science **314**, 97 (2006), astro-ph/0609417.

[179] K. Stovall, R. S. Lynch, S. M. Ransom, A. M. Archibald, S. Banaszak, C. M. Biwer, J. Boyles, L. P. Dartez, D. Day, A. J. Ford, J. Flanigan, A. Garcia, J. W. T. Hessels, J. Hinojosa, F. A. Jenet, D. L. Kaplan, C. Karako-Argaman, V. M. Kaspi, V. I. Kondratiev, S. Leake, D. R. Lorimer, G. Lunsford, J. G. Martinez, A. Mata, M. A. McLaughlin, M. S. E. Roberts, M. D. Rohr, X. Siemens, I. H. Stairs, J. van Leeuwen, A. N. Walker, and B. L. Wells, ApJ **791**, 67 (2014), arXiv:1406.5214 [astro-ph.HE].

[180] K. M. Smith, ArXiv e-prints (2016), arXiv:1610.06831 [astro-ph.HE].

[181] K. Bandura, G. E. Addison, M. Amiri, J. R. Bond, D. Campbell-Wilson, L. Connor, J.-F. Cliche, G. Davis, M. Deng, N. Denman, M. Dobbs, M. Fandino, K. Gibbs, A. Gilbert, M. Halpern, D. Hanna, A. D. Hincks, G. Hinshaw, C. Höfer, P. Klages, T. L. Landecker, K. Masui, J. Mena Parra, L. B. Newburgh, U.-l. Pen, J. B. Peterson, A. Recnik, J. R. Shaw, K. Sigurdson, M. Sitwell, G. Smecher, R. Smegal, K. Vanderlinde, and D. Wiebe, in *Society of Photo-Optical Instrumentation Engineers (SPIE) Conference Series*, Society of Photo-Optical Instrumentation Engineers (SPIE) Conference Series, Vol. 9145 (2014) p. 22, arXiv:1406.2288 [astro-ph.IM].

[182] D. R. DeBoer, A. R. Parsons, J. E. Aguirre, P. Alexander, Z. S. Ali, A. P. Beardsley, G. Bernardi, J. D. Bowman, R. F. Bradley, C. L. Carilli, C. Cheng, E. de Lera Acedo, J. S. Dillon, A. Ewall-Wice, G. Fadana, N. Fagnoni, R. Fritz, S. R. Furlanetto, B. Glendenning, B. Greig, J. Grobbelaar, B. J. Hazelton, J. N. Hewitt, J. Hickish, D. C. Jacobs, A. Julius, M. Kariseb, S. A. Kohn, T. Lekalake, A. Liu, A. Loots, D. MacMahon, L. Malan, C. Malgas, M. Maree, Z. Martinot, N. Mathison, E. Matsetela, A. Mesinger, M. F. Morales, A. R. Neben, N. Patra, S. Pieterse, J. C. Pober, N. Razavi-Ghods, J. Ringuette, J. Robnett, K. Rosie, R. Sell, C. Smith, A. Syce, M. Tegmark, N. Thyagarajan, P. K. G. Williams, and H. Zheng, Publications of the Astronomical Society of the Pacific **129**, 045001 (2017).

[183] J. C. Pober, A. R. Parsons, J. E. Aguirre, Z. Ali, R. F. Bradley, C. L. Carilli, D. DeBoer, M. Dexter, N. E. Gugliucci, D. C. Jacobs, P. J. Klima, D. MacMahon, J. Manley, D. F. Moore, I. I. Stefan, and W. P. Walbrugh, ApJ **768**, L36 (2013), arXiv:1301.7099.

[184] S. Tingay, R. Goeke, J. N. Hewitt, E. Morgan, R. A. Remillard, C. L. Williams, J. D. Bowman, E. Emrich, S. M. Ord, T. Booler, B. Crosse, D. Pallot, W. Arcus, T. Colegate, P. J. Hall, D. Herne, M. J. Lynch, F. Schlagenhaufer, S. Tremblay, R. B. Wayth, M. Waterson, D. A. Mitchell, R. J. Sault, R. L. Webster, J. S. B. Wyithe, M. F. Morales, B. J. Hazelton, A. Wicenec, A. Williams, D. Barnes, G. Bernardi, L. J. Greenhill, J. C. Kasper, F. Briggs, B. McKinley, J. D. Bunton, L. deSouza, R. Koenig, J. Pathikulangara, J. Stevens, R. J. Cappallo, B. E. Corey, B. B. Kincaid, E. Kratzenberg, C. J. Lonsdale, S. R. McWhirter, A. E. E. Rogers, J. E. Salah, A. R. Whitney, A. Deshpande, T. Prabu, A. Roshi, N. Udaya-Shankar, K. S. Srivani, R. Subrahmanyan, B. M. Gaensler, M. Johnston-Hollitt, D. L. Kaplan, and D. Oberoi, in *Resolving The Sky - Radio Interferometry: Past, Present and Future* (2012) p. 36, arXiv:1212.1327 [astro-ph.IM].

[185] X. Chen, in *International Journal of Modern Physics Conference Series*, International Journal of Modern Physics Conference Series, Vol. 12 (2012) pp. 256–263, arXiv:1212.6278 [astro-ph.IM].

[186] M. P. van Haarlem, M. W. Wise, A. W. Gunst, G. Heald, J. P. McKean, J. W. T. Hessels, A. G. de Bruyn, R. Nijboer, J. Swinbank, R. Fallows, M. Brentjens, A. Nelles, R. Beck, H. Falcke, R. Fender, J. Hörandel, L. V. E. Koopmans, G. Mann, G. Miley, H. Röttgering, B. W. Stappers, R. A. M. J. Wijers, S. Zaroubi, M. van den Akker, A. Alexov, J. Anderson, K. Anderson, A. van Ardenne, M. Arts, A. Asgekar, I. M. Avruch, F. Batejat, L. Bähren, M. E. Bell, M. R. Bell, I. van Bemmel, P. Bennema, M. J. Bentum, G. Bernardi, P. Best, L. Bîrzan, A. Bonafede, A.-J. Boonstra, R. Braun, J. Bregman, F. Breitling, R. H. van de Brink, J. Broderick, P. C. Broekema, W. N. Brouw, M. Brüggen, H. R. Butcher, W. van Cappellen, B. Ciardi, T. Coenen, J. Conway, A. Coolen, A. Corstanje, S. Damstra, O. Davies, A. T. Deller, R.-J. Dettmar, G. van Diepen, K. Dijkstra, P. Donker, A. Doorduin, J. Dromer, M. Drost, A. van Duin, J. Eislöffel, J. van Enst, C. Ferrari, W. Frieswijk, H. Gankema, M. A. Garrett, F. de Gasperin, M. Gerbers, E. de Geus, J.-M. Grießmeier, T. Grit, P. Gruppen, J. P. Hamaker, T. Hassall, M. Hoeft, H. A. Holties, A. Horneffer, A. van der Horst, A. van Houwelingen, A. Huijgen, M. Iacobelli, H. Intema, N. Jackson, V. Jelic, A. de Jong, E. Juette, D. Kant, A. Karastergiou, A. Koers, H. Kollen, V. I. Kondratiev, E. Kooistra, Y. Koopman, A. Koster, M. Kuniyoshi, M. Kramer, G. Kuper, P. Lambropoulos, C. Law, J. van Leeuwen, J. Lemaitre, M. Loose, P. Maat, G. Macario, S. Markoff, J. Masters, R. A. McFadden, D. McKay-Bukowski, H. Meijering, H. Meulman, M. Mevius, E. Middelberg, R. Millenaar, J. C. A. Miller-Jones, R. N. Mohan, J. D. Mol, J. Morawietz, R. Morganti, D. D. Mulcahy, E. Mulder,

H. Munk, L. Nieuwenhuis, R. van Nieuwpoort, J. E. Noordam, M. Norden, A. Noutsos, A. R. Offringa, H. Olofsson, A. Omar, E. Orrú, R. Overeem, H. Paas, M. Pandey-Pommier, V. N. Pandey, R. Pizzo, A. Polatidis, D. Rafferty, S. Rawlings, W. Reich, J.-P. de Reijer, J. Reitsma, G. A. Renting, P. Riemers, E. Rol, J. W. Romein, J. Roosjen, M. Ruiter, A. Scaife, K. van der Schaaf, B. Scheers, P. Schellart, A. Schoenmakers, G. Schoonderbeek, M. Serylak, A. Shulevski, J. Sluman, O. Smirnov, C. Sobey, H. Spreeuw, M. Steinmetz, C. G. M. Sterks, H.-J. Stiepel, K. Stuurwold, M. Tagger, Y. Tang, C. Tasse, I. Thomas, S. Thoudam, M. C. Toribio, B. van der Tol, O. Usov, M. van Veelen, A.-J. van der Veen, S. ter Veen, J. P. W. Verbiest, R. Vermeulen, N. Vermaas, C. Vocks, C. Vogt, M. de Vos, E. van der Wal, R. van Weeren, H. Weggemans, P. Weltevrede, S. White, S. J. Wijnholds, T. Wilhelmsson, O. Wucknitz, S. Yatawatta, P. Zarka, A. Zensus, and J. van Zwieten, A&A **556**, A2 (2013), arXiv:1305.3550 [astro-ph.IM].

[187] R. A. Monsalve, A. E. E. Rogers, J. D. Bowman, and T. J. Mozdzen, ApJ **835**, 49 (2017), arXiv:1602.08065 [astro-ph.IM].

[188] L. J. Greenhili, D. Werthimer, G. B. Taylor, and S. W. Ellingson, in *2012 International Conference on Electromagnetics in Advanced Applications* (2012) pp. 1117–1120.

[189] S. Rawlings, F. B. Abdalla, S. L. Bridle, C. A. Blake, C. M. Baugh, L. J. Greenhill, and J. M. van der Hulst, New A Rev. **48**, 1013 (2004), astro-ph/0409479.

[190] K. Bandura, J. F. Cliche, M. A. Dobbs, A. J. Gilbert, D. Ittah, J. Mena Parra, and G. Smecher, Journal of Astronomical Instrumentation **5**, 1641004 (2016).

[191] P. Berger, L. B. Newburgh, M. Amiri, K. Bandura, J.-F. Cliche, L. Connor, M. Deng, N. Denman, M. Dobbs, M. Fandino, A. J. Gilbert, D. Good, M. Halpern, D. Hanna, A. D. Hincks, G. Hinshaw, C. Hofer, A. M. Johnson, T. L. Landecker, K. W. Masui, J. M. Parra, N. Oppermann, U.-L. Pen, J. B. Peterson, A. Recnik, T. Robishaw, J. R. Shaw, S. Siegel, K. Sigurdson, K. Smith, E. Storer, I. Tretyakov, K. Van Gassen, K. Vanderlinde, and D. Wiebe, arXiv.org (2016), 1607.01473v1.

[192] L. B. Newburgh, G. E. Addison, M. Amiri, K. Bandura, J. R. Bond, L. Connor, J.-F. Cliche, G. Davis, M. Deng, N. Denman, M. Dobbs, M. Fandino, H. Fong, K. Gibbs, A. Gilbert, E. Griffin, M. Halpern, D. Hanna, A. D. Hincks, G. Hinshaw, C. Höfer, P. Klages, T. Landecker, K. Masui, J. M. Parra, U.-L. Pen, J. Peterson, A. Recnik, J. R. Shaw, K. Sigurdson, M. Sitwell, G. Smecher, R. Smegal, K. Vanderlinde, and D. Wiebe, in *Society of Photo-Optical Instrumentation Engineers (SPIE) Conference Series*, Society of Photo-Optical Instrumentation Engineers (SPIE) Conference Series, Vol. 9145 (2014) p. 4, arXiv:1406.2267 [astro-ph.IM].

[193] P. Procopio, R. B. Wayth, J. Line, C. M. Trott, H. T. Intema, D. A. Mitchell, B. Pindor, J. Riding, S. J. Tingay, M. E. Bell, J. R. Callingham, K. S. Dwarakanath, B.-Q. For, B. M. Gaensler, P. J. Hancock, L. Hindson, N. Hurley-Walker, M. Johnston-Hollitt, A. D. Kapińska, E. Lenc, B. McKinley, J. Morgan, A. Offringa, L. Staveley-Smith, C. Wu, and Q. Zheng, PASA **34**, e033 (2017), arXiv:1707.02288 [astro-ph.IM].

[194] H.-J. Seo and C. M. Hirata, MNRAS **456**, 3142 (2016), arXiv:1508.06503.

[195] A. Liu and M. Tegmark, MNRAS **419**, 3491 (2012), arXiv:1106.0007 [astro-ph.CO].

[196] J. R. Shaw, K. Sigurdson, M. Sitwell, A. Stebbins, and U.-L. Pen, arXiv.org (2014a), 1401.2095v1.

[197] J. R. Shaw, K. Sigurdson, U.-L. Pen, A. Stebbins, and M. Sitwell, arXiv.org (2013), 1302.0327v1.

[198] M. Tegmark and M. Zaldarriaga, Phys. Rev. D **79**, 083530 (2009), arXiv:0805.4414.

[199] A. R. Offringa, R. B. Wayth, N. Hurley-Walker, D. L. Kaplan, N. Barry, A. P. Beardsley, M. E. Bell, G. Bernardi, J. D. Bowman, F. Briggs, J. R. Callingham, R. J. Cappallo, P. Carroll, A. A. Deshpande, J. S. Dillon, K. S. Dwarakanath, A. Ewall-Wice, L. Feng, B.-Q. For, B. M. Gaensler, L. J. Greenhill, P. Hancock, B. J. Hazelton, J. N. Hewitt, L. Hindson, D. C. Jacobs, M. Johnston-Hollitt, A. D. Kapińska, H.-S. Kim, P. Kittiwisit, E. Lenc, J. Line, A. Loeb, C. J. Lonsdale, B. McKinley, S. R. McWhirter, D. A. Mitchell, M. F. Morales, E. Morgan, J. Morgan, A. R. Neben, D. Oberoi, S. M. Ord, S. Paul, B. Pindor, J. C. Pober, T. Prabu, P. Procopio, J. Riding, N. Udaya Shankar, S. Sethi, K. S. Srivani, L. Staveley-Smith, R. Subrahmanyan, I. S. Sullivan, M. Tegmark, N. Thyagarajan, S. J. Tingay, C. M. Trott, R. L. Webster, A. Williams, C. L. Williams, C. Wu, J. S. Wyithe, and Q. Zheng, PASA **32**, e008 (2015), arXiv:1501.03946 [astro-ph.IM].

[200] A. R. Offringa, J. J. van de Gronde, and J. B. T. M. Roerdink, A&A **539**, A95 (2012), arXiv:1201.3364 [astro-ph.IM].

[201] B. S. Arora, J. Morgan, S. M. Ord, S. J. Tingay, N. Hurley-Walker, M. Bell, G. Bernardi, N. D. R. Bhat, F. Briggs, J. R. Callingham, A. A. Deshpande, K. S. Dwarakanath, A. Ewall-Wice, L. Feng, B.-Q. For, P. Hancock, B. J. Hazelton, L. Hindson, D. Jacobs, M. Johnston-Hollitt, A. D. Kapińska, N. Kudryavtseva, E. Lenc, B. McKinley, D. Mitchell, D. Oberoi, A. R. Offringa, B. Pindor, P. Procopio, J. Riding, L. Staveley-Smith, R. B. Wayth, C. Wu, Q. Zheng, J. D. Bowman, R. J. Cappallo, B. E. Corey, D. Emrich, R. Goeke, L. J. Greenhill, D. L. Kaplan, J. C. Kasper, E. Kratzenberg, C. J. Lonsdale, M. J. Lynch, S. R. McWhirter, M. F. Morales, E. Morgan, T. Prabu, A. E. E. Rogers, A. Roshi, N. U. Shankar, K. S. Srivani, R. Subrahmanyan, M. Waterson, R. L. Webster, A. R. Whitney, A. Williams, and C. L. Williams, PASA **32**, e029 (2015), arXiv:1507.01184 [astro-ph.IM].

[202] G. Hovey, L. Baker, G. Cortes, D. DeBoer, M. Fleming, W. Imbriale, G. Lacy, B. Veidt, P. Byrnes, J. Fitzsimmons, L. Knee, and M. Kesteven, in *2015 1st URSI Atlantic Radio Science Conference (URSI AT-RASC)* (2015) pp. 1–1.

[203] A. Liu, M. Tegmark, S. Morrison, A. Lutomirski, and M. Zaldarriaga, MNRAS **408**, 1029 (2010), arXiv:1001.5268 [astro-ph.IM].

[204] C. L. Carilli, B. Nikolic, N. Thyagarajan, K. Gale-Sides, Z. Abdurashidova, J. E. Aguirre, P. Alexander, Z. S. Ali, Y. Balfour, A. P. Beardsley, G. Bernardi, J. D. Bowman, R. F. Bradley, J. Burba, C. Cheng, D. R. DeBoer, M. Dexter, E. de˜Lera˜Acedo, J. S. Dillon, A. Ewall-Wice, G. Fadana, N. Fagnoni, R. Fritz, S. R. Furlanetto, A. Ghosh, B. Glendenning, B. Greig, J. Grobbelaar, Z. Halday, B. J. Hazelton, J. N. Hewitt, J. Hickish, D. C. Jacobs, A. Julius, M. Kariseb, S. A. Kohn, M. Kolopanis, T. Lekalake, A. Liu, A. Loots, D. MacMahon, L. Malan, C. Malgas, M. Maree, Z. Martinot, E. Matsetela, A. Mesinger, M. Molewa, M. F. Morales, A. R. Neben, A. R. Parsons, N. Patra, S. Pieterse, P. La Plante, J. C. Pober, N. Razavi-Ghods, J. Ringuette, J. Robnett, K. Rosie, R. Sell, P. Sims, C. Smith, A. Syce, P. K. ˜G. Williams, and H. Zheng, ArXiv e-prints (2018), arXiv:1805.00953 [astro-ph.IM].

[205] J. S. Dillon, S. A. Kohn, A. R. Parsons, J. E. Aguirre, Z. S. Ali, G. Bernardi, N. S. Kern, W. Li, A. Liu, C. D. Nunhokee, and J. C. Pober, MNRAS **477**, 5670 (2018), arXiv:1712.07212 [astro-ph.IM].

[206] V. Ram Marthi and J. Chengalur, in *Astronomical Society of India Conference Series*, Astronomical Society of India Conference Series, Vol. 13 (2014) pp. 393–394, arXiv:1310.1449 [astro-ph.IM].

[207] J. S. Dillon and A. R. Parsons, ApJ **826**, 181 (2016), arXiv:1602.06259 [astro-ph.IM].

[208] J. L. Sievers, ArXiv e-prints (2017), arXiv:1701.01860 [astro-ph.IM].
[209] U.-L. Pen, New A **9**, 417 (2004), astro-ph/0305387.
[210] M. Tegmark and M. Zaldarriaga, Phys. Rev. D **82**, 103501 (2010), arXiv:0909.0001 [astro-ph.CO].
[211] K. W. Masui, J. R. Shaw, C. Ng, K. M. Smith, K. Vanderlinde, and A. Paradise, ArXiv e-prints (2017), arXiv:1710.08591 [astro-ph.IM].
[212] M. Sokolowski, T. Colegate, A. T. Sutinjo, D. Ung, R. Wayth, N. Hurley-Walker, E. Lenc, B. Pindor, J. Morgan, D. L. Kaplan, M. E. Bell, J. R. Callingham, K. S. Dwarakanath, B.-Q. For, B. M. Gaensler, P. J. Hancock, L. Hindson, M. Johnston-Hollitt, A. D. Kapińska, B. McKinley, A. R. Offringa, P. Procopio, L. Staveley-Smith, C. Wu, and Q. Zheng, PASA **34**, e062 (2017), arXiv:1710.07478 [astro-ph.IM].
[213] D. C. Jacobs, J. Burba, J. Bowman, A. R. Neben, B. Stinnett, and L. Turner, ArXiv e-prints (2016), arXiv:1610.02607 [astro-ph.IM].
[214] G. Virone, A. M. Lingua, M. Piras, A. Cina, F. Perini, J. Monari, F. Paonessa, O. A. Peverini, G. Addamo, and R. Tascone, IEEE Antennas and Wireless Propagation Letters **13**, 169 (2014).
[215] G. Pupillo, G. Naldi, G. Bianchi, A. Mattana, J. Monari, F. Perini, M. Poloni, M. Schiaffino, P. Bolli, A. Lingua, I. Aicardi, H. Bendea, P. Maschio, M. Piras, G. Virone, F. Paonessa, Z. Farooqui, A. Tibaldi, G. Addamo, O. A. Peverini, R. Tascone, and S. J. Wijnholds, Experimental Astronomy **39**, 405 (2015).
[216] C. Chang, C. Monstein, A. Refregier, A. Amara, A. Glauser, and S. Casura, PASP **127**, 1131 (2015), arXiv:1505.05885 [astro-ph.IM].
[217] L. R. D'Addario and D. Wang, in *2016 United States National Committee of URSI National Radio Science Meeting (USNC-URSI NRSM)* (2016) pp. 1–2.
[218] S. E. Harper and C. Dickinson, MNRAS **479**, 2024 (2018), arXiv:1803.06314 [astro-ph.IM].
[219] H.-J. Seo, S. Dodelson, J. Marriner, D. Mcginnis, A. Stebbins, C. Stoughton, and A. Vallinotto, ApJ **721**, 164 (2010), arXiv:0910.5007 [astro-ph.CO].
[220] J. C. Pober, MNRAS **447**, 1705 (2015), arXiv:1411.2050.
[221] J. Jewell, S. Levin, and C. H. Anderson, ApJ **609**, 1 (2004), arXiv:astro-ph/0209560 [astro-ph].
[222] D. J. Eisenstein, H.-J. Seo, E. Sirko, and D. N. Spergel, ApJ **664**, 675 (2007), astro-ph/0604362.
[223] N. Padmanabhan, M. White, and J. D. Cohn, Phys. Rev. D **79**, 063523 (2009), arXiv:0812.2905.
[224] D. Alonso, P. G. Ferreira, and M. G. Santos, MNRAS **444**, 3183 (2014), arXiv:1405.1751.
[225] P. Monaco, E. Sefusatti, S. Borgani, M. Crocce, P. Fosalba, R. K. Sheth, and T. Theuns, MNRAS **433**, 2389 (2013), arXiv:1305.1505.
[226] F.-S. Kitaura and S. Heß, MNRAS **435**, L78 (2013), arXiv:1212.3514.
[227] S. Avila, S. G. Murray, A. Knebe, C. Power, A. S. G. Robotham, and J. Garcia-Bellido, MNRAS **450**, 1856 (2015), arXiv:1412.5228.
[228] C.-H. Chuang, F.-S. Kitaura, F. Prada, C. Zhao, and G. Yepes, MNRAS **446**, 2621 (2015), arXiv:1409.1124.
[229] M. Vakili, F.-S. Kitaura, Y. Feng, G. Yepes, C. Zhao, C.-H. Chuang, and C. Hahn, MNRAS **472**, 4144 (2017), arXiv:1701.03765.
[230] S. Tassev, M. Zaldarriaga, and D. J. Eisenstein, J. Cosmology Astropart. Phys. **6**, 036 (2013), arXiv:1301.0322 [astro-ph.CO].
[231] M. White, J. L. Tinker, and C. K. McBride, MNRAS **437**, 2594 (2014), arXiv:1309.5532.
[232] Y. Feng, M.-Y. Chu, U. Seljak, and P. McDonald, MNRAS **463**, 2273 (2016), arXiv:1603.00476.
[233] G. Stein, M. A. Alvarez, and J. R. Bond, ArXiv e-prints (2018), arXiv:1810.07727.
[234] G. Prézeau and M. Reinecke, ApJS **190**, 267 (2010), arXiv:1002.1050 [astro-ph.IM].
[235] A. J. Cianciara, C. J. Anderson, X. Chen, Z. Chen, J. Geng, J. Li, C. Liu, T. Liu, W. Lu, J. B. Peterson, H. Shi, C. N. Steffel, A. Stebbins, T. Stucky, S. Sun, P. T. Timbie, Y. Wang, F. Wu, and J. Zhang, Journal of Astronomical Instrumentation **6**, 1750003-40 (2017), arXiv:1705.04435 [astro-ph.IM].
[236] M. Deng, D. Campbell-Wilson, and for the CHIME Collaboration, ArXiv e-prints (2017), arXiv:1708.08521 [astro-ph.IM].
[237] A. Ewall-Wice, R. Bradley, D. Deboer, J. Hewitt, A. Parsons, J. Aguirre, Z. S. Ali, J. Bowman, C. Cheng, A. R. Neben, N. Patra, N. Thyagarajan, M. Venter, E. de Lera Acedo, J. S. Dillon, R. Dickenson, P. Doolittle, D. Egan, M. Hedrick, P. Klima, S. Kohn, P. Schaffner, J. Shelton, B. Saliwanchik, H. A. Taylor, R. Taylor, M. Tegmark, and B. Wirt, ApJ **831**, 196 (2016), arXiv:1602.06277.
[238] "Vla data rate," `https://science.nrao.edu/facilities/vla/docs/manuals/oss/performance/tim-res`, accessed: 2018-07-10.
[239] "Alma data rate," `https://library.nrao.edu/public/memos/naasc/NAASC_110.pdf`, accessed: 2018-07-10.
[240] "Lhc data rate," `https://home.cern/about/computing/processing-what-record`, accessed: 2018-07-10.
[241] "Lsst data rate," `https://www.lsst.org/about/camera/features`, accessed: 2018-07-10.
[242] J. Thayer, D. Damiani, C. Ford, M. Dubrovin, I. Gaponenko, C. P. O'Grady, W. Kroeger, J. Pines, T. J. Lane, A. Salnikov, D. Schneider, T. Tookey, M. Weaver, C. H. Yoon, and A. Perazzo, Advanced Structural and Chemical Imaging **3**, 3 (2017).
[243] "Lcls-ii data rate," `http://www.esrf.eu/files/live/sites/www/files/events/conferences/2018/IFDEPS/S8.02.Thayer.pdf`, accessed: 2018-07-10.
[244] "Xfel data rate," `http://www.esrf.eu/files/live/sites/www/files/events/conferences/2018/IFDEPS/S8.01.Kuster.pdf`, accessed: 2018-07-10.
[245] "Ska i data rate," `https://indico.cern.ch/event/184526/contributions/322917/attachments/253364/354189/PAlexander_SKA_Computational_Challenges.pdf`, accessed: 2018-07-10.
[246] "Chime data rate," `https://chime-experiment.ca/instrument`, accessed: 2018-07-10.
[247] S. Das, C. J. Anderson, R. Ansari, J.-E. Campagne, D. Charlet, X. Chen, Z. Chen, A. J. Cianciara, P. Colom, Y. Cong, K. G. Gayley, J. Geng, J. Hao, Q. Huang, C. S. Keith, C. Li, J. Li, Y. Li, C. Liu, T. Liu, C. Magneville, J. P. Marriner, J.-M. Martin, M. Moniez, T. M. Oxholm, U.-l. Pen, O. Perdereau, J. B. Peterson, H. Shi, L. Shu, A. Stebbins, S. Sun, P. T. Timbie, S. Torchinsky, G. S. Tucker, G. Wang, R. Wang, X. Wang, Y. Wang, F. Wu, Y. Xu, K. Yu, J. Zhang, J. Zhang, L. Zhang, J. Zhu, and S. Zuo, in *Society of Photo-Optical Instrumentation Engineers (SPIE) Conference Series*, Society of Photo-Optical Instrumentation Engineers (SPIE) Conference Series, Vol. 10708 (2018) p. 1070836, arXiv:1806.04698 [astro-ph.IM].
[248] A. R. Parsons, D. C. Backer, G. S. Foster, M. C. H. Wright, R. F. Bradley, N. E. Gugliucci, C. R. Parashare, E. E. Benoit, J. E. Aguirre, D. C. Jacobs, C. L. Carilli, D. Herne, M. J. Lynch, J. R. Manley, and D. J. Werthimer, AJ **139**, 1468 (2010).

[249] S. J. Tingay, R. Goeke, J. D. Bowman, D. Emrich, S. M. Ord, D. A. Mitchell, M. F. Morales, T. Booler, B. Crosse, R. B. Wayth, C. J. Lonsdale, S. Tremblay, D. Pallot, T. Colegate, A. Wicenec, N. Kudryavtseva, W. Arcus, D. Barnes, G. Bernardi, F. Briggs, S. Burns, J. D. Bunton, R. J. Cappallo, B. E. Corey, A. Deshpande, L. Desouza, B. M. Gaensler, L. J. Greenhill, P. J. Hall, B. J. Hazelton, D. Herne, J. N. Hewitt, M. Johnston-Hollitt, D. L. Kaplan, J. C. Kasper, B. B. Kincaid, R. Koenig, E. Kratzenberg, M. J. Lynch, B. Mckinley, S. R. Mcwhirter, E. Morgan, D. Oberoi, J. Pathikulangara, T. Prabu, R. A. Remillard, A. E. E. Rogers, A. Roshi, J. E. Salah, R. J. Sault, N. Udaya-Shankar, F. Schlagenhaufer, K. S. Srivani, J. Stevens, R. Subrahmanyan, M. Waterson, R. L. Webster, A. R. Whitney, A. Williams, C. L. Williams, and J. S. B. Wyithe, PASA **30**, e007 (2013), arXiv:1206.6945 [astro-ph.IM].
[250] G. Paciga, J. G. Albert, K. Bandura, T.-C. Chang, Y. Gupta, C. Hirata, J. Odegova, U.-L. Pen, J. B. Peterson, J. Roy, J. R. Shaw, K. Sigurdson, and T. Voytek, MNRAS **433**, 639 (2013).
[251] J. D. Bowman, A. E. E. Rogers, R. A. Monsalve, T. J. Mozdzen, and N. Mahesh, Nature **555**, 67 (2018).
[252] C. Feng and G. Holder, ArXiv e-prints (2018), arXiv:1802.07432.
[253] R. Hills, G. Kulkarni, P. D. Meerburg, and E. Puchwein, (2018), arXiv:1805.01421 [astro-ph.CO].
[254] S. Fraser, A. Hektor, G. Hütsi, K. Kannike, C. Marzo, L. Marzola, C. Spethmann, A. Racioppi, M. Raidal, V. Vaskonen, and H. Veermäe, ArXiv e-prints (2018), arXiv:1803.03245 [hep-ph].
[255] R. Barkana, N. J. Outmezguine, D. Redigolo, and T. Volansky, ArXiv e-prints (2018), arXiv:1803.03091 [hep-ph].
[256] A. Berlin, D. Hooper, G. Krnjaic, and S. D. McDermott, ArXiv e-prints (2018), arXiv:1803.02804 [hep-ph].
[257] R. Barkana, Nature **555**, 71 (2018), arXiv:1803.06698.
[258] T. R. Slatyer and C.-L. Wu, ArXiv e-prints (2018), arXiv:1803.09734.
[259] S. Hirano and V. Bromm, ArXiv e-prints (2018), arXiv:1803.10671.
[260] D. A. Neufeld, G. R. Farrar, and C. F. McKee, ArXiv e-prints (2018), arXiv:1805.08794.
[261] S. Yoshiura, K. Takahashi, and T. Takahashi, ArXiv e-prints (2018), arXiv:1805.11806.
[262] M. Chianese, P. Di Bari, K. Farrag, and R. Samanta, ArXiv e-prints (2018), arXiv:1805.11717 [hep-ph].
[263] A. A. Costa, R. C. G. Landim, B. Wang, and E. Abdalla, ArXiv e-prints (2018), arXiv:1803.06944.
[264] J. C. Hill and E. J. Baxter, ArXiv e-prints (2018), arXiv:1803.07555.
[265] T. Moroi, K. Nakayama, and Y. Tang, ArXiv e-prints (2018), arXiv:1804.10378 [hep-ph].
[266] N. Houston, C. Li, T. Li, Q. Yang, and X. Zhang, ArXiv e-prints (2018), arXiv:1805.04426 [hep-ph].
[267] P. Sikivie, ArXiv e-prints (2018), arXiv:1805.05577.
[268] Y. Wang and G.-B. Zhao, ArXiv e-prints (2018), arXiv:1805.11210.
[269] G. D'Amico, P. Panci, and A. Strumia, ArXiv e-prints (2018), arXiv:1803.03629.
[270] Y. Yang, ArXiv e-prints (2018), arXiv:1803.05803.
[271] K. Cheung, J.-L. Kuo, K.-W. Ng, and Y.-L. Sming Tsai, ArXiv e-prints (2018), arXiv:1803.09398.
[272] S. Clark, B. Dutta, Y. Gao, Y.-Z. Ma, and L. E. Strigari, ArXiv e-prints (2018), arXiv:1803.09390 [astro-ph.HE].
[273] A. Hektor, G. Hütsi, L. Marzola, M. Raidal, V. Vaskonen, and H. Veermäe, ArXiv e-prints (2018), arXiv:1803.09697.
[274] A. Lidz and L. Hui, ArXiv e-prints (2018), arXiv:1805.01253.
[275] M. Safarzadeh, E. Scannapieco, and A. Babul, ArXiv e-prints (2018), arXiv:1803.08039.
[276] A. Schneider, ArXiv e-prints (2018), arXiv:1805.00021.
[277] A. Liu, J. R. Pritchard, M. Tegmark, and A. Loeb, Phys. Rev. D **87**, 043002 (2013), arXiv:1211.3743 [astro-ph.CO].
[278] J. Silk, ApJ **151**, 459 (1968).
[279] Y. Ali-Haimoud, P. D. Meerburg, and S. Yuan, Phys. Rev. **D89**, 083506 (2014), arXiv:1312.4948 [astro-ph.CO].
[280] K. Sigurdson and S. R. Furlanetto, Phys. Rev. Lett. **97**, 091301 (2006), arXiv:astro-ph/0505173 [astro-ph].
[281] A. Loeb and M. Zaldarriaga, Phys. Rev. Lett. **92**, 211301 (2004), arXiv:astro-ph/0312134 [astro-ph].
[282] A. Lewis and A. Challinor, Phys. Rev. **D76**, 083005 (2007), arXiv:astro-ph/0702600 [ASTRO-PH].
[283] S. Jester and H. Falcke, New A Rev. **53**, 1 (2009), arXiv:0902.0493 [astro-ph.CO].
[284] J. O. Burns, R. Bradley, K. Tauscher, S. Furlanetto, J. Mirocha, R. Monsalve, D. Rapetti, W. Purcell, D. Newell, D. Draper, R. MacDowall, J. Bowman, B. Nhan, E. J. Wollack, A. Fialkov, D. Jones, J. C. Kasper, A. Loeb, A. Datta, J. Pritchard, E. Switzer, and M. Bicay, ApJ **844**, 33 (2017), arXiv:1704.02651 [astro-ph.IM].
[285] M. K. Wolt, and D. Collaboration (2013) pp. 1–2.
[286] P. Adshead, R. Easther, J. Pritchard, and A. Loeb, JCAP **1102**, 021 (2011), arXiv:1007.3748 [astro-ph.CO].
[287] J. B. Muñoz, Y. Ali-Haïmoud, and M. Kamionkowski, Phys. Rev. D **92**, 083508 (2015), arXiv:1506.04152.
[288] X. Chen, P. D. Meerburg, and M. Münchmeyer, JCAP **1609**, 023 (2016), arXiv:1605.09364 [astro-ph.CO].
[289] D. Baumann, G. Goon, H. Lee, and G. L. Pimentel, (2017), arXiv:1712.06624 [hep-th].
[290] A. H. Guth, Phys. Rev. D **23**, 347 (1981).
[291] J. L. Cook and L. Sorbo, Phys. Rev. **D85**, 023534 (2012), [Erratum: Phys. Rev.D86,069901(2012)], arXiv:1109.0022 [astro-ph.CO].
[292] R. Namba, M. Peloso, M. Shiraishi, L. Sorbo, and C. Unal, JCAP **1601**, 041 (2016), arXiv:1509.07521 [astro-ph.CO].
[293] J. Khoury, B. A. Ovrut, P. J. Steinhardt, and N. Turok, Phys. Rev. **D64**, 123522 (2001), arXiv:hep-th/0103239 [hep-th].
[294] D. H. Lyth, Phys. Rev. Lett. **78**, 1861 (1997), arXiv:hep-ph/9606387 [hep-ph].
[295] P. D. Meerburg, J. Meyers, K. M. Smith, and A. van Engelen, Phys. Rev. **D95**, 123538 (2017), arXiv:1701.06992 [astro-ph.CO].
[296] P. D. Meerburg, R. Hložek, B. Hadzhiyska, and J. Meyers, Phys. Rev. **D91**, 103505 (2015), arXiv:1502.00302 [astro-ph.CO].
[297] E. Alizadeh and C. M. Hirata, Phys. Rev. D **85**, 123540 (2012), arXiv:1201.5374 [astro-ph.CO].
[298] K. W. Masui and U.-L. Pen, Physical Review Letters **105**, 161302 (2010), arXiv:1006.4181 [astro-ph.CO].
[299] K. W. Masui, U.-L. Pen, and N. Turok, Phys. Rev. Lett. **118**, 221301 (2017), arXiv:1702.06552 [astro-ph.CO].
[300] S. Dodelson, E. Rozo, and A. Stebbins, Phys. Rev. Lett. **91**, 021301 (2003), arXiv:astro-ph/0301177 [astro-ph].
[301] C. Li and A. Cooray, Phys. Rev. **D74**, 023521 (2006), arXiv:astro-ph/0604179 [astro-ph].
[302] L. Book, M. Kamionkowski, and F. Schmidt, Phys. Rev. Lett. **108**, 211301 (2012), arXiv:1112.0567 [astro-ph.CO].

[303] N. E. Chisari, C. Dvorkin, and F. Schmidt, Phys. Rev. **D90**, 043527 (2014), arXiv:1406.4871 [astro-ph.CO].
[304] C. Sheere, A. van Engelen, P. D. Meerburg, and J. Meyers, Phys. Rev. **D96**, 063508 (2017), arXiv:1610.09365 [astro-ph.CO].
[305] F. Schmidt and D. Jeong, Phys. Rev. **D86**, 083513 (2012), arXiv:1205.1514 [astro-ph.CO].
[306] A. Lewis, A. Challinor, and A. Lasenby, Astrophys. J. **538**, 473 (2000), arXiv:astro-ph/9911177 [astro-ph].
[307] S. Saga, D. Yamauchi, and K. Ichiki, Phys. Rev. **D92**, 063533 (2015), arXiv:1505.02774 [astro-ph.CO].
[308] S. Saga, Phys. Rev. **D94**, 063523 (2016), arXiv:1607.03973 [astro-ph.CO].
[309] D. Baumann, P. J. Steinhardt, K. Takahashi, and K. Ichiki, Phys. Rev. **D76**, 084019 (2007), arXiv:hep-th/0703290 [hep-th].
[310] S. Foreman, H. Perrier, and L. Senatore, JCAP **1605**, 027 (2016), arXiv:1507.05326 [astro-ph.CO].
[311] Y.-Z. Ma and D. Scott, Phys. Rev. **D93**, 083510 (2016), arXiv:1510.08309 [astro-ph.CO].
[312] R. A. Battye, I. W. A. Browne, C. Dickinson, G. Heron, B. Maffei, and A. Pourtsidou, MNRAS **434**, 1239 (2013), arXiv:1209.0343 [astro-ph.CO].
[313] N. H. M. Crighton, M. T. Murphy, J. X. Prochaska, G. Worseck, M. Rafelski, G. D. Becker, S. L. Ellison, M. Fumagalli, S. Lopez, A. Meiksin, and J. M. O'Meara, MNRAS **452**, 217 (2015), arXiv:1506.02037.
[314] A. de Oliveira-Costa, M. Tegmark, B. M. Gaensler, J. Jonas, T. L. Landecker, and P. Reich, MNRAS **388**, 247 (2008), arXiv:0802.1525.
[315] Planck Collaboration, R. Adam, P. A. R. Ade, N. Aghanim, M. I. R. Alves, M. Arnaud, M. Ashdown, J. Aumont, C. Baccigalupi, A. J. Banday, and et al., A&A **594**, A10 (2016), arXiv:1502.01588.
[316] V. Jelić, S. Zaroubi, P. Labropoulos, R. M. Thomas, G. Bernardi, M. A. Brentjens, A. G. de Bruyn, B. Ciardi, G. Harker, L. V. E. Koopmans, V. N. Pandey, J. Schaye, and S. Yatawatta, MNRAS **389**, 1319 (2008), arXiv:0804.1130.
[317] A. Datta, J. D. Bowman, and C. L. Carilli, ApJ **724**, 526 (2010), arXiv:1005.4071 [astro-ph.CO].
[318] H. Vedantham, N. Udaya Shankar, and R. Subrahmanyan, ApJ **745**, 176 (2012), arXiv:1106.1297 [astro-ph.IM].
[319] M. F. Morales, B. Hazelton, I. Sullivan, and A. Beardsley, ApJ **752**, 137 (2012), arXiv:1202.3830 [astro-ph.IM].
[320] C. M. Trott, R. B. Wayth, and S. J. Tingay, ApJ **757**, 101 (2012), arXiv:1208.0646 [astro-ph.CO].
[321] N. Thyagarajan, N. Udaya Shankar, R. Subrahmanyan, W. Arcus, G. Bernardi, J. D. Bowman, F. Briggs, J. D. Bunton, R. J. Cappallo, B. E. Corey, L. deSouza, D. Emrich, B. M. Gaensler, R. F. Goeke, L. J. Greenhill, B. J. Hazelton, D. Herne, J. N. Hewitt, M. Johnston-Hollitt, D. L. Kaplan, J. C. Kasper, B. B. Kincaid, R. Koenig, E. Kratzenberg, C. J. Lonsdale, M. J. Lynch, S. R. McWhirter, D. A. Mitchell, M. F. Morales, E. H. Morgan, D. Oberoi, S. M. Ord, J. Pathikulangara, R. A. Remillard, A. E. E. Rogers, D. Anish Roshi, J. E. Salah, R. J. Sault, K. S. Srivani, J. B. Stevens, P. Thiagaraj, S. J. Tingay, R. B. Wayth, M. Waterson, R. L. Webster, A. R. Whitney, A. J. Williams, C. L. Williams, and J. S. B. Wyithe, ApJ **776**, 6 (2013), arXiv:1308.0565 [astro-ph.CO].
[322] J. C. Pober, A. R. Parsons, J. E. Aguirre, Z. Ali, R. F. Bradley, C. L. Carilli, D. DeBoer, M. Dexter, N. E. Gugliucci, D. C. Jacobs, P. J. Klima, D. MacMahon, J. Manley, D. F. Moore, I. I. Stefan, and W. P. Walbrugh, ApJ **768**, L36 (2013), arXiv:1301.7099 [astro-ph.CO].
[323] J. S. Dillon, A. Liu, C. L. Williams, J. N. Hewitt, M. Tegmark, E. H. Morgan, A. M. Levine, M. F. Morales, S. J. Tingay, G. Bernardi, J. D. Bowman, F. H. Briggs, R. C. Cappallo, D. Emrich, D. A. Mitchell, D. Oberoi, T. Prabu, R. Wayth, and R. L. Webster, Phys. Rev. D **89**, 023002 (2014).
[324] B. J. Hazelton, M. F. Morales, and I. S. Sullivan, ApJ **770**, 156 (2013), arXiv:1301.3126 [astro-ph.IM].
[325] N. Thyagarajan, D. C. Jacobs, J. D. Bowman, N. Barry, A. P. Beardsley, G. Bernardi, F. Briggs, R. J. Cappallo, P. Carroll, B. E. Corey, A. de Oliveira-Costa, J. S. Dillon, D. Emrich, A. Ewall-Wice, L. Feng, R. Goeke, L. J. Greenhill, B. J. Hazelton, J. N. Hewitt, N. Hurley-Walker, M. Johnston-Hollitt, D. L. Kaplan, J. C. Kasper, H.-S. Kim, P. Kittiwisit, E. Kratzenberg, E. Lenc, J. Line, A. Loeb, C. J. Lonsdale, M. J. Lynch, B. McKinley, S. R. McWhirter, D. A. Mitchell, M. F. Morales, E. Morgan, A. R. Neben, D. Oberoi, A. R. Offringa, S. M. Ord, S. Paul, B. Pindor, J. C. Pober, T. Prabu, P. Procopio, J. Riding, A. E. E. Rogers, A. Roshi, N. Udaya Shankar, S. K. Sethi, K. S. Srivani, R. Subrahmanyan, I. S. Sullivan, M. Tegmark, S. J. Tingay, C. M. Trott, M. Waterson, R. B. Wayth, R. L. Webster, A. R. Whitney, A. Williams, C. L. Williams, C. Wu, and J. S. B. Wyithe, ApJ **804**, 14 (2015), arXiv:1502.07596 [astro-ph.IM].
[326] N. Thyagarajan, D. C. Jacobs, J. D. Bowman, N. Barry, A. P. Beardsley, G. Bernardi, F. Briggs, R. J. Cappallo, P. Carroll, A. A. Deshpande, A. de Oliveira-Costa, J. S. Dillon, A. Ewall-Wice, L. Feng, L. J. Greenhill, B. J. Hazelton, L. Hernquist, J. N. Hewitt, N. Hurley-Walker, M. Johnston-Hollitt, D. L. Kaplan, H.-S. Kim, P. Kittiwisit, E. Lenc, J. Line, A. Loeb, C. J. Lonsdale, B. McKinley, S. R. McWhirter, D. A. Mitchell, M. F. Morales, E. Morgan, A. R. Neben, D. Oberoi, A. R. Offringa, S. M. Ord, S. Paul, B. Pindor, J. C. Pober, T. Prabu, P. Procopio, J. Riding, N. Udaya Shankar, S. K. Sethi, K. S. Srivani, R. Subrahmanyan, I. S. Sullivan, M. Tegmark, S. J. Tingay, C. M. Trott, R. B. Wayth, R. L. Webster, A. Williams, C. L. Williams, and J. S. B. Wyithe, ApJ **807**, L28 (2015), arXiv:1506.06150.
[327] E. Chapman, S. Zaroubi, F. B. Abdalla, F. Dulwich, V. Jelić, and B. Mort, MNRAS **458**, 2928 (2016).
[328] J. C. Pober, B. J. Hazelton, A. P. Beardsley, N. A. Barry, Z. E. Martinot, I. S. Sullivan, M. F. Morales, M. E. Bell, G. Bernardi, N. D. R. Bhat, J. D. Bowman, F. Briggs, R. J. Cappallo, P. Carroll, B. E. Corey, A. de Oliveira-Costa, A. A. Deshpande, J. S. Dillon, D. Emrich, A. M. Ewall-Wice, L. Feng, R. Goeke, L. J. Greenhill, J. N. Hewitt, L. Hindson, N. Hurley-Walker, D. C. Jacobs, M. Johnston-Hollitt, D. L. Kaplan, J. C. Kasper, H.-S. Kim, P. Kittiwisit, E. Kratzenberg, N. Kudryavtseva, E. Lenc, J. Line, A. Loeb, C. J. Lonsdale, M. J. Lynch, B. McKinley, S. R. McWhirter, D. A. Mitchell, E. Morgan, A. R. Neben, D. Oberoi, A. R. Offringa, S. M. Ord, S. Paul, B. Pindor, T. Prabu, P. Procopio, J. Riding, A. E. E. Rogers, A. Roshi, S. K. Sethi, N. Udaya Shankar, K. S. Srivani, R. Subrahmanyan, M. Tegmark, N. Thyagarajan, S. J. Tingay, C. M. Trott, M. Waterson, R. B. Wayth, R. L. Webster, A. R. Whitney, A. Williams, C. L. Williams, and J. S. B. Wyithe, ApJ **819**, 8 (2016), arXiv:1601.06177 [astro-ph.IM].
[329] H.-J. Seo and C. M. Hirata, MNRAS **456**, 3142 (2016), arXiv:1508.06503.
[330] H. Jensen, S. Majumdar, G. Mellema, A. Lidz, I. T. Iliev, and K. L. Dixon, MNRAS **456**, 66 (2016), arXiv:1509.02277.
[331] S. A. Kohn, J. E. Aguirre, C. D. Nunhokee, G. Bernardi, J. C. Pober, Z. S. Ali, R. F. Bradley, C. L. Carilli, D. R. DeBoer, N. E. Gugliucci, D. C. Jacobs, P. Klima, D. H. E. MacMahon, J. R. Manley, D. F. Moore, A. R. Parsons, I. I. Stefan, and W. P. Walbrugh, ApJ **823**, 88 (2016), arXiv:1602.02635 [astro-ph.IM].
[332] J. C. Pober, A. Liu, J. S. Dillon, J. E. Aguirre, J. D. Bowman, R. F. Bradley, C. L. Carilli, D. R. DeBoer, J. N. Hewitt, D. C. Jacobs, M. McQuinn, M. F. Morales, A. R. Parsons, M. Tegmark, and D. J. Werthimer, ApJ **782**, 66 (2014), arXiv:1310.7031.

[333] D. J. Bacon *et al.*, PASA 2018 (in prep).
[334] R. Braun *et al.*, SKA-TEL-SKO-0000818 (2017).
[335] M. Remazeilles, C. Dickinson, A. J. Banday, M.-A. Bigot-Sazy, and T. Ghosh, MNRAS **451**, 4311 (2015), arXiv:1411.3628 [astro-ph.IM].
[336] C. Howlett, M. Manera, and W. J. Percival, Astronomy and Computing **12**, 109 (2015), arXiv:1506.03737.
[337] M. Davis, G. Efstathiou, C. S. Frenk, and S. D. M. White, ApJ **292**, 371 (1985).
[338] The LSST Dark Energy Science Collaboration, R. Mandelbaum, T. Eifler, R. Hložek, T. Collett, E. Gawiser, D. Scolnic, D. Alonso, H. Awan, R. Biswas, J. Blazek, P. Burchat, N. E. Chisari, I. Dell'Antonio, S. Digel, J. Frieman, D. A. Goldstein, I. Hook, Ž. Ivezić, S. M. Kahn, S. Kamath, D. Kirkby, T. Kitching, E. Krause, P.-F. Leget, P. J. Marshall, J. Meyers, H. Miyatake, J. A. Newman, R. Nichol, E. Rykoff, F. J. Sanchez, A. Slosar, M. Sullivan, and M. A. Troxel, ArXiv e-prints (2018), arXiv:1809.01669.
[339] S.-F. Chen, E. Castorina, M. White, and A. Slosar, in prep. (2018).